NTNU

Norwegian University of
Science and Technology

Quasi-static and dynamic behaviour of fillet welded connections

Martin Flottorp Paus

Civil and Environmental Engineering
Submission date: December 2016
Supervisor: Arild Holm Clausen, KT
Co-supervisor: Erik Løhre Grimsmo, KT

Norwegian University of Science and Technology
Department of Structural Engineering

Department of Structural Engineering
Faculty of Engineering Science and Technology
NTNU- Norwegian University of Science and Technology

ACCESSIBILITY

OPEN

MASTER THESIS 2016

SUBJECT AREA:	DATE:	NO. OF PAGES:
Computational Mechanics	20.12.2016	10+86

TITLE:

Quasi-static and dynamic behaviour of fillet welded connections

Kvasistatisk og dynamisk oppførsel av forbindelser med kilsveiser

BY:

Martin Flottorp Paus

SUMMARY:

Introduction
Understanding the behaviour of the joints in a construction is crucial for structural engineers. In fact, the behaviour of steel joints exposed to static loading is well documented. Steel joints exposed to impact loading have received limited attention in the literature. In recent years, however, the interest in steel structures and joints under extreme conditions has grown. The main purposes of this master thesis were to

- observe experimentally how fillet welded joints respond to impact and compare it to their response to quasi-static loading.
- carry out material test and determine the material properties of the weld and base materials.
- create representative numerical models and carry out final element simulations and compare the experimental results with the results from numerical simulations and Eurocode calculations.

Method
Two different component test specimen types were created, one with transverse and one with longitudinal fillet welds. Each specimen type was tested with both impact and quasi-static loading. DIC was employed to measure the deformations of the welds. The applied load was registered using strain gauges. Load and displacement curves were presented as the results for all the component tests.

Material test specimens were machined from an unused test specimen. The material test specimens were tested in tension at three different loading rates. The extracted properties were determined and inserted into the numerical models. Creating representative numerical 3D models of the component test specimens, and carrying out final element simulations of those models, have been significant parts of the work for this thesis.

Results and discussion
The component tests with transverse fillet welds showed higher strength and less deformation capacity than the component tests with longitudinal fillet welds. There were no significant differences in the strength of the component tests measured at impact and at quasi-static loading. The numerical simulations gave good compliance to the experimental results. However, the strengths in the numerical models, particularly for the quasi-static simulations, were somewhat reduced with respect to the experimental results. The results do not indicate that the resistance formulas in the Eurocode should be altered.

RESPONSIBLE TEACHER: Arild Holm Clausen

SUPERVISOR(S): Arild Holm Clausen, Erik Løhre Grimsmo

CARRIED OUT AT: SIMLab, Department of Structural Engineering, NTNU

NORGES TEKNISK-NATURVITENSKAPELIGE UNIVERSITET
INSTITUTT FOR KONSTRUKSJONSTEKNIKK

MASTER THESIS 2016

Martin Flottorp Paus

Quasi-static and dynamic behaviour of fillet welded connections

(Kvasistatisk og dynamisk oppførsel av forbindelser med kilsveiser)

Welded connections are very common in most steel structures such as office buildings, offshore platforms, etc. The static behavior of welded connections has been well known for several decades, but the behavior of welded connections under transient dynamic loading is unknown. The latter load condition can arise due to for instance explosions, dropped objects and collisions.

The Eurocode NS-EN 1993-1-8 provides resistance formulas for fillet welds. However, these formulas assume static loading. In recent years, there has been an increased interest in the design of connections that may be subjected to blast or impact loading. It is therefore appropriate to investigate whether the resistance of fillet welds depend on the load rate. Furthermore, the ductility of the fillet welds is another important property, which becomes particularly important in transient dynamic load conditions because the energy absorption capacity is crucial in such load conditions. In this master thesis, fillet welds will be tested quasi-statically and dynamically. Moreover, the base and weld material behavior will be tested over a large range of load rates. Numerical simulations will be employed for further investigations.

The research project has three main objectives: (1) determine the material properties of the base and weld material, (2) investigate experimentally the quasi-static and dynamic behavior of fillet welds, (3) compare the experimental results with finite element analyses and Eurocode calculations.

The main topics in the research project will be as follows

1. **Literature study**: find and read relevant literature; *e.g.* scientific papers, Eurocodes, and textbooks.
2. **Material experiments**: uniaxial tension tests and identification of material properties.
3. **Component tests**: quasi-static and dynamic tests on specimens comprising of structural steel and fillet welds with emphasise on the resistance and ductility of the welds.
4. **Numerical analyses**: nonlinear finite element analyses of the component tests where the material properties should be determined from the material tests.
5. **Validation**: the finite element model should be validated against test results.
6. **Comparison with Eurocode**: the resistance of the fillet welds obtained from experiments and numerical analyses should be compared with estimates from Eurocode NS-EN 1993-1-8. The student should evaluate whether a modification of the resistance formulas is appropriate for transient dynamic load conditions.

The candidate may agree with the supervisors to pay particular attention to specific parts of the investigation, or include other aspects than those already mentioned.

The thesis is to be organized as a research report, recognising the guidelines provided by Department of Structural Engineering.

Supervisors: Erik Grimsmo and Arild Holm Clausen

The report is to be handed in not later than 21 December 2016.

NTNU, 3 August 2016

Arild Holm Clausen

Preface

The work of this master thesis has been carried out at the Norwegian University of Science and Technology (NTNU) for the research group Structural Impact Laboratory (SIMLab) at the Department of Structural Engineering.

Working with this master thesis has given me a better understanding of welds and steel as structural components and how of how the research in material and structural behaviour is being carried out. Besides, the work with this thesis has given me a great experience with working with Abaqus and final elements simulations.

I would like to thank my supervisors, Professor Arild Holm Clausen and PhD candidate Erik Løhre Grimsmo, for great support along the way. Their assistance has been a crucial factor in the work of this thesis and I am very grateful. I would also like to show my gratitude to Trond Auestad for his help during the experiments. Further, I would like to thank PhD candidate Petter Henrik Holmstrøm for his help with various problems, particularly problems related to Abaqus. Finally I wish to thank Torodd Berstad for his help with the debugging of my Abqus simulations and Egil Fagerholt for his guidance in the use of the eCorr software.

Trondheim, 20^{th} Desember, 2016

Martin Flottorp Paus

Abstract

Introduction

Understanding the behaviour of the joints in a construction is crucial for structural engineers. In fact, the behaviour of steel joints exposed to static loading is well documented. Steel joints exposed to impact loading have received limited attention in the literature. In recent years, however, the interest in steel structures and joints under extreme conditions has grown. The main purposes of this master thesis were to

- observe experimentally how fillet welded joints respond to impact and compare it to their response to quasi-static loading.
- carry out material test and determine the material properties of the weld and base materials.
- create representative numerical models and carry out final element simulations and compare the experimental results with the results from numerical simulations and Eurocode calculations.

Method

Two different component test specimen types were created, one with transverse and one with longitudinal fillet welds. Each specimen type was tested with both impact and quasi-static loading. DIC was employed to measure the deformations of the welds. The applied load was registered using strain gauges. Load and displacement curves were presented as the results for all the component tests.

Material test specimens were machined from an unused test specimen. The material test specimens were tested in tension at three different loading rates. The extracted properties were determined and inserted into the numerical models. Creating representative numerical 3D models of the component test specimens, and carrying out final element simulations of those models, have been significant parts of the work for this thesis.

Results and discussion

The component tests with transverse fillet welds showed higher strength and less deformation capacity than the component tests with longitudinal fillet welds. There were no significant differences in the strength of the component tests measured at impact and at quasi-static loading. The numerical simulations gave good compliance to the experimental results. However, the strengths in the numerical models, particularly for the quasi-static simulations, were somewhat reduced with respect to the experimental results. The results do not indicate that the resistance formulas in the Eurocode should be altered.

Sammendrag

Introduksjon

Det å forstå oppførslene til forbindelsene i en konstruksjon er avgjørende for en bygningsingeniør. Oppførselen til stålforbindelser utsatt for statisk belastning av den grunn godt dokumentert. Stålforbindelser utsatt for støt har dog ikke fått like stor oppmerksomhet i litteraturen. I de siste årene har riktignok interessen vokst for stålstrukturer og -forbindelser under ekstreme forhold. Hovedmålene med denne masteroppgaven var å

- observere eksperimentelt hvordan forbindelser med kilsveiser responderer ved påføring av støt og sammenlikne det med deres respons på kvasistatisk belastning.
- gjennomføre materialtester og fastslå materialegenskapene til både sveisene og grunnmaterialene.
- lage representative numeriske 3D modeller, kjøre elementmetodesimuleringer og sammenligne de eksperimentelle resultatene med resultatene fra simuleringene og fra beregninger gjort med Euocode.

Metode

To forskjellige komponentprøvestykker ble laget, èn med transverse og èn med langsgående kilsveiser. Hver av komponentprøvestykketypene ble testet med både støt og kvasistatisk belastning. DIC ble brukt for å måle deformasjonene i sveisene. De påførte kreftene ble registrert ved hjelp av strekklapper. Kurver med kraft mot relativ forskyvning ble presentert som resultater for alle komponentprøvestykkene.

Materialprøvestykker fra et ubrukt komponentprøvestykke ble strekktestet med tre forskjellige deformasjonshastigheter. De resulterende materialegenskapene ble brukt i de numeriske modellene. En stor del av arbeidet med denne masteroppgaven har gått med på å lage representative numeriske 3D modeller av komponentprøvestykkene og å kjøre elementmetodesimuleringer av disse modellene.

Resultater og diskusjon

Komponentprøvestykkene med transverse kilsveiser viste større styrke og mindre deformasjonskapasitet enn komponentprøvestykkene med langsgående kilsveiser. Det var ingen signifikant forskjell i styrken av komponentprøvestykkene målt ved støt og ved kvasistatisk belastning. De numeriske simuleringene ga god overenstemmelse med resultatene fra eksperimentene. Det var dog en viss forskjell. Styrken i de numeriske modellene, spesielt for modellene utsatt for kvasistatiske belastning, var noe redusert i forhold til de eksperimentelle resultatene. Resultatene tyder ikke på at det er behov for å endre formlene for dimensjonering i Eorocode.

Quasi-static and dynamic behaviour of fillet welded connections

Martin Flottorp Paus
Supervisors: Arild Holm Clausen and Erik Løhre Grimsmo
NTNU

December 20, 2016

Contents

1 Introduction

1.1 Background

Steel joints are usually minor parts in large constructions. However, the joints determines much of the behaviour and cost of the entire construction. Understanding the behaviour of the joints in a construction is therefore crucial for structural engineers. In fact, the behaviour of steel joints exposed to static loading is well documented. The design codes for joints in steel structures today are based on static conditions [15]. Steel joints exposed to impact loading has received limited attention in literature. After the attack on the World Trade Center in 2001 however, the interest in steel structures and joints under extreme conditions has grown.

1.2 Purpose of the study

Welded connections are among the most common steel joints. Welds are used in many different structures such as offshore platforms, bridges, cars, office buildings, etc. The purpose of this study was to observe and explain how fillet welded joints respond to impact and compare it to their response to quasi-static loading. To do this, two different component specimen types were tested, one with component test with transverse fillet welds and one with longitudinal fillet welds. Each component specimen type was tested with both impact and quasi-static loading for comparison.

Another goal of this study was to be able to create representative numerical final element models of both the quasi-static and the dynamic component tests used in the experiments. To be able to do this in a satisfying manner, material tests of the base and weld materials were carried out and the extracted material properties were inserted into the numerical models.

A final purpose of this study was to compare the results from the experiment and the numerical simulations with calculations of the strength in the different component tests according to the regulations in Eurocode.

This study has been carried out in collaboration with PhD candidate Erik L. Grimsmo. Grimsmo has previously carried out related studies regarding other types of steel joints [1–3].

2 Theory

2.1 Direction of fillet welds

A fillet weld can be loaded at any angle between 0° and 90° relative to the orientation of the weld. The behaviour of the weld during deformation is greatly dependent on the direction of the weld [5]. A fillet weld normal to the force applied is stronger and less ductile than a fillet weld parallel to the force applied.

2.2 Direction method for fillet welds in Eurocode [16]

There are two methods described in the Eurocode for designing the resistance of welded joints. The two methods are called the direction method and the simplified method. Of the two methods, the direction method gives the most realistic results [4] and is therefore used in this thesis. The simplified method is also allowed to use because the results will always be equal or more conservative than the results from the direction method.

With the direction method, the forces applied on the weld need to be decomposed into the stresses illustrated in Figure 2.1:

- $\sigma_\perp$ is the normal stress perpendicular to the throat.
- $\tau_\perp$ is the shear stress component (in the plane of the throat) perpendicular to the axis of the weld.
- $\tau_\parallel$ is the shear stress component (in the plane of the throat) parallel to the axis of the weld.

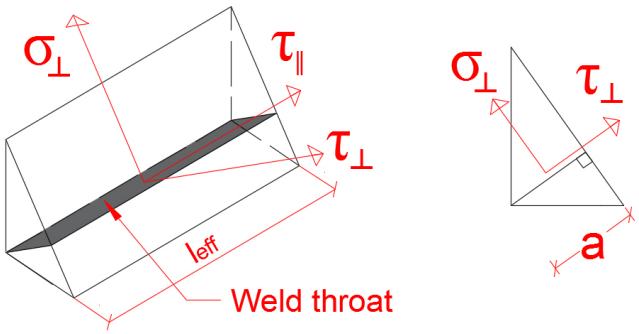

Figure 2.1: Decomposed stresses for the direction method

The design resistance of the fillet weld will be sufficient if the following are both satisfied:

$$\sqrt{\sigma_{\perp}^2 + 3(\tau_{\perp}^2 + \tau_{\parallel}^2)} \leq \frac{f_u}{\gamma_{M2} \cdot \beta_w} \tag{2.1}$$

and

$$\sigma_{\perp} \leq 0.9 \frac{f_u}{\gamma_{M2}} \tag{2.2}$$

where:

- $\gamma_{M2} = 1.25$ is a partial safety factor [17].
- f_u is the nominal ultimate tensile strength of the weaker part joined.
- β_w is a correlation factor and is found in Table 2.1.

Table 2.1: Correlation factor β_w for fillet welds [18]

Steel grade	f_u (N/mm^2)	β_w
S 235	360	0.8
S 275	430	0.85
S 355	510	0.9
S 420	520	1.0
S 460	540	1.0

2.2.1 Resistance of transverse fillet welds

A fillet weld normal to the force applied is only subjected to normal stress and normal shear stress, hence $\tau_{\parallel} = 0$. Assuming fillet welds with equally sized legs, so that the angle between the throat direction and the direction of the force is 45°, the stress components are equal.

$$\sigma_{\perp} = \tau_{\perp} = \frac{F}{\sqrt{2} \cdot A_{w,tot}} \tag{2.3}$$

where F is the force applied and $A_{w,tot}$ is the total area of the weld throat. The criterion from (3.1) gives

$$\sqrt{\sigma_{\perp}^2 + 3\tau_{\perp}^2} = \sqrt{1+3} \cdot \frac{F}{\sqrt{2} \cdot A_{w,tot}} = \sqrt{2} \cdot \frac{F}{A_{w,tot}} \leq \frac{f_u}{\gamma_{M2} \cdot \beta_w} \tag{2.4}$$

$$F_{max} = \frac{f_u \cdot A_{w,tot}}{\sqrt{2} \cdot \gamma_{M2} \cdot \beta_w} \tag{2.5}$$

2.2.2 Resistance of longitudinal fillet welds

A fillet weld parallel to the force applied is only subjected to parallel shear stress, hence $\tau_\perp = \sigma_\perp = 0$.

$$\tau_\parallel = \frac{F}{A_{w,tot}} \tag{2.6}$$

The criterion from (3.1) gives

$$\sqrt{3\tau_\parallel^2} = \sqrt{3} \cdot \frac{F}{A_{w,tot}} \leq \frac{f_u}{\gamma_{M2} \cdot \beta_w} \tag{2.7}$$

$$F_{max} = \frac{f_u \cdot A_{w,tot}}{\sqrt{3} \cdot \gamma_{M2} \cdot \beta_w} \tag{2.8}$$

3 Experimental set-up and method

Two different specimen types were produced, both in steel S355, one specimen with only transverse fillet welds, and the other with only longitudinal fillet welds. The specimens were assembled with shielded metal arc welding using stick electrodes of the type Elga P47 with nominal yield stress of 460 MPa.

3.1 Component test specimens

Both types of the component test specimens were made of two parallel plates welded to a block. The upper plate was welded to the upper side of the block, and the lower plate was welded to the lower side of the block. The main difference in the two specimen types was the weld orientation. One specimen type had transverse fillet welds and the other had longitudinal fillet welds, relative to the direction of the applied force.

3.1.1 Transverse fillet welds

Figure 3.1 gives an illustration of the specimen with transverse fillet welds. The force was applied to the specimen at the backside of the block, see Figure 3.1c, so the direction of the force was from the back to the front of the test specimen. The two transverse fillet welds, joining the plates to the block, were 60 mm long each and had a 4 mm thick throat.

3.1.2 Longitudinal fillet welds

Figure 3.2 illustrates the second test specimen type with four fillet welds joining the plates to the block. All the welds were parallel to the force direction, going back to front. To be able to weld in that direction, it was necessary to produce the plates with a small rectangular opening over and under the block. Each of the four fillet welds were 30 mm long and had a 4 mm thick throat.

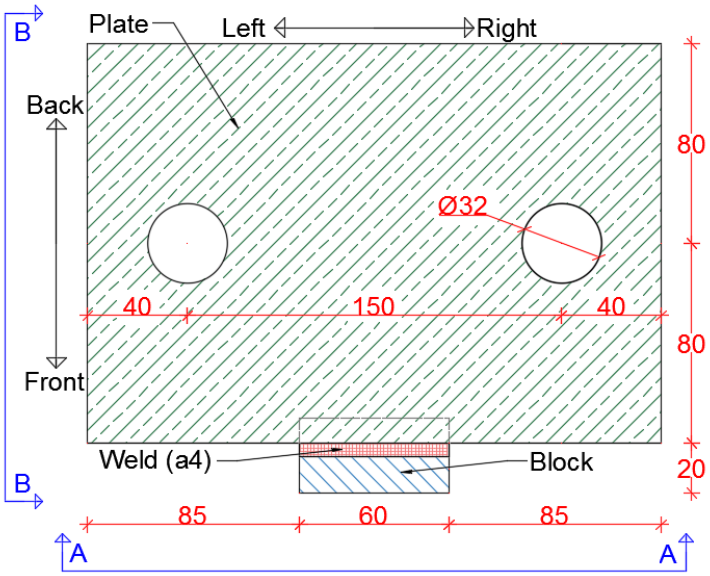

(a) Upper view

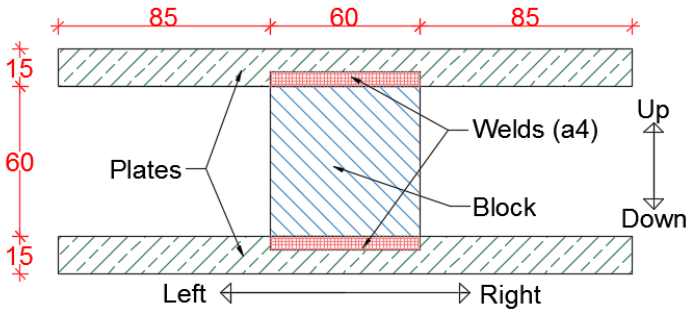

(b) Section A-A

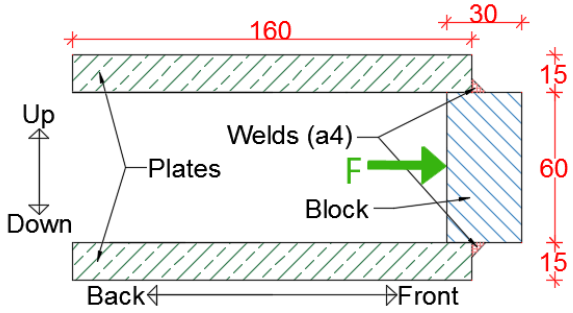

(c) Section B-B

Figure 3.1: Test specimen with transverse welds

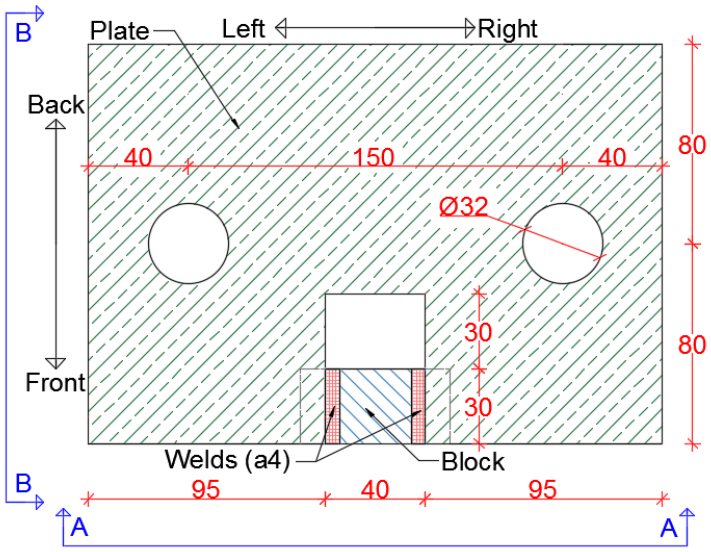

(a) Upper view

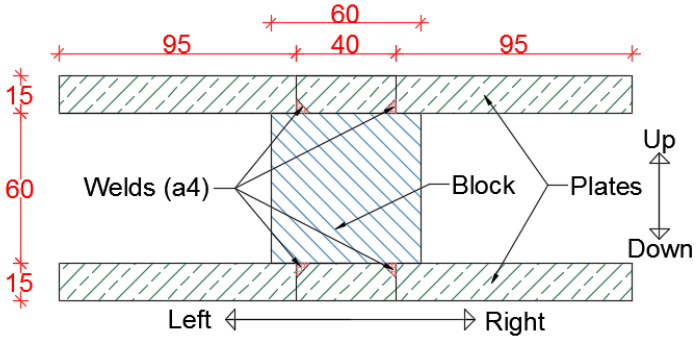

(b) Section A-A

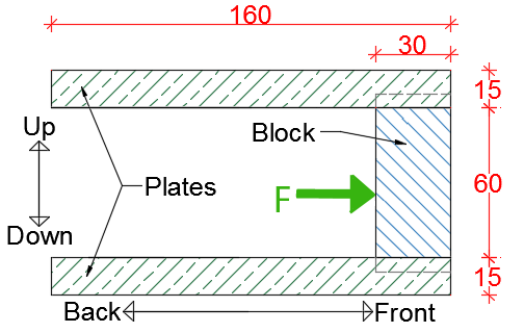

(c) Section B-B

Figure 3.2: Test specimen with longitudinal welds

3.2 Experimental program

The test specimens employed in the quasi-static and dynamic tests were labelled *QS* and *DYN*, respectively. The test specimens with longitudinal fillet welds were labelled with *L*, and the test specimens with transverse fillet welds were labelled with *T*. The replicates within each series were labelled with consecutive numbers *01*, *02* etc. From the example in Figure 3.3, *QS T 02* was the second quasi-static test with transverse fillet welds, while *DYN L 01* was the first dynamic test with longitudinal fillet welds.

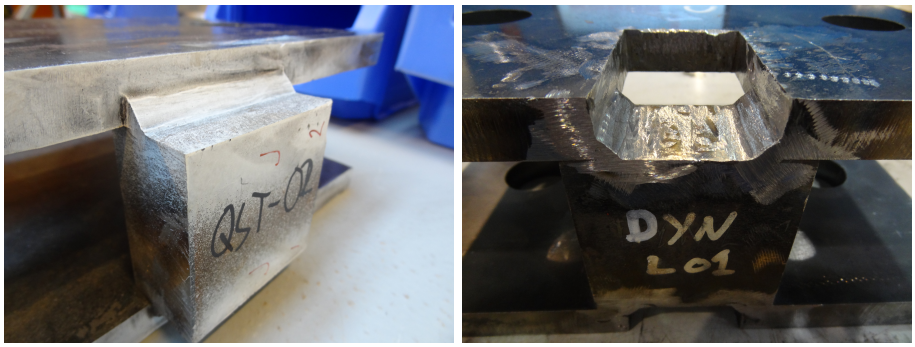

(a) Test specimen with transverse fillet welds

(b) Test specimen with longitudinal fillet welds

Figure 3.3: The two test specimen types

A total of twenty specimens, ten of each specimen type, were successfully tested during this study. In addition, one test specimen was used for material testing. Five samples of each specimen type were tested under quasi-static load conditions, whereas the other five samples were subjected to impact loading.

Table 3.1: Number of successful component tests

Weld type	Quasi-static tests	Dynamic tests (impact velocity $\approx$ 2 m/s)
Transverse	5 *(0.4 mm/min)*	5
Longitudinal	5 *(0.6 mm/min)*	5

3.3 Set-up

3.3.1 Nose

A circular end plate and a solid cylinder create the nose, see Figure 3.4. The nose was used to inflict a force on the test specimen. To create this force the nose was pushed into the block, indicated with the letter *F* in Figure 3.1c and 3.2c, so that deformation and eventually fracture of the welds occurred.

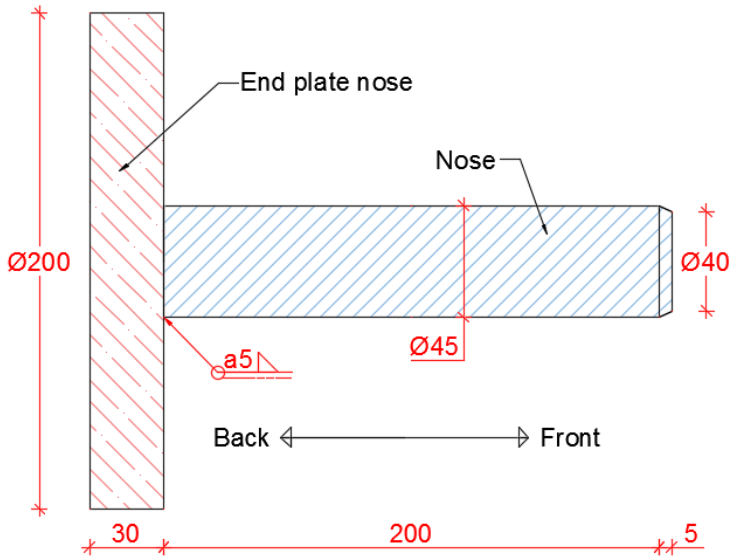

Figure 3.4: Nose

The nose cylinder was 200 mm long and had a diameter of 45 mm. In the last 5 mm in the free end of the cylinder, the diameter narrowed down from 45 mm to 40 mm. The cylinder was welded concentric to the end plate, and the end plate was bolted to the moving part of the test machine. Four strain gauges were attached evenly around the nose 135 mm from its free end. They registered the elastic deformation in the nose and could also monitor possible bending in the nose.

3.3.2 Fixture

The test specimens were mounted to the test machines with the fixture depicted in Figure 3.5. The fixture was made of a rectangular end plate and two thick beams. The two beams were welded to the end plate like cantilever beams. The beams were 250 mm long. At a distance of 170 mm from the fixed end, it was created a vertical hole with 32 mm diameter in each beam. The purpose of these holes was to bolt the specimens to the fixture. Also a horizontal hole, going left to right, was made in the two beams 100 mm from the fixed end. The purpose of these holes was to get a better view of of the deformations during the tests. The end plate of the fixture was fixed to the quasi-static or dynamic test machine with bolts.

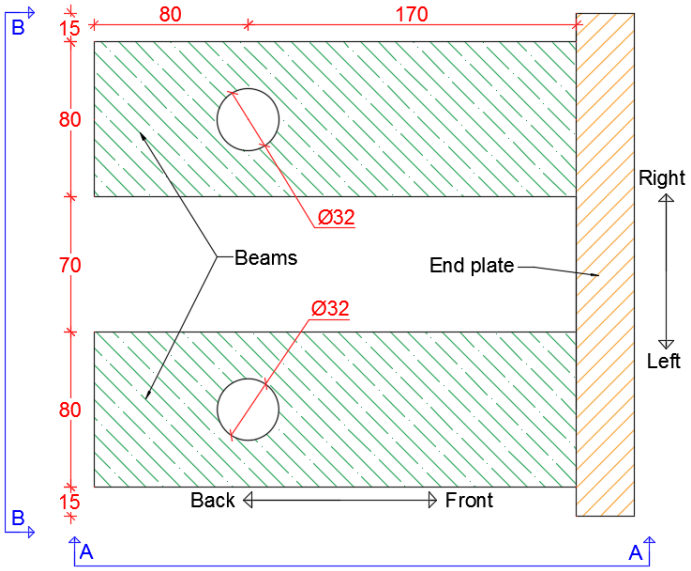

(a) Upper view

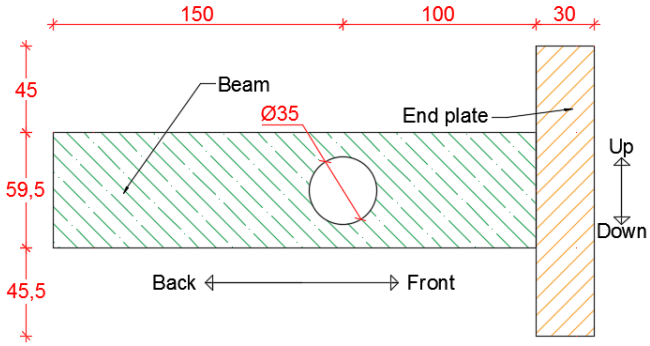

(b) Section A-A

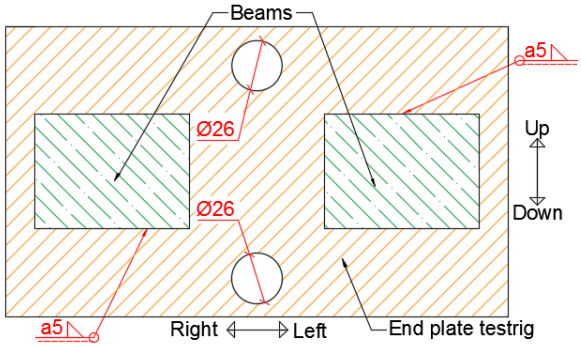

(c) Section B-B

Figure 3.5: Fixture

3.3.3 Bolts

Bolts were used to fix the component test specimens to the fixture. Bolt number 1, see Figure 3.6, was used in nearly all the tests. Inside the holes in the upper plates, the bolts were unthreaded and they had a smooth contact surface against the plate holes. In the lower plates on the other hand, when using bolt number 1, the threads on the bolts caused an irregular contact surface between the bolts and the plates. The total contact area was smaller between the bolts and the lower plate holes than for the upper plate holes. This could cause increased stress and possibly unwanted plastic deformations in the lower plates, which would create asymmetry in the component test specimen. Besides, the plastic deformation in the plate would absorb energy that was supposed to go to the deformations of the welds.

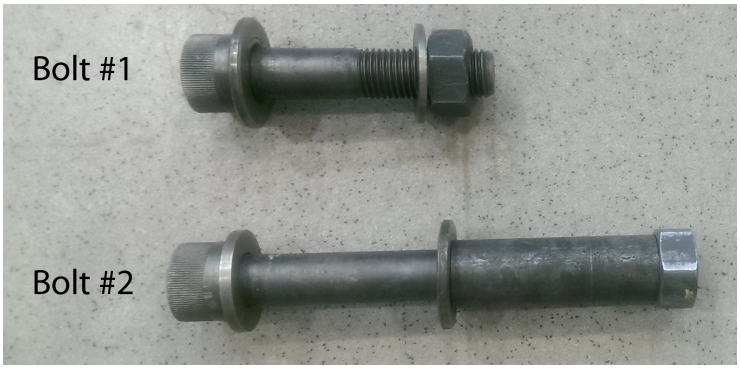

Figure 3.6: The two different bolts used

Bolt number 2 was long enough to avoid bolt threads in the plate holes. Unfortunately, only two component tests were tested with bolt number 2, one quasi-static component test specimen with transverse fillet welds and one quasi-static component test specimen with longitudinal fillet welds. All the other component test specimen were tested with bolt number 1. How important this was for the final results is discussed further in Sectinon 8.

3.4 Quasi-static test set-up

A standard hydraulic tension/compression test machine was used for the quasi-static tests. The nose was bolted to a the moving part in the test machine. The fixture was fixed in the opposite side of the machine, and the test specimen was bolted to the fixture, see Figure 3.7. The bolts used to fasten the test specimen were finger-tightened to avoid too much friction between the test specimen and the rig. The nose was led down towards the block to make sure that the contact between the nose and the block was as plane as possible. For the test specimen

with transverse fillet welds, the holes on the sides of the fixture was used to observe the contact between the nose and the block. For the test specimen with longitudinal fillet welds, this was observed directly from the upside or underside of the test specimen.

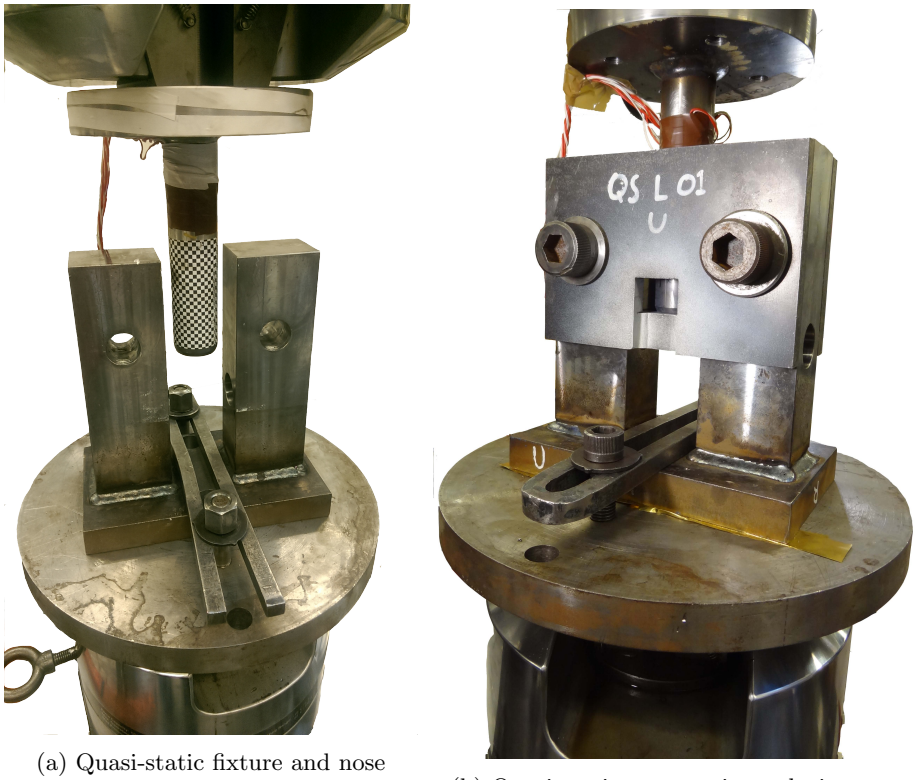

(a) Quasi-static fixture and nose before inserting the test specimen

(b) Quasi-static test specimen during test

Figure 3.7: Quasi-static test rig

When the test specimen was in place, two cameras were set up to acquire images of the fillet welds on both sides of the block. The images in Figure 3.11 are examples of images taken by these cameras. The cameras were synchronised to the tension/compression machine, so that they recorded data at the same time with a rate of 1 Hz. The nose was pushed into the block with a constant speed until the fillet welds fractured. The speed of the nose was set to 0.4 mm/min for the QS L component tests and 0.6 mm/min for the QS T component tests.

3.5 Dynamic test set-up

In the dynamic test, the nose was mounted to the front of a trolley in a machine used for impact tests, see Figure 3.8a. The total mass of the trolley including the nose was 1440 kg. The trolley was rolling on rails with a given velocity and impacted the test specimen to fracture the fillet welds. The test specimen was bolted to the fixture which was fixed to an end wall of the machine as shown in Figure 3.8b. Aluminium buffers were set up to stop the trolley after the impact with the test specimen. These buffers deform and absorb energy to avoid damage on the fixture, the wall and the trolley. The bolts between the test specimen and the fixture were finger-tightened as it was done in the quasi-static tests. Before starting the test, the trolley was slowly brought to the test specimen to control the contact plane between the nose and the block. The visual control was the same as for the quasi-static tests.

(a) Trolley with nose

(b) fixture with test specimen and aluminium buffers on the sides

(c) Dynamic test machine

Figure 3.8: Dynamic test set-up

Two high-speed cameras monitored the dynamic tests. As for the quasi-static tests, one camera was placed above the test specimen to track the block and welds on the upper side while the other camera was placed below to track the block and welds from the underside. The cameras were set to capture images at a frequency of 30 kHz. Figure 3.9 illustrates the views from the two cameras. The trolley was accelerated to about 2 m/s and was crashed into the test specimen to fracture the welds with an impact. Closely before the impact with the test specimen, the trolley passed two photocells with a distance Δd = 250 mm from each other. The time of the passing trolley was registered in both photocells. In this way the initial velocity v_0 of the trolley for each dynamic component test was calculated as

$$v_0 = \frac{\Delta d}{\Delta T} \tag{3.1}$$

where ΔT is the time interval between the two photocells. The load from the impact was measured from the strain gauges on the nose just as for the quasi-static tests. The load registration frequency was 250 kHz.

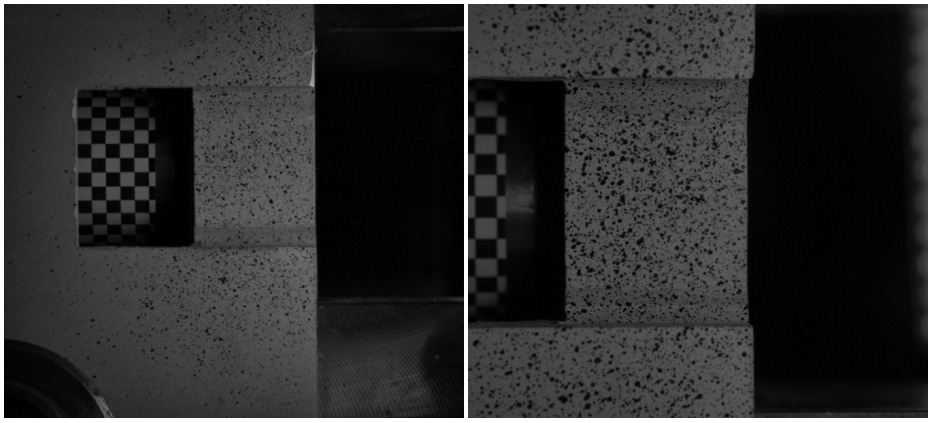

(a) Image from above (b) Image from below

Figure 3.9: Example of images taken during the dynamic tests. These images are from the test specimen with longitudinal fillet welds

3.6 Data acquisition

3.6.1 DIC - digital image correlation

DIC is a method to optically register displacements or deformations in 2D or 3D using a series of digital images. Before starting the deformations in the experiment, the test specimen is first painted white before a black spray pattern is added. The black pattern is made out of small dots with different sizes which is randomly distributed over the test specimen. In this way, every part of the test specimen is visually unique.

During the deformations of the test specimen, images are captured with a fixed time interval. The first image in this series is defined as the undeformed state of the test specimen. A grid with relatively small elements is created for this first image. An example of this is illustrated in Figure 3.10a. Each element in the grid will contain a random pattern with different amount of black and white. This makes it possible for the DIC-software to recognize and track each element and its deformations from one image to the next, as long as the deformations are small enough between the two images.

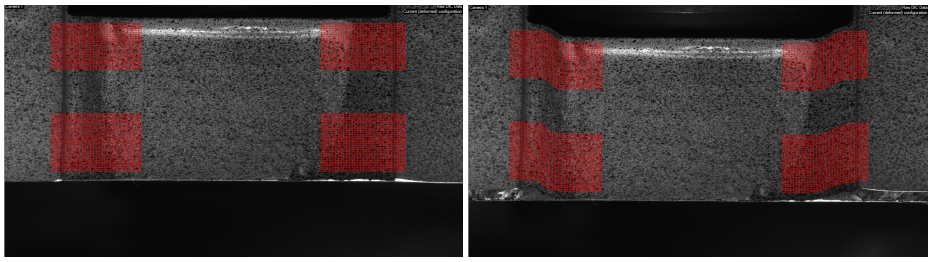

(a) Undeformed mesh in DIC, frame 1 (b) Deformed mesh in DIC, frame 422

Figure 3.10: Painting and mesh in DIC

3.6.2 Procedure

In this study the test specimens were painted white and sprayed with a black dot spray. The size of the black dots varied over the test specimen to uniquely define different elements in the test specimen. The DIC-software eCorr v4.0(2016) [19], developed by researcher Egil Fagerholt at NTNU, was used to track the deformations from the image series.

With the combined use of a camera taking photos at a given frame rate and a DIC-software, it was possible to obtain a good estimation of the time-displacement curves of selected points in the tests, see Figure 3.11. Subtracting the displacement in one point from the displacement in another made it possible to get the relative displacement between the two points. Measuring the displacement in two points on each side of the welds, one point on the block

and one on the plate, it was possible to get a relative deformation in the weld between those two points.

The yellow dots in Figure 3.11 mark the positions of the selected points where the displacements were tracked using DIC. The four letters symbolises the directions in the image. The points were selected in pairs with one point on each side of the welds. In this way it was possible to get an estimation of the relative displacement of the block relative to the plate. The transverse fillet welds had 3 point pairs named *left*, *mid* and *right*. The longitudinal fillet welds had 4 point pair named *BL*, *BF*, *BR* and *FR* using the four letters in the figure.

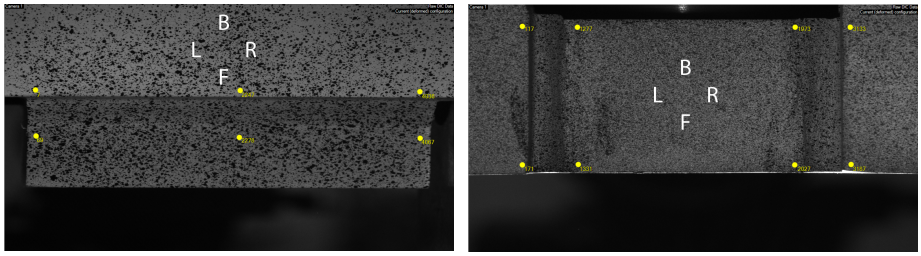

(a) Transverse fillet welds (b) Longitudinal fillet welds

Figure 3.11: Two examples of images used in DIC

The force applied to the test specimen was also registered during the experiment. Deformation in the nose, registered by the strain gauges, was converted into force assuming only elastic deformation in the nose. In addition to the strain gauges, the quasi-static test machine had a built-in load cell. This was used as a quality control of the forces registered with the strain gauges. For the dynamic tests, only the strain gauges were available.

3.6.3 Procedure example, QS T 02

As mentioned, for the component tests with transverse fillet welds, three pairs of points were tracked on the upside, and another three pairs of points were tracked on the underside of the component test specimen. Figure 3.11a illustrates the location of the three pair of points on the upside of a component test specimen. The location of the points was similar on the underside.

By tracking the points in time, both from the upside and the underside, the graphs in Figure 3.12 were created. There is an evident distinction between the displacement of the points on the plates and the displacement of the points on the block. This is caused by the deformations of the welds. Subtracting the displacement of the points on the plates from the displacement of their respective point pair on the block, the relative displacement of each point pair was obtained. This is illustrated in Figure 3.13.

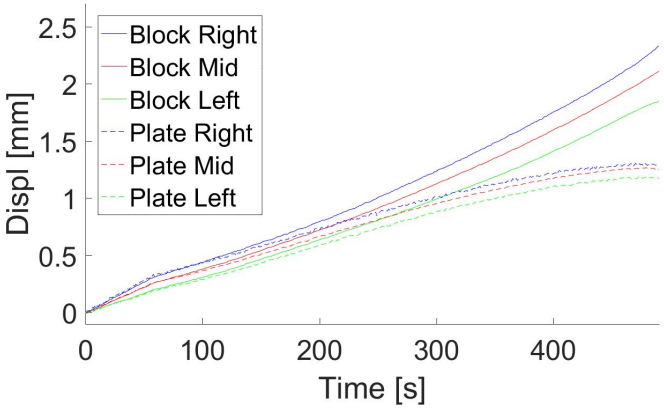

(a) QS T 02, point displacement, up

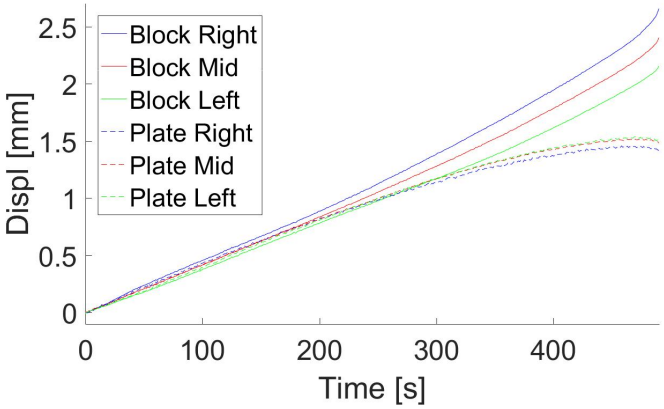

(b) QS T 02, point displacement, down

Figure 3.12: QS T 02, point displacement

Comparing the loads measured in the strain gauges with the load from the the test machine, it was possible compare the results and validate the use of the strain gauges. In the dynamic tests, the load were measured only with strain gauges. The load from the strain gauges and the machine gave very similar results, see Figure 3.14. This was the case for all the tests, and hence the load from the strain gauges was reliable and could be trusted in the dynamic tests. The mean loads from the strain gauges were used as the representative loads for this study.

Merging the relative displacement curves with the load curves, the load-displacement curves were created. The graphs in Figure 3.15 were calculated from the mean relative displacement of certain point pairs. The curve named *Right* for example is the mean relative displacement of the right point pair from

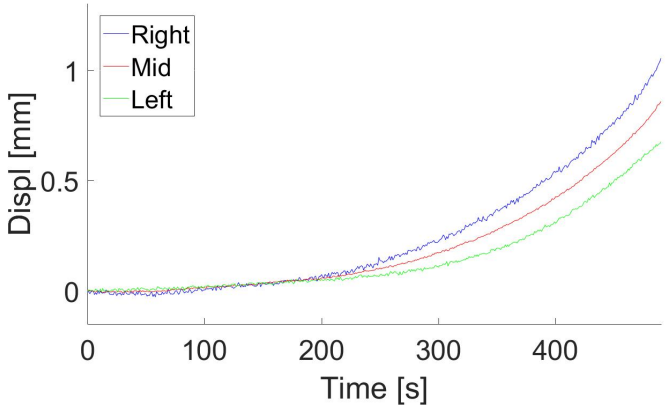

(a) Q ST 02, relative displacement, up

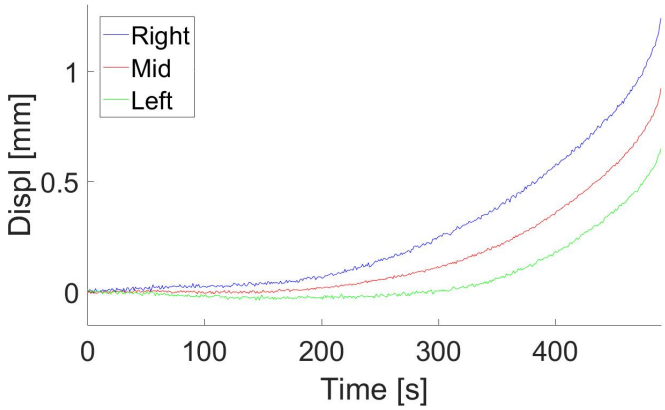

(b) QS T 02, relative displacement, up

Figure 3.13: QS T 02, relative displacement

the upside and the right nod pair from the underside. Similar calculations were made for the curves *Left*, *Up* and *Down*, while *Mean* was the mean relative displacement of all the six point pairs.

The *Mean* curve is the most relevant curve, and it is therefore the main result from the of the component tests. Assuming an ideal test specimen with perfect symmetry, the *Mean* curve would describe the whole response in the test specimen. However, the other curves in Figure 3.15 give information about possible unwanted rotations of the block relative to the plates. For this particular component test, it is possible to notice a clear left/right rotation, and also a small up/down rotation. The left/right rotations varied seemingly randomly for the the different tests. The up/down rotations on the other hand are discussed further in Section 8.

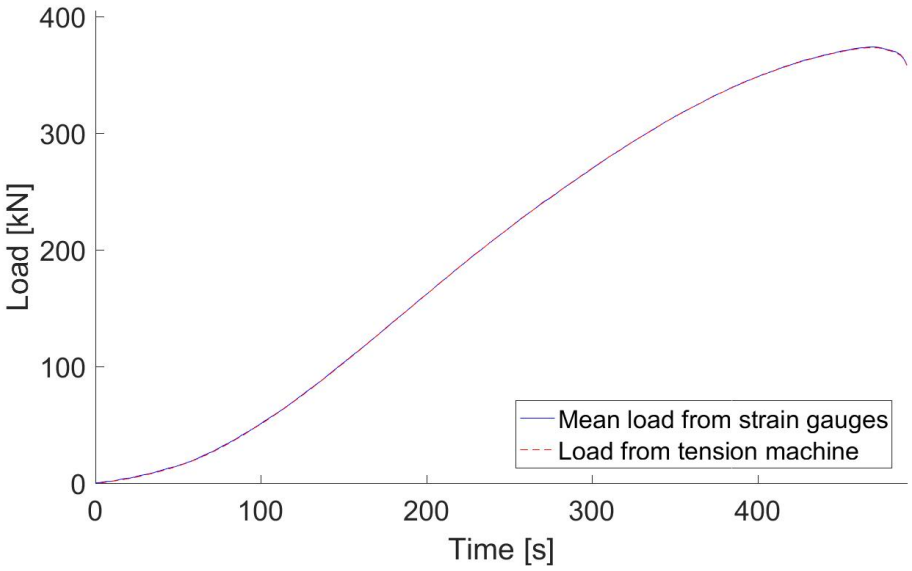

Figure 3.14: QS T 02, load

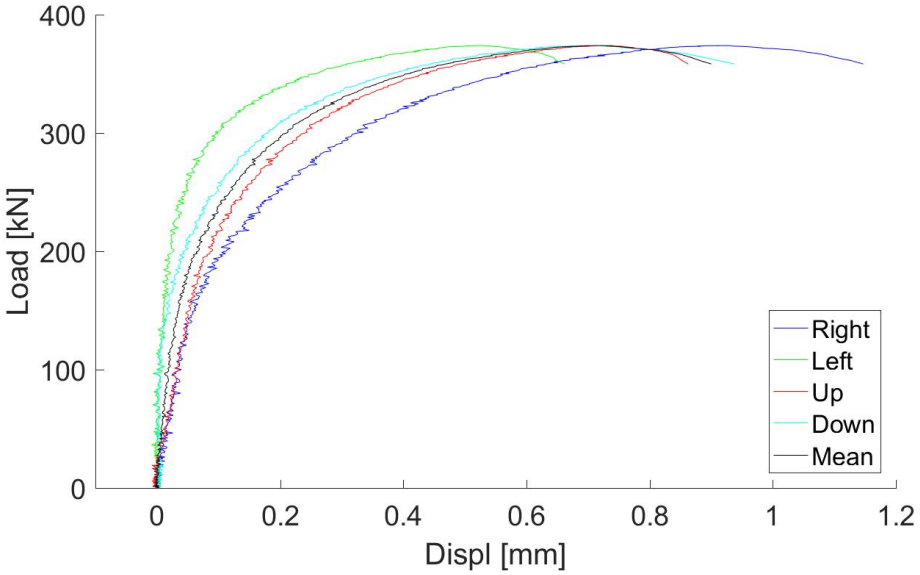

Figure 3.15: QS T 02, load - mean relative displacement

4 Experimental results

4.1 Quasi-static tests

4.1.1 Transverse fillet welds

Five successful tests were carried out with the QS T components, see Figure 4.1. QS T 01 was not successful however, and is therefore left out of this paper. Notice also that QS T 06 was tested with different bolts according to Section 3.3.3.

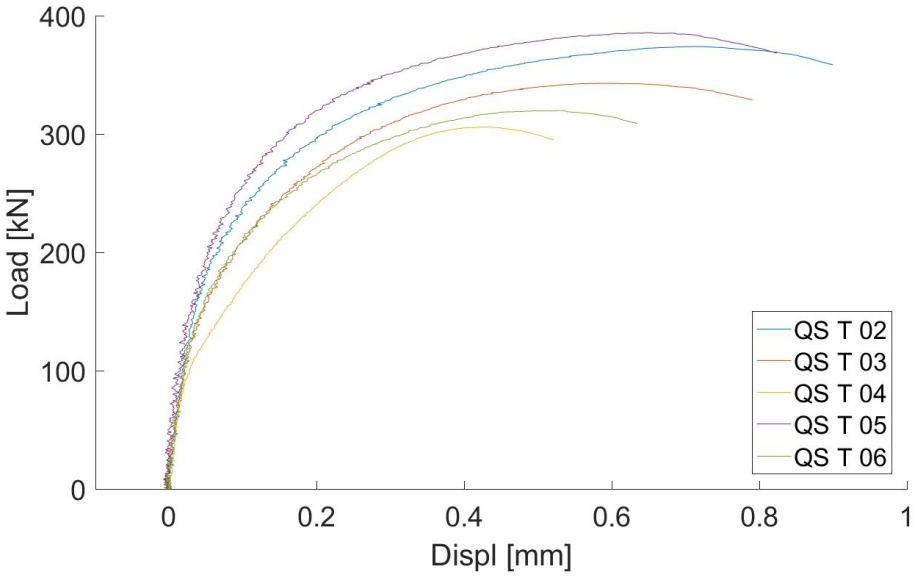

Figure 4.1: Load-mean relative displacement for QS T

According to Table 4.1, there was a clear scatter in the maximum loads measured in the QS T component tests. The standard deviation of the measured maximum loads was 30.5 kN, which is about 9% of the mean value. The QS T component test with the lowest maximum load, QS T 04, had a maximum load of about 79 kN lower than the test specimen with the highest maximum load, QS T 05. There was also a significant difference in the deformation capacity of these tests. A standard deviation of 0.14 mm represents about 19% of the mean value. Further, according to the same table, the size of the welds in the QS T component tests were rather consistent. However, the mean value of the measured throat size of these component tests was 0.4 mm larger than anticipated.

Table 4.1: Max load, mean relative displacement at fracture and mean throat measure in the QS T component tests

	QST02	QST03	QST04	QST05	QST06	Mean	SD
Max load [kN]	374	343	306	385	320	346	30.5
Displ. [mm]	0.90	0.79	0.52	0.82	0.63	0.73	0.14
a [mm]	4.6	4.4	4.4	4.3	4.2	4.4	0.13

4.1.2 Longitudinal fillet welds

The procedure for the QS L component tests was similar to the QS T component tests only with different points in the DIC tracking. Eight pair of points were tracked with DIC. Four of the point pairs were on the upside of the component test specimen, as illustrated in Figure 3.11b, and the other four pairs of points were on the underside. Five successful tests were preformed with the QS L components, see Figure 4.2. Notice that QS L 05 was tested with different bolts, according to Section 3.3.3.

The maximum loads measured in the QS L component tests, presented in Table 4.1, were less scattered than for the QS T component tests. The standard deviation of the maximum load measured in the QS L component tests was only 7.3 kN, which represents about 3% of the mean value for the QS L component tests. The lowest maximum load measured in the QS L component tests, from QS L 01, was only about 20 kN lower than the highest maximum load, from QS L 05. The deformation capacity of the QS L component tests were higher than for the QS T component tests. The QS L component tests had a standard deviation for the relative displacement at fracture of 0.4 mm, which is about 15% of the calculated mean value.

The size of the welds for these test had a mean throat size of 4.0 mm, which was as anticipated. The variations in the weld size was also small. The throat sizes of the QS L 01, Dyn L 01 and Dyn T 01 component tests were measured using a welding gauge. All the other other component tests were measured with a more reliable CMM machine. The two measuring methods gave very different results and therefore the throat sizes measured for the mentioned component tests were not considered when calculating the mean value and the standard deviation. The measured throat size of these component tests is still presented in the tables, but marked with a star to illustrate that they were not further considered.

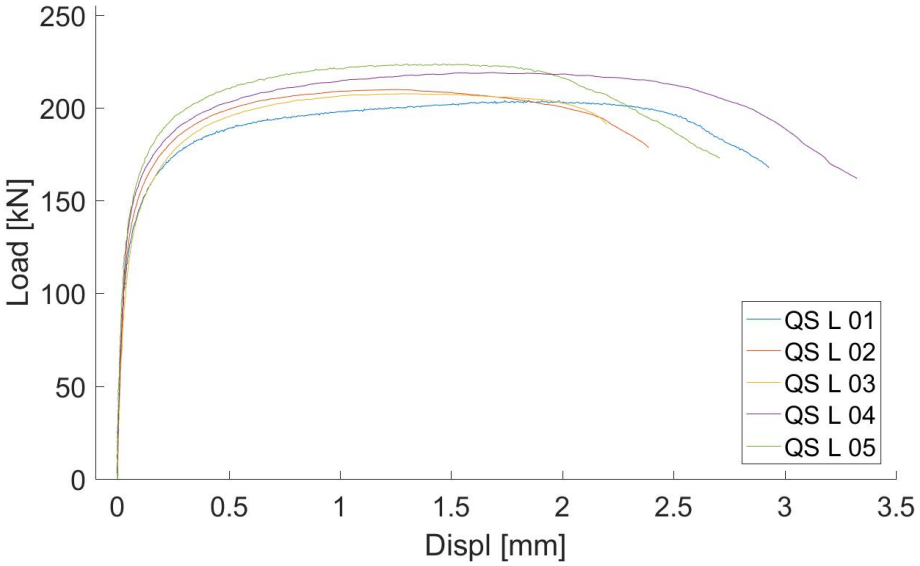

Figure 4.2: Load-mean relative displacement for QS L

Table 4.2: Max load, mean relative displacement at fracture and mean throat measure in the QS L component tests

	QSL01	QSL02	QSL03	QSL04	QSL05	Mean	SD
Max load [kN]	204	210	208	219	224	213	7.3
Displ. [mm]	2.93	2.39	2.20	3.33	2.71	2.71	0.40
a [mm]	3.2 *	4.0	4.1	4.1	4.0	4.0	0.04

4.2 Dynamic tests

4.2.1 Transverse fillet welds

Five successful tests were preformed with the Dyn T component tests, see Figure 4.3. The procedure for registration and calculations of the results for the Dyn T component tests was the same as for the QS T component tests, explained in Section 3.6.3. During the Dyn T 01 component test, only the camera from above was used. Therefore only the three point pairs on the upper side of that component test specimen were tracked.

The maximum loads of the Dyn T component tests had some spread, according to Table 4.3. The standard deviation of the maximum loads measured in the Dyn T component tests were 22.5 kN. That is about 6% of the mean value. The lowest maximum load measured, from Dyn T 05, was only about 56 kN lower than the highest maximum load, from Dyn T 02. Notice also that the mean maximum load for the Dyn T component tests is about 24 kN higher

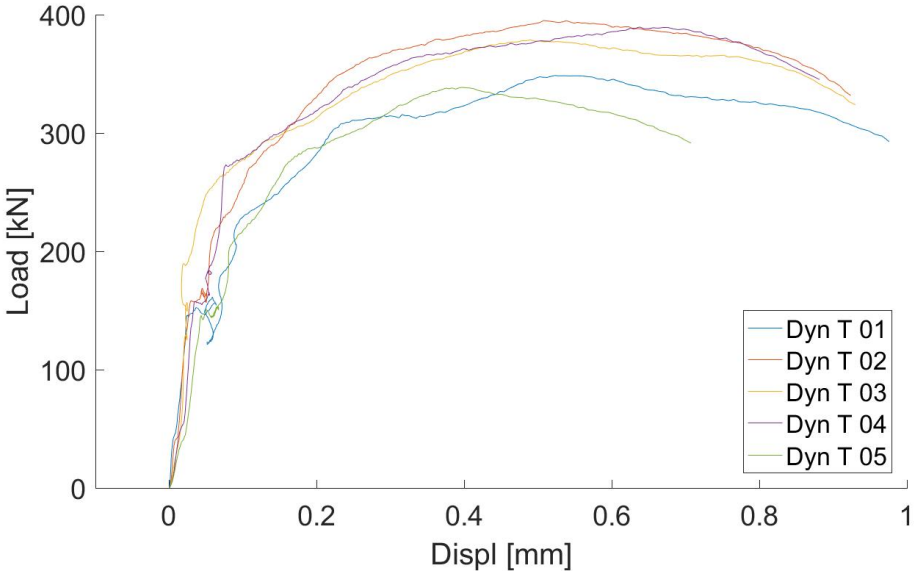

Figure 4.3: Load-mean relative displacement for Dyn T

than that for the QS T component tests. That is an increase in mean maximum load of about 7%. The standard deviation of the mean relative displacements for the Dyn T component tests was 0.09 mm, which is about 10% of the mean value. Further, the measured throat sizes of the Dyn T component tests varied a great deal, giving a standard deviation of about 0.3 mm.

With increasing velocities of the trolley before impact, the strain rate in the welds would increase the hardening causing higher stress levels. At the same time, increasing the strain rate would cause increased thermal softening causing a reduction in the stress. Therefore, to have comparable results it was important to have similar initial velocities of the trolley before the impacts. The initial velocities for the Dyn T component tests were quite similar with a mean value of 2453 mm/s. The standard deviation was only 35.4 mm/s which is about 1.4% of the mean value. The test specimen with the highest initial velocity was Dyn T 04, and the test specimen with the lowest inital velocity was Dyn T 02. Note that the results in Figure 4.3 for these two tests are very similar.

Table 4.3: Max load, mean relative displacement at fracture, mean throat measure and initial speed of trolley in the Dyn T component tests

	DynT01	DynT02	DynT03	DynT04	DynT05	Mean	SD
Max load [kN]	349	395	379	390	338	370	22.5
Displ. [mm]	0.98	0.92	0.93	0.88	0.71	0.88	0.09
a [mm]	3.9 *	4.4	4.6	4.2	3.8	4.2	0.30
v_0 [mm/s]	2440	2393	2475	2497	2461	2453	35.4

4.2.2 Longitudinal fillet welds

Five successful tests were preformed with the Dyn L component tests, see Figure 4.4. The procedure for registration and calculation of the results for the Dyn L component tests were the same as for the QS L component tests, explained in Section 4.1.2 during the Dyn L 01 component test, only the camera from above was used. Hence only the four point pairs on the upper side of that component test specimen were tracked. Further, a technical error occurred during the Dyn L 02 tests. The data registration did not start as planned, hence there were no images nor forces registered for the test. The Dyn L 02 component test was therefore not considered.

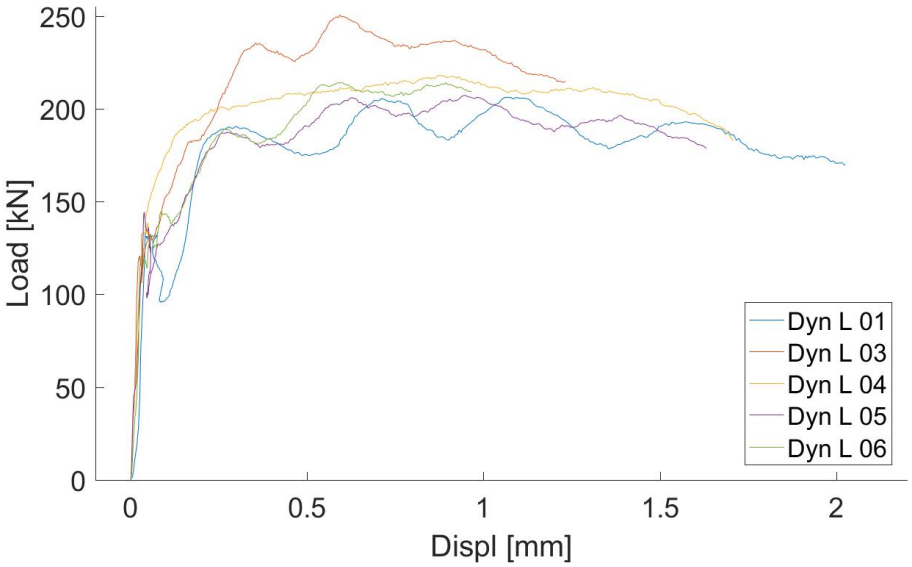

Figure 4.4: Load-mean relative displacement for Dyn L

The maximum loads of the Dyn L component tests had some variations, according to Table 4.4. The standard deviation of the Dyn L component tests was 16.2 kN, which represents roughly 7% of the mean value. The lowest max load measured in the Dyn L component tests, from Dyn L 05, was only about 44 kN lower than the highest max load, from Dyn L 02. The mean maximum load for the Dyn L component tests was very similar to that for the QS L compoent test. In fact the former was only about 6 kN bigger, which is an increase of nearly 3% from the quasi-static to the dynamic version of the component tests with longitudinal welds.

The standard deviation of the mean relative displacements for the Dyn L component tests was 0.37 mm, which is about 25% of the mean value. The variation in the throat size was rather small and the mean value of the throat sizes was as expected.

Table 4.4: Max load, mean relative displacement at fracture, mean throat measure and initial speed of trolley in the Dyn L component tests

	DynL01	DynL03	DynL04	DynL05	DynL06	Mean	SD
Max load [kN]	206	250	218	207	214	219	16.2
Displ. [mm]	2.03	1.23	1.71	1.63	0.97	1.51	0.37
a [mm]	3.0 *	4.2	4.1	3.9	4.0	4.0	0.08
v_0 [mm/s]	2434	2211	2356	2356	2405	2353	76.6

The variation of the initial velocities of the trolley was bigger for the Dyn L component tests than for the Dyn T component tests. The mean initial volocity was 2353 mm/s. This is about 100 mm/s slower than the mean value for the Dyn T component tests. The standard variation is 76.6 mm/s which constitutes about 3.3% of the mean value. However, the the variations in the trolley velocities still were relatively small. It was therefore assumed that the measured variations in the trolley velocities did not have any significant influence to the experimental results. The test with the biggest deviation from the mean value in the initial speed is Dyn L 03. An interesting remark is that the same test seems to de be deviating from the rest in the results in Figure 4.4. It is difficult to say whether this is an arbitrary coincidence without carrying out more tests.

5 Material tests

Material tests were performed to determine the mechanical properties of the different materials used. The material properties from the plates, the blocks and the welds were assumed to be different and therefore tested separately. The different materials were also tested under both quasi-static and dynamic conditions. Table 5.1 illustrates the number of successfully executed material tests.

Table 5.1: Number of successful material tests

	QS slow (0.007 mm/s)	QS fast (0.5 mm/s)	Dyn (SHTB)
Block	3	0	0
Plate	2	1	4
Weld	3	2	3

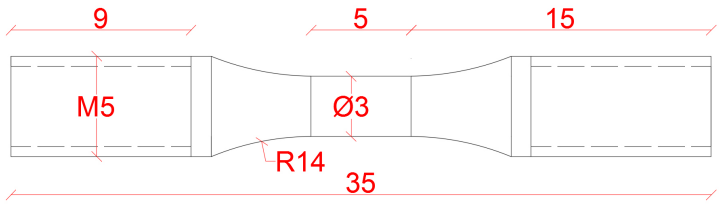

Figure 5.1: Material test specimens with dimensions in mm

Material test specimens for the plate and the block were machined from an unused component test specimen. The welds on the component test specimen were too small and could therefore not be used to create material test specimens. A larger weld was produced instead, see Figure 5.2a. This new weld was created as similar as possible to the welds in the test specimens, and the material test specimens for the welds were carved the center part of the big weld according to Figure 5.2b. All the material test specimens were machined as illustrated in Figure 5.1.

5.1 Quasi-static test set-up

A servohydraulic test machine was used for the quasi-static material tests. A lamp was set up to create a very bright background and a well defined contrast to the edge of the test specimen as shown in Figure 5.3. Assuming isotropy in the material tests, only one camera was used to capture the deformations during the tests. As for the component tests, series of images were taken with a given frame rate, see Table 5.2. The servohydraulic test machine tracked and registered the force during the tests.

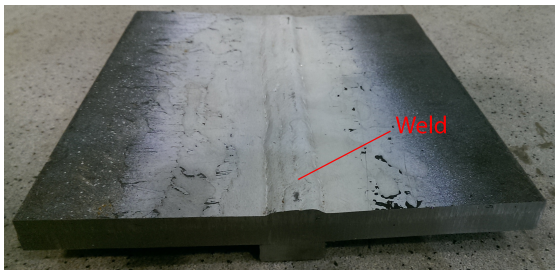

(a) The larger weld

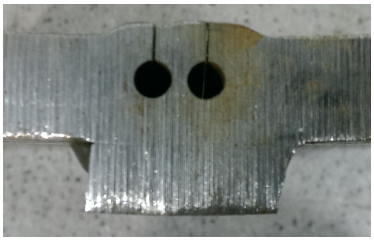

(b) Positions of the material test specimens

Figure 5.2: Weld for the material test

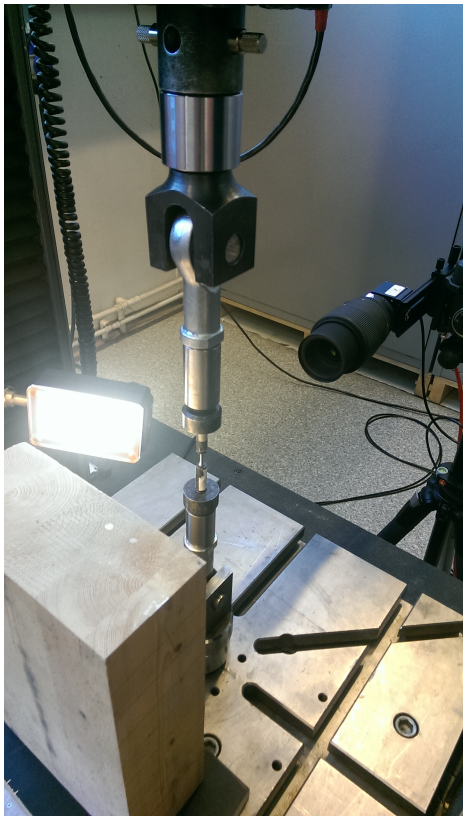

(a) The set-up

(b) Image from the camera during a material test

Figure 5.3: Quasi-static material tests

Table 5.2: Data logging frequency in material tests

	QS slow (0.007 mm/s)	QS fast (0.5 mm/s)	Dyn (SHTB)
Images	1 Hz	15 Hz	100 kHz
Load	1 Hz	15 Hz	1000 kHz

5.2 Dynamic test set-up, the split-Hopkinson tension bar

A split-Hopkinson tension bar (SHTB), see Figure 5.4a, was used to carry out the dynamic material tests [6, 7]. The material test specimen was attached in both ends, uniting two long bars, as illustrated in Figure 5.4b. Similar as for the quasi-static material tests, isotropy was assumed so that only one camera was needed and lamps were set up to give a well defined contrast for the material test specimen edge. The camera used in the dynamic tests was a high-speed camera capturing images at a frequency of 100 kHz.

(a) Split-Hopkinson tension bar

(b) The material test specimen was attached between two long bars

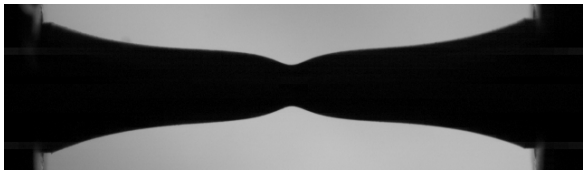

(c) Image taken during a split-Hopkinson test

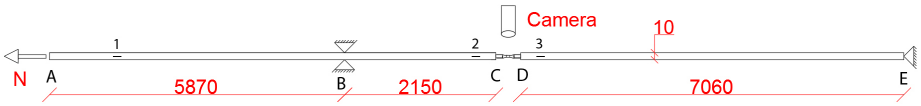

(d) Split-Hopkinson tension bar set-up

Figure 5.4: Split-Hopkinson tension bar

In point B in the Slit-Hopkinson tension bar, according to Figure 5.4d, there was a friction lock. This friction lock would, when activated, fix the bar at that point so it could not move longitudinally. After activating the friction lock, a force N was applied to point A to create tension in AB. Strain gauges were placed in the three places labelled *1*,*2* and *3* in the figure. The tension created in AB was monitored with the strain gauge *1*. The applied force N was not big

enough to cause plastic deformation in the bar, but it was more than sufficient to eventually cause fracture of the material test specimen.

When an appropriate level of tension was applied to AB, the lock in B was broken and the bar was suddenly free to move along its axis. This caused a propagating stress wave moving from AB to the rest of the bar and through the material test specimen, causing the material test specimen to fracture. The strain in *2* and *3* was registered with a frequency of 1000 kHz, making it possible to calculate the force applied to the material test specimen during the test.

5.3 Data acquisition

To calculate the material parameters, it was essential to calibrate the relation between the true strain and the true stress in the material tests. The true stress in a cross section, assuming that the stress is only in the longitudinal direction, is given as

$$\sigma_t = \frac{F}{A_t} \tag{5.1}$$

where F is the force applied, and A_t is the true area of the cross section, changing with the deformations. Assuming a one-dimensional stress state is a simplification of course, especially after necking when the deformations are big. To minimize the possible errors that could come from this simplification, material calibrations were performed to find the equivalent stress that could be implemented in the numerical simulations. The material calibration part is described in Section 6.

Given the three-dimensional strain state in the material tests, it was possible to decompose the strain into one longitudinal strain component ε^L, and two transverse strain components ε^{t1} and ε^{t2}, as illustrated in Figure 5.5. Assuming that the material test specimens had perfectly circular cross sections that remained perfectly circular during the deformations, the two transverse strains were equal.

$$\varepsilon^{t1} = \varepsilon^{t2} = ln(\frac{d}{d_0}) \tag{5.2}$$

where d_0 is the diameter of the test specimen before the deformations and d is the diameter during the deformation. Furthermore, by assuming conservation of the volume

$$\varepsilon_v = \varepsilon^L + \varepsilon^{t1} + \varepsilon^{t2} = 0 \tag{5.3}$$

Using Equation 5.2 and 5.3, the following expression was derived for the longitudinal strain in the material test specimens. Notice that the only variable is the diameter of the material test specimen during the deformations.

$$\varepsilon^L = -2 \cdot ln(\frac{d}{d_0}) \tag{5.4}$$

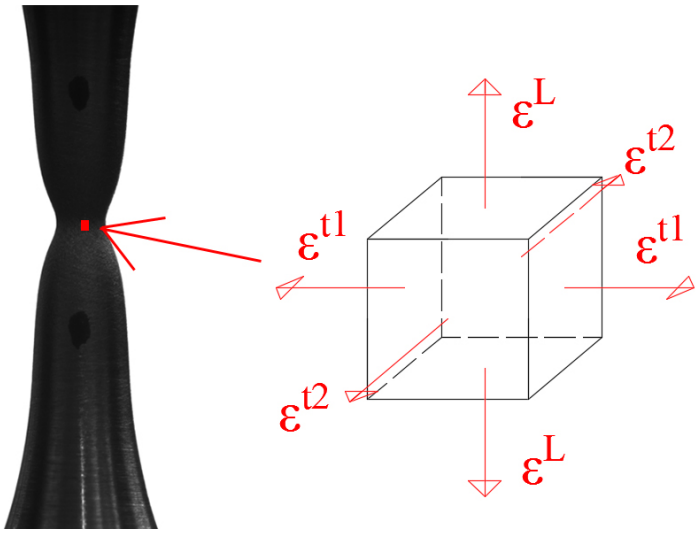

Figure 5.5: Strain components

According to Equation 5.1 and 5.4, still assuming that the cross sections remain perfectly circular during the deformations, the diameter of the test specimen during deformations was the only variable missing to be able to define the true strain and true stress of the material tests.

The diameter of the test specimen was registered using Edge Tracing in eCorr 4.0, the same software used to run DIC analysis. Much similar to the DIC procedure, the Edge Tracing tracks an edge in a series of images during a deformation. In the first image in a series, the two edges of the test specimen were defined, as illustrated in Figure 5.6a. Because of the big contrast in the image from inside to the outside of the edge, the software manages to track the pixels along the edges from one image to the nest in a series. The critical cross section is the cross section where the necking is happening, see Figure 5.6b. Tracking the minimum distance between the two edges of the material test specimen, it was possible to get the diameter of the material test specimens during the deformations, and hence also the true strain and true stress.

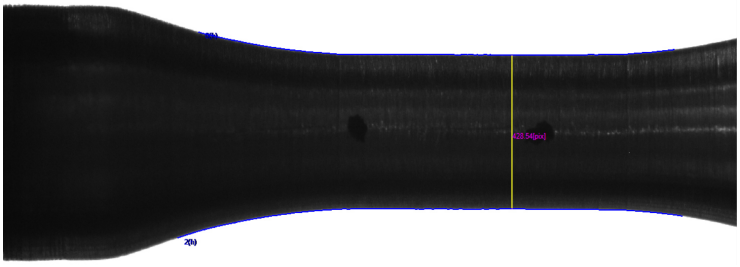

(a) Distance between edges, undeformed, frame 1

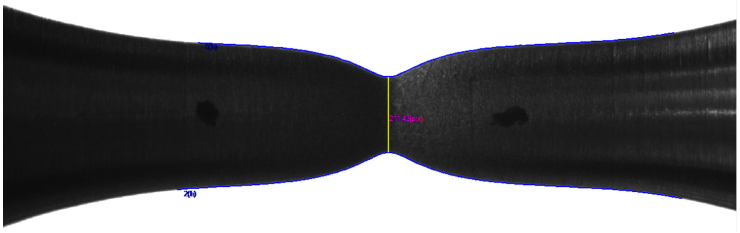

(b) Distance between edges, deformed, frame 561

Figure 5.6: Edge tracing

5.4 Results

The results from the material tests are given as true strain/true stress curves. These curves were used to calibrate the material parameters for the numerical model, as described in Section 6.

5.4.1 Quasi-static tests

The results from the three quasi-static material tests for the block are illustrated in Figure 5.7. All three tests were performed with 0.007 mm/s deformation rate. There was a considerable variation in the results of the three tests.

Four quasi-static tests were performed with the plate material, but unfortunately the QS P 03 material test was defect and therefore not considered further. The two first tests were performed at 0.007 mm/s deformation rate, while the QS P 04 material test was performed at 0.5 mm/s deformation rate, as the black markers on the curve indicates in Figure 5.8. Note that the two first curves are very similar, while the curve for QS P 04 seems to be slightly different from the others. As expected because of a higher strain rate, the QS P 04 gets a little higher stress level at low strains. However the curve seems to get some unexpected softening with the increased strain. While this could be explained as an effect of thermal softening, that does not seem probable because thermal softening normally only plays an important role at higher strain rates.

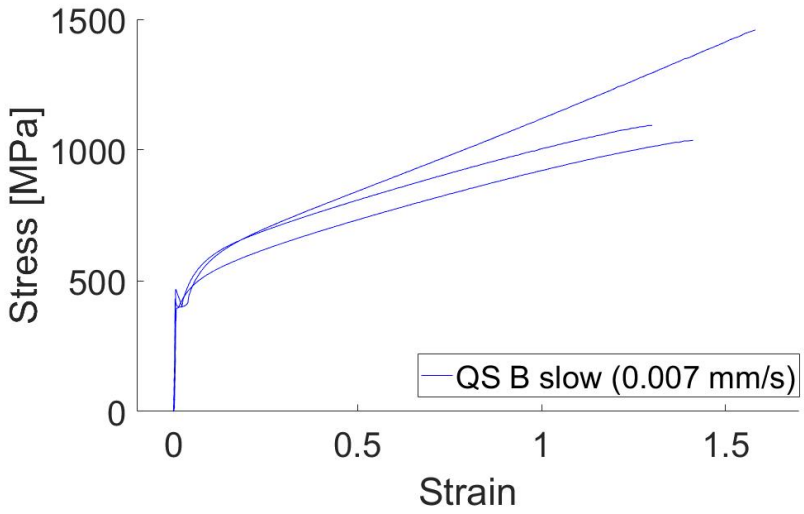

Figure 5.7: Material tests, QS Block

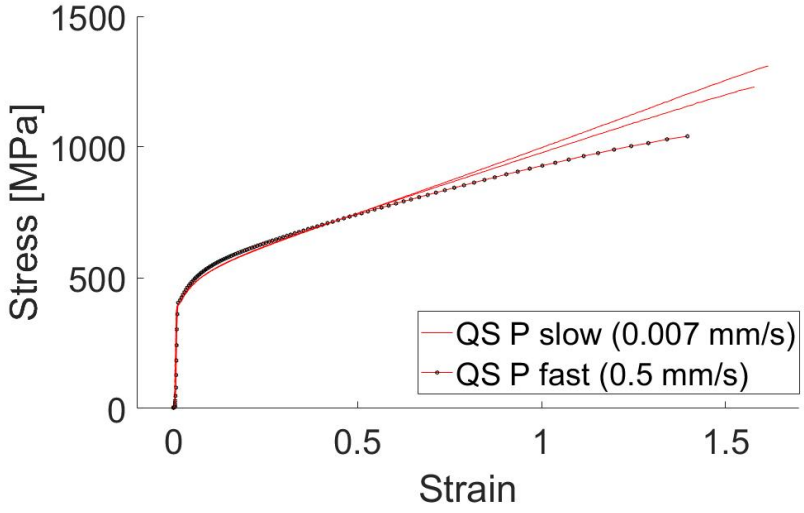

Figure 5.8: Material tests, QS Plate

Five quasi-static material tests were performed for the welds, three at a slow speed, and the two last at a higher speed rate of deformations, as illustrated in Figure 5.8. Notice that all the curves are very similar, but that there still is a clear distinguishable trend between the tests with slow speed and the tests with higher speed. This is just as expected.

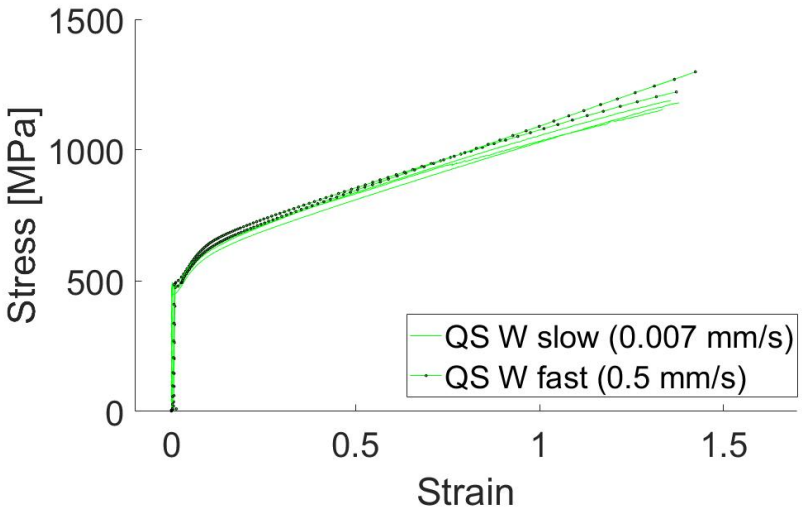

Figure 5.9: Material tests, QS Weld

5.4.2 Dynamic tests

A total of four dynamic material tests for the plate material were performed, as illustrated in Figure 5.11. The four curves are fairly similar, but they seem to diverge from one another with increased strain.

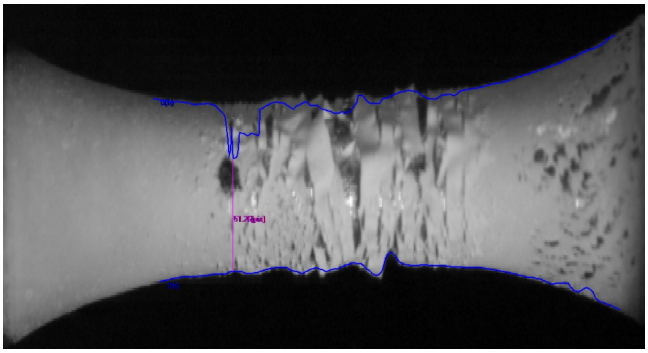

Figure 5.10: Problems with Dyn L 02 in edge tracing

Five dynamic material tests were performed for the weld material. Unfortunately, two of these tests came out faulted. A technical problem was the cause for the Dyn W 05 test, where no data was registered during the test. Further, the two first tests were painted white before they were tested. A black background was used to create a sharp edge on the material test specimen. However, during deformations, the painting started peeling off creating problems for the

edge tracing software, see Figure 5.10. The results for the Dyn W 01 test still were usable, but unfortunately that was not the case for the Dyn L 02 test. After this, for the other material tests, the material test specimens were no longer painted, but the background was lighted up white instead.

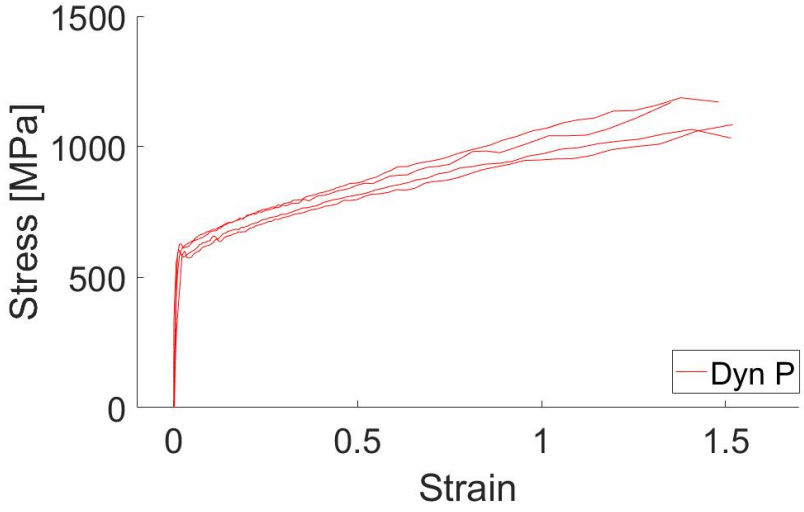

Figure 5.11: Material tests, Dyn Plate

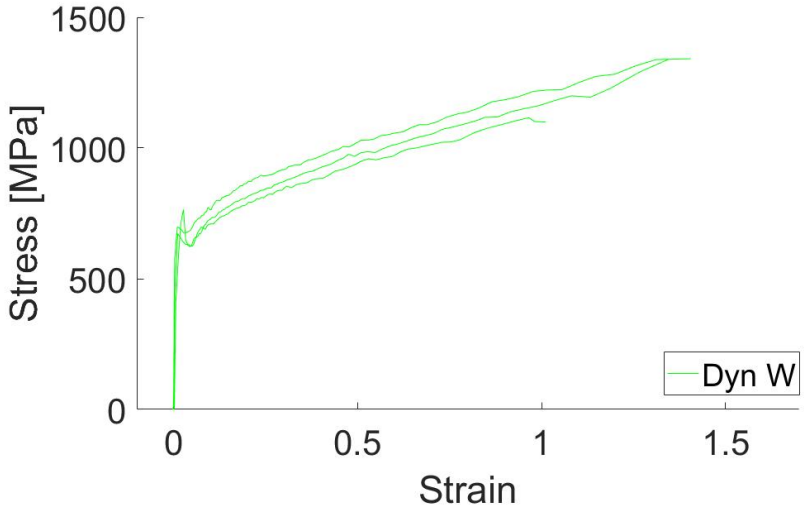

Figure 5.12: Material tests, Dyn Weld

6 Material calibration

When calculating the true stress in the quasi-static material tests, a one-dimensional stress state was assumed. As mentioned, this was a simplification, and could cause deviations in the results from the numerical simulations. Material calibrations were performed to find an equivalent stress that would better describe the behaviour of the materials.

6.1 Numerical model of the material tests

The numerical model of the material test specimen was created as 3D deformable solid in Abaqus 6.14 (implicit). All the materials were given the same elastic properties, according to Table 7.1, while the plastic material properties were derived as explained in Section 6.2. The SIMLab material model library was utilized to run the simulations.

Table 6.1: Elastic material properties

Young's modulus [MPa]	Poisson's ratio
210 000	0.3

Two perpendicular planes along the longitudinal center axis of the material test specimen create two symmetry planes. Therefore it was only necessary to build one quarter of the material test specimen, as illustrated in Figure 6.1. This was a simplified model since the ends parts were created with smooth surfaces without screw threads. Anyhow this simplification was considered to have little influence on the numerical results because all the plastic deformations were assumed to occur in the middle part of the test specimen.

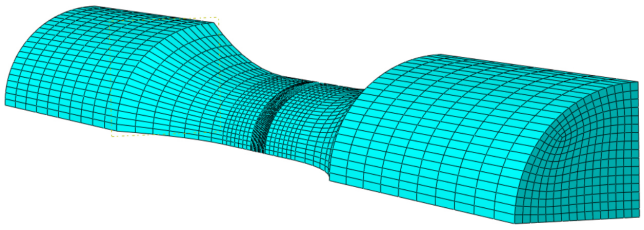

Figure 6.1: Numerical simulation of the material tests

In the experiment, the outer 9 mm at the ends of the material test specimens were covered with screw threads which were screwed into the hydraulic tension machine. To get a similar effect in the numerical model, the surfaces of the material test specimen at the outer 9 mm were defined as two different sets. These sets were given a displacement, the left end going left and the right end going right causing deformation in the centre part.

6.2 Calibration procedure

A material calibration was performed for each material type. One representative curve from the slow going quasi-static material tests for each material was selected, as illustrated for the block in Figure 6.5. A first estimation of a representative equivalent stress curve for each material was achieved by estimating the value of the Voce parameters in the following equation.

$$\sigma_{eq} = \sigma_y + \sum_i (Q_i - Q_i \cdot exp(-\frac{\theta_i}{Q_i} \cdot p)) \tag{6.1}$$

where σ_{eq} is the equivalent stress, σ_y is the yield stress, Q_i and θ_i are Voce parameters and p is the plastic strain. While this equation might seem complex, it is simply a summation of terms where each term represents a curve. The yield stress is a constant straight line, while each Voce term is a particular curve that has initial inclination θ_i and then saturates at Q_i. For example, given the parameters in Table 6.2 it is possible to illustrate the equivalent stress as the sum of the curves in Figure 6.2.

Table 6.2: Example of parameter values for the equivalent stress, using two Voce terms

σ_y	Q_1	Θ_1	Q_2	Θ_2
500	250	5000	5000	250

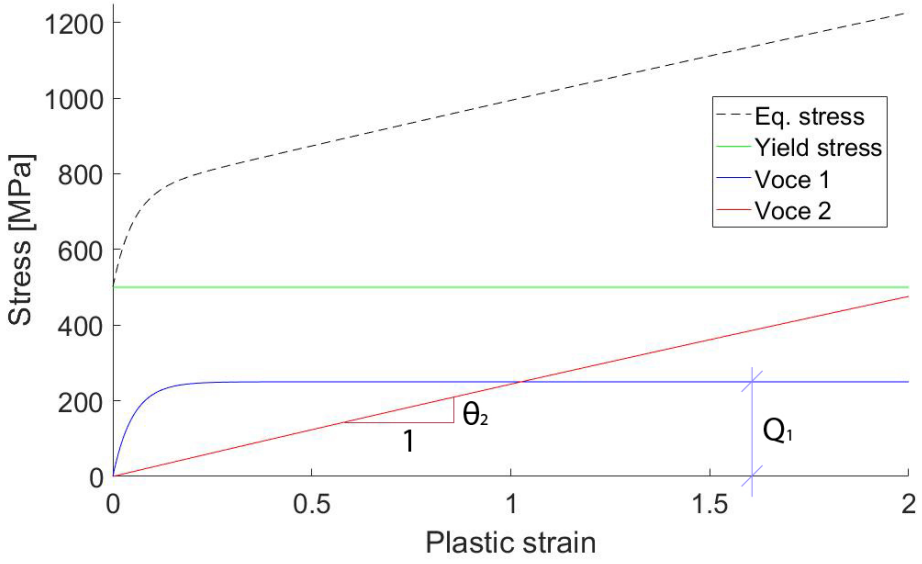

Figure 6.2: Example equivalent stress curve, using Table 6.2

The goal of the calibration was to create an equivalent stress that would, when inserted into the numerical model, make the numerical model of the material test specimen behave in the same way as the selected representative material test specimen from the experiment. Similar to the material tests in the laboratory, the data outputs from the numerical models were the load applied and the reduction in diameter in the middle of the tests. After running the first simulation with the estimated equivalent stress it was expected that the results from the numerical simulation would be different from the results from the material tests. An example of this is illustrated in Figure 6.3. The figure illustrates the results from the numerical model with the first version of the equivalent stress for the welds.

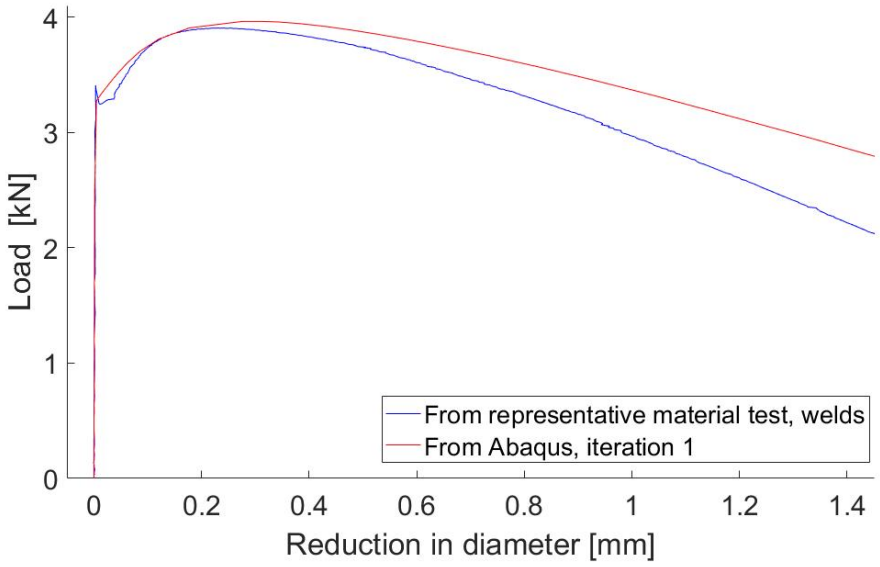

Figure 6.3: Reduction in diameter, first iteration weld material

To obtain better results, another iteration was needed. The voce parameters were changed to create a second equation for the equivalent stress and in that way to begin the second iteration. The new equivalent stress was inserted into a second numerical simulation, and again the results were compared with the results from the representative material test. This cycle of iteration continued until the results had converged satisfactorily. The final equation for the equivalent stress was defined as the equivalent stress for the current material, and was later used in the numerical simulation of the component tests.

Three different meshes were used to do the material calibrations. The first mesh was a coarse mesh, saving time in the first few iterations to get close to a good solution. Then a finer mesh was used to do the successive iterations until the result was satisfactory. Then at last, an even finer mesh was used to control the results of the second mesh. The three meshes are illustrated in Figure 6.4. Eight-node brick elements with full integration was used.

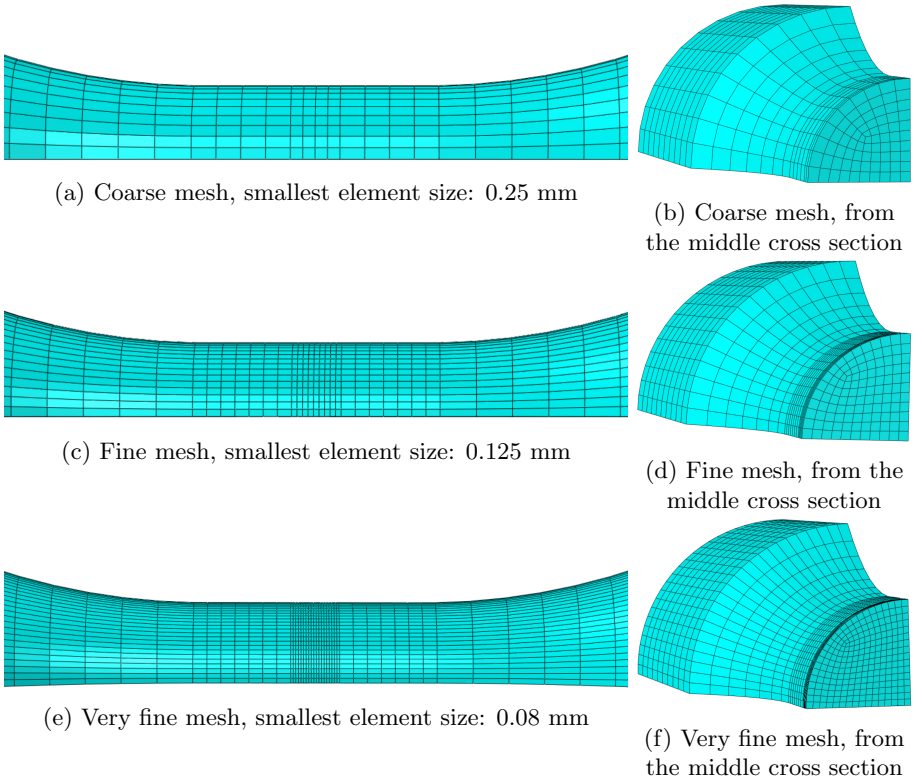

(a) Coarse mesh, smallest element size: 0.25 mm

(b) Coarse mesh, from the middle cross section

(c) Fine mesh, smallest element size: 0.125 mm

(d) Fine mesh, from the middle cross section

(e) Very fine mesh, smallest element size: 0.08 mm

(f) Very fine mesh, from the middle cross section

Figure 6.4: Material test meshes

6.3 Calibrating the material properties

6.3.1 Selecting representative curves

For each material it was necessary to choose one representative curve from the material tests. The purpose for the numerical models was to achieve the same results as the representative material tests. When choosing the representative curves, only the slow (0.007 mm/s) quasi-static material tests were considered to avoid effects from the strain rate. For the block material, the curve from the QS B 01 material tests was selected as the representative curve, being the middle curve according to Figure 6.5. The three curves varied more than expected and ideally it would be better to preform further material tests of the block before choosing a representative curve.

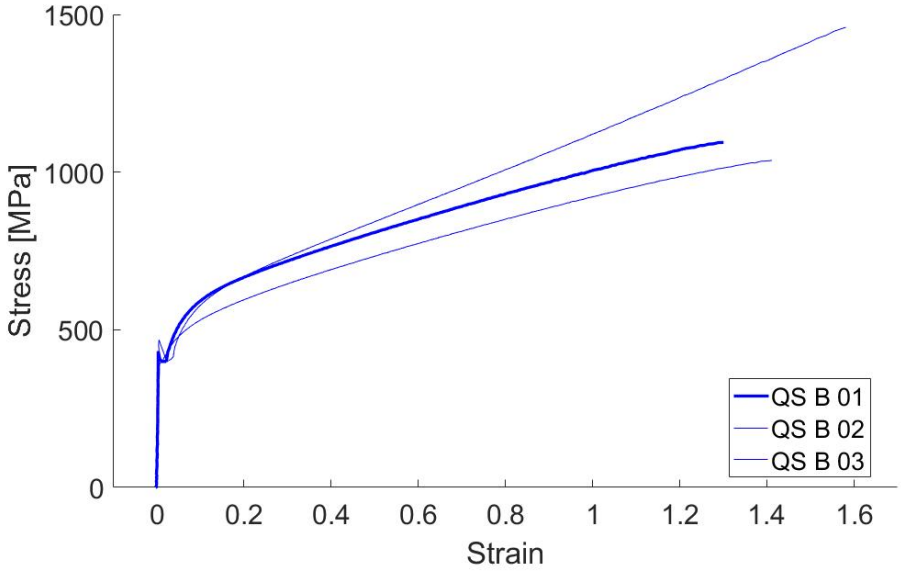

Figure 6.5: The representative curves from the slow going quasi-static material tests from the block

The two slow quasi-static material tests from the plates were very similar, as illustrated in Figure 6.6. Choosing one curve or the other as the representative curve would probably not make a great difference for the numerical model. QS P 02 was chosen because it was the middle curve when also including the fast going quasi-static test for the plates, as illustrated in Figure 5.8.

The three slow quasi-static material tests from the weld material were almost identical, see Figure 6.7. Again, selecting one or another would make little difference to the final results. QS W 01 was chosen as the representative curve.

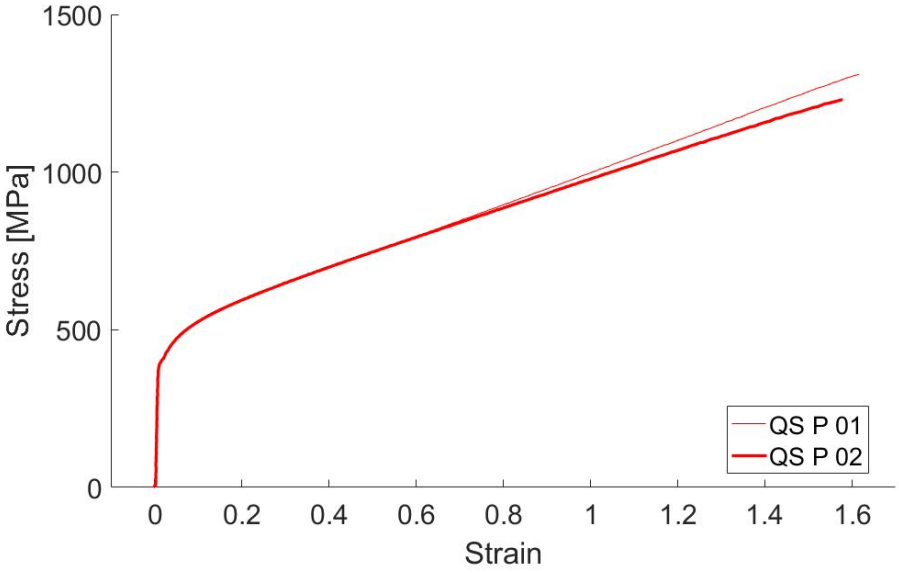

Figure 6.6: The representative curves from the slow going quasi-static material tests from the plates

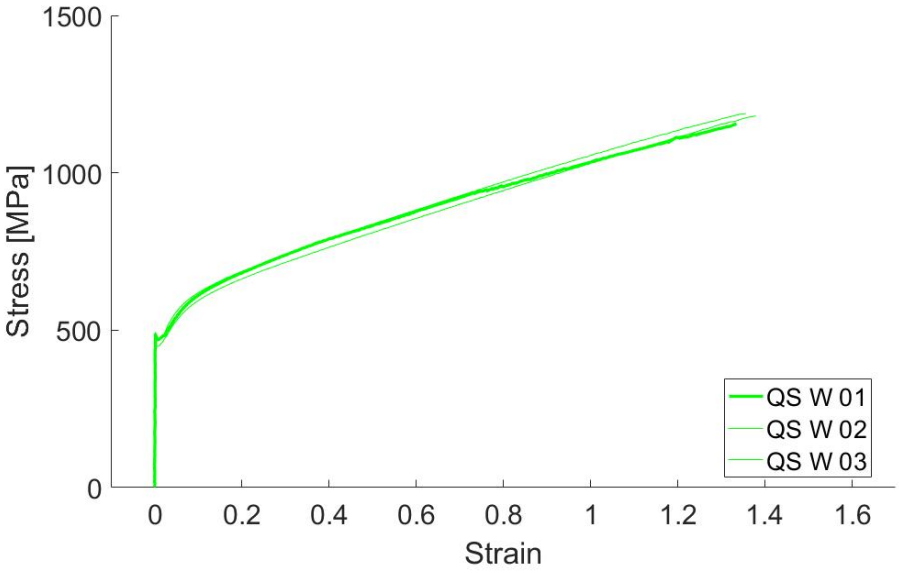

Figure 6.7: The representative curves from the slow going quasi-static material tests from the weld

6.3.2 Final results for the material calibrations

After running various iterations for each material, the results finally gave satisfactory convergences as illustrated in Figure 6.8 for the block material, in Figure 6.9 for the plate material and in Figure 6.10 weld material. Notice that the very fine mesh and the fine mesh, illustrated in Figure 6.4, give almost identical results in all three plots.

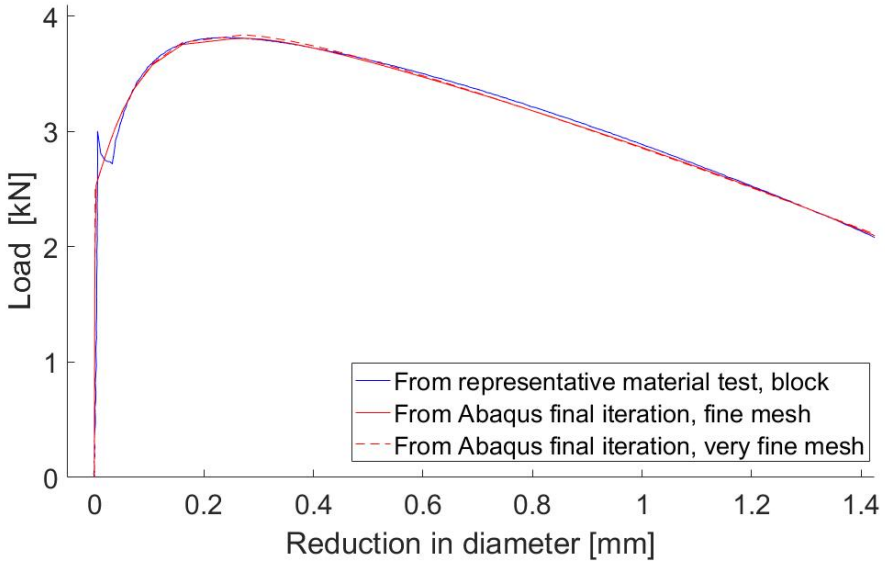

Figure 6.8: Converged results, block material

The final Voce parameters for each material are presented in Table 6.3. The respective equivalent stress curves are compared to the results from the representative material tests in Figure 6.11. Notice that the transformation from the the material test curves to the equivalent stress curves is fairly similar for all three materials.

Notice also the relatively large difference in the results between the block and the plate. This was not expected since both were made of steel S355. The reason for the difference in the two could of course be related to the choice of representative curves. As mentioned, there was a big variation in the results from the material test of the block, and selecting another material test would perhaps have resulted in more representative material properties for the block. However, it is also possible that the block had different material properties than the plate. Without doing further material tests for the block, this cannot be determined.

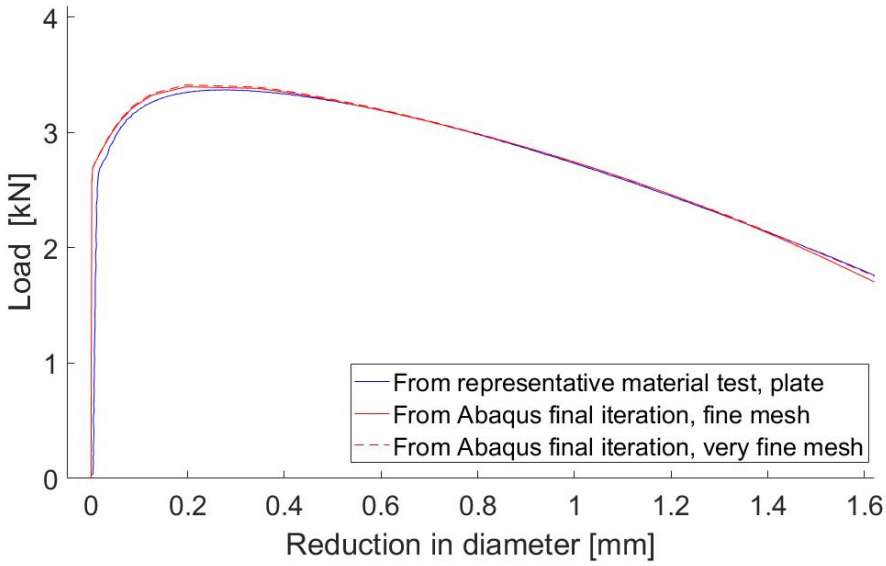

Figure 6.9: Converged results, plate material

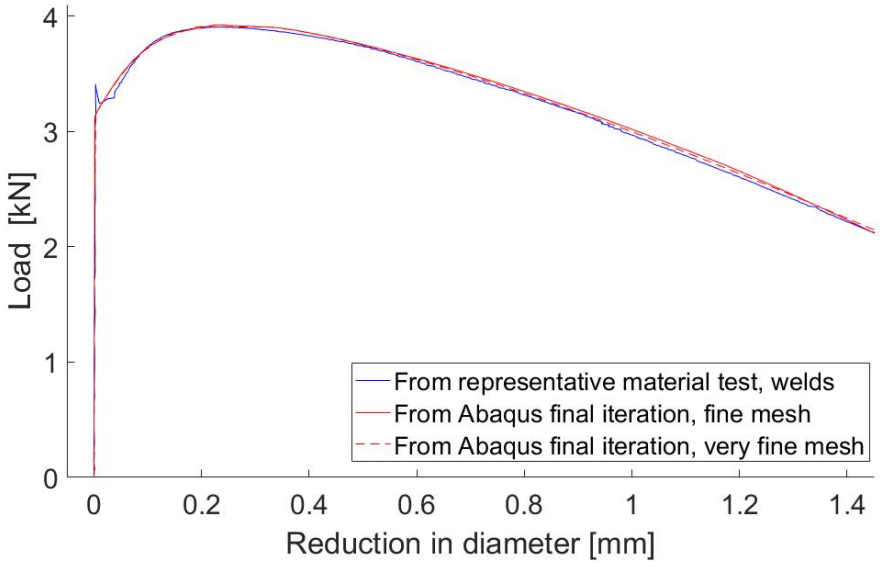

Figure 6.10: Converged results, weld material

Table 6.3: Final Voce terms for the materials

	σ_y	Q_1	Θ_1	Q_2	Θ_2	Q_3	Θ_3
Block	360	298	4000	20000	140	-	-
Plate	384	140	2300	600	300	50	100
Weld	450	200	2200	300	200	50	100

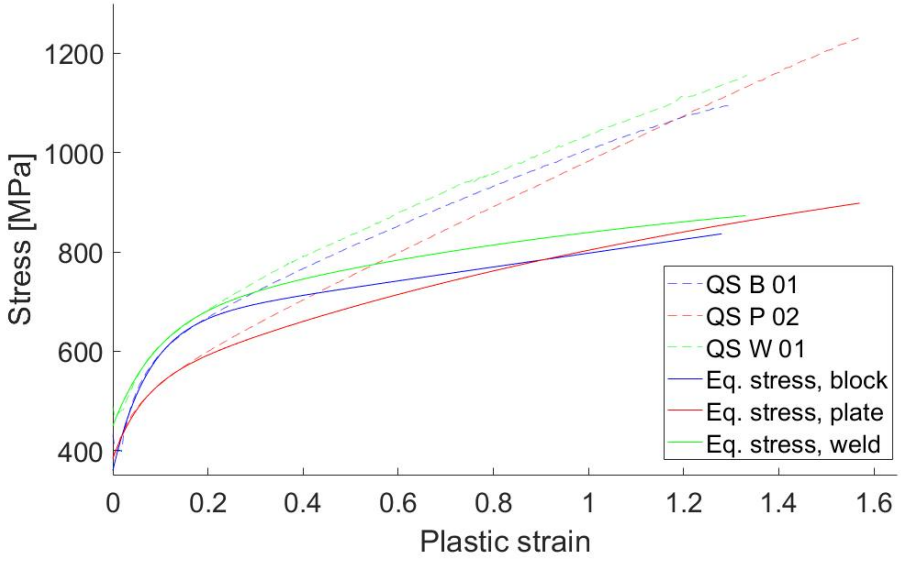

Figure 6.11: The final equivalent stress curves compared to the results from the representative material tests

6.4 Including strain rate and temperature dependencies

For the dynamic material parameters, Equation 6.1 was multiplied with two dynamic factors to become Equation 6.2. The first dynamic factors handles viscosity, and the second includes adiabatic heating and thermal softening.

$$\sigma_{eq} = (\sigma_y + \sum_i (Q_i - Q_i \cdot exp(-\frac{\theta_i}{Q_i} \cdot p))) \cdot (1 + \frac{\dot{p}}{\dot{p}_0})^C \cdot (1 - T_h^m) \tag{6.2}$$

where $\dot{p}$ is the plastic strain rate, $\dot{p}_0 = 10^{-3}s^{-1}$ is the reference plastic strain rate, C is a plastic strain rate sensitivity coefficient and m is a temperature coefficient. For the quasi-static tests, $\dot{p}$ was assumed to be zero and hence the viscosity term was neglected when running the quasi-static simulations. Further, T_h is a dimensionless temperature defined as

$$T_h = \frac{T - T_r}{T_m - T_r} \tag{6.3}$$

where $T = T_r + \Delta T$ is the current temperature, T_r is the room temperature and T_m is the melting temperature. ΔT is defined as

$$\Delta T = \int_0^p \chi \cdot \frac{\sigma_{eq}}{\rho \cdot C_p} dp \tag{6.4}$$

where ρ is the material density, C_p is the specific heat and χ is the Taylor-Quinney coefficient that represents the proportion of plastic work converted into heat. Notice that when $T \approx T_r \implies T_h^m \approx 0$. This implies that the temperature factor can be neglected as long as the change in temperature is small, which is the case for low strain rates.

Table 6.4: Material properties steel alloys [9]

T_r (K)	T_m (K)	ρ (kg/m^3)	C_p (J/kg K)	χ	m
293	1800	7821	452	0.9	1.0

6.4.1 Finding the strain rate sensitivity coefficient C

Assuming neglectable the change in temperature in the material test specimen at relatively low strains, Equation 6.2 can be rewritten as

$$\sigma_{eq} = \underbrace{(\sigma_y + \sum_i (Q_i - Q_i \cdot exp(-\frac{\theta_i}{Q_i} \cdot p)))}_{\text{Voce}} \cdot (1 + \frac{\dot{p}}{\dot{p}_0})^C \tag{6.5}$$

for small strain. Dividing both sides with the *Voce* term and then taking the logarithms, the equation can be written as

$$\underbrace{log(\frac{\sigma_{eq}}{Voce})}_{\text{Y}} = C \cdot \underbrace{log(1 + \frac{\dot{p}}{\dot{p}_0})}_{\text{X}} \tag{6.6}$$

Notice that Equation 6.6 is an equation for a simple linear curve where C gives the slope of the curve. Hence, by plotting $log(\frac{\sigma_{eq}}{Voce})$ against $log(1+\frac{\dot{p}}{\dot{p}_0})$, the slope of the curves would define C for each material. The equivalent stress σ_{eq} was assumed equal to the calculated true stress from the material test specimens for small strains. This is a fair assumption because the one dimensional stress state is a good representation in the material tests before the deformations get too big.

Looking at the first part of the plastic strains, for $p \leq 0.1$, the strain in time curves are close to linear for almost all of the material tests. This is illustrated in the plots in Figure 6.12b, in Figure 6.13b and in Figure 6.14b. The strain rate $\dot{p}$ for each curve was therefore assumed constant for $p \leq 0.1$ and it was calculated by taking the mean slope of each curve in this interval.

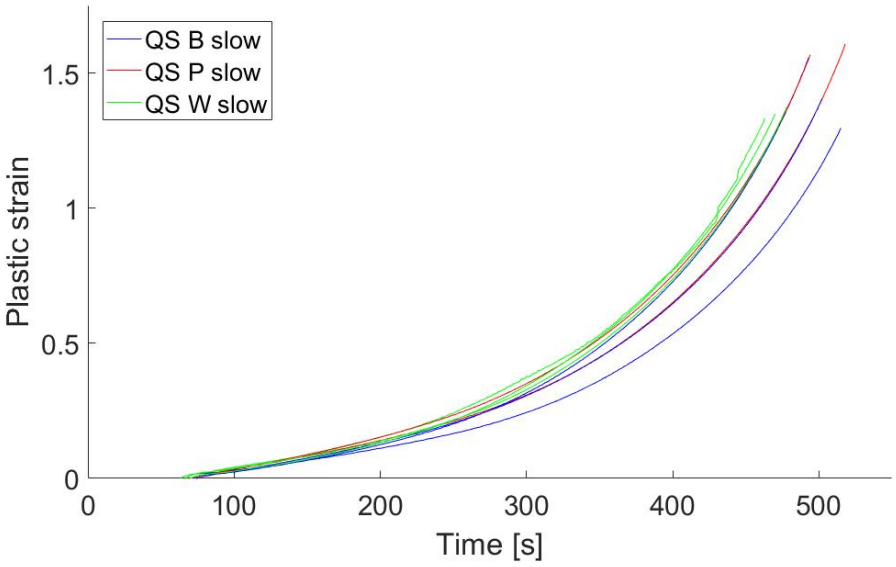

(a) Plastic strains in time

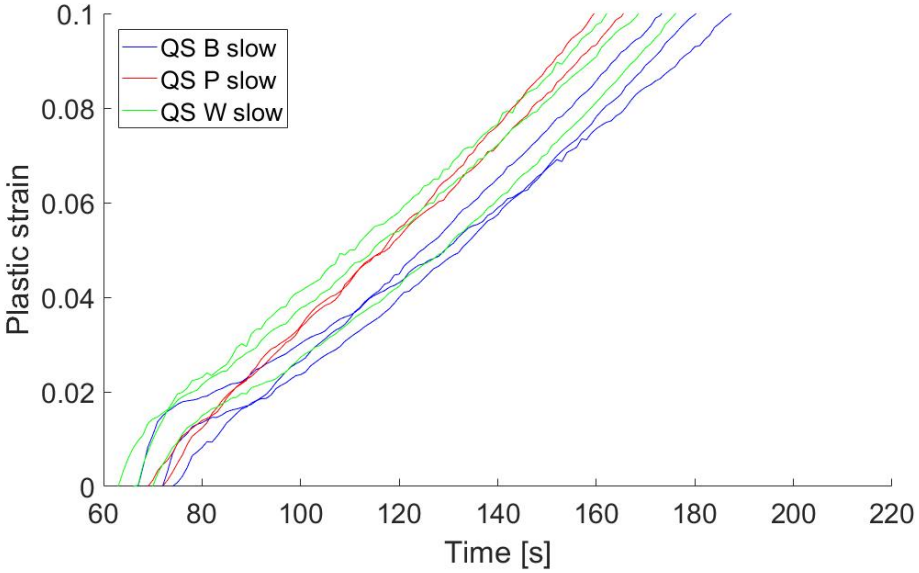

(b) "Linear" part at small strains

Figure 6.12: Plastic strain in time, slow going quasi-static material tests

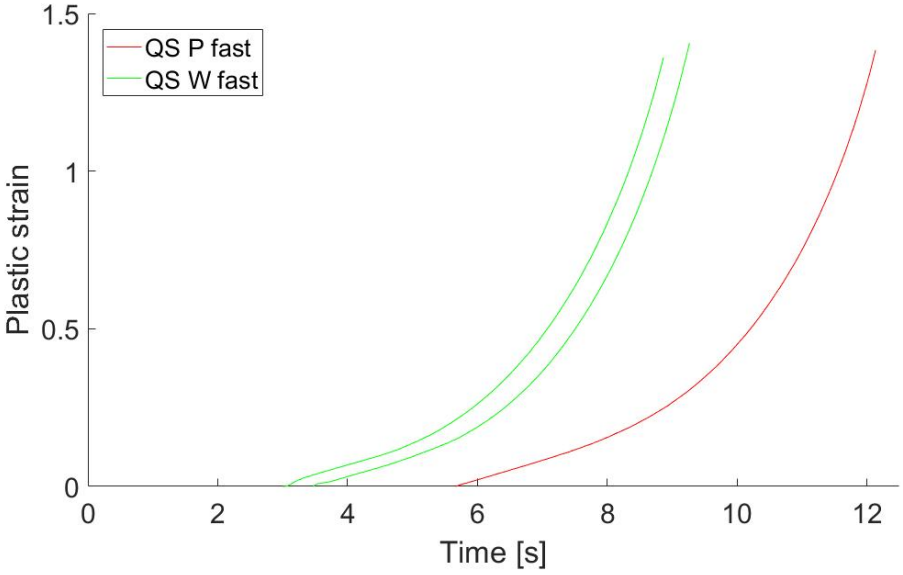

(a) Plastic strains in time

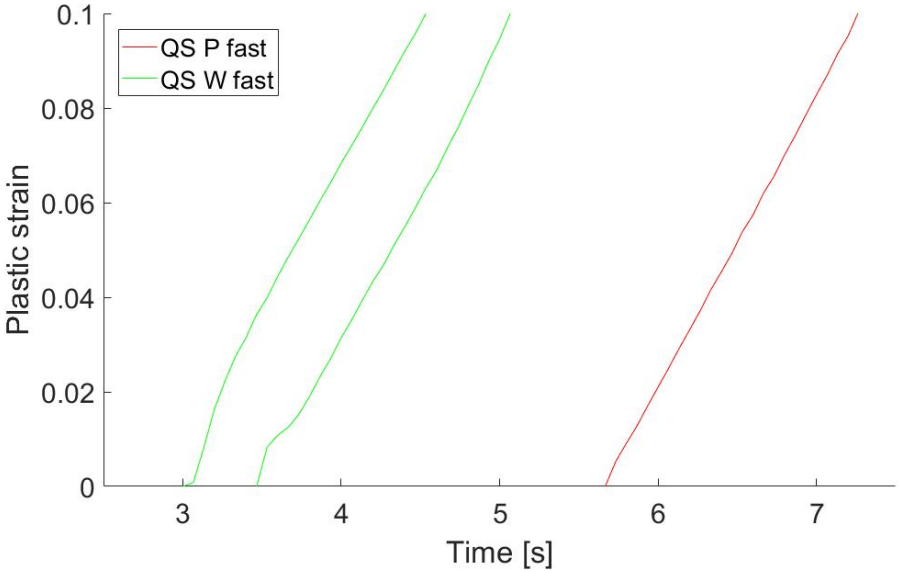

(b) "Linear" part at small strains

Figure 6.13: Plastic strains in time, fast going quasi-static material tests

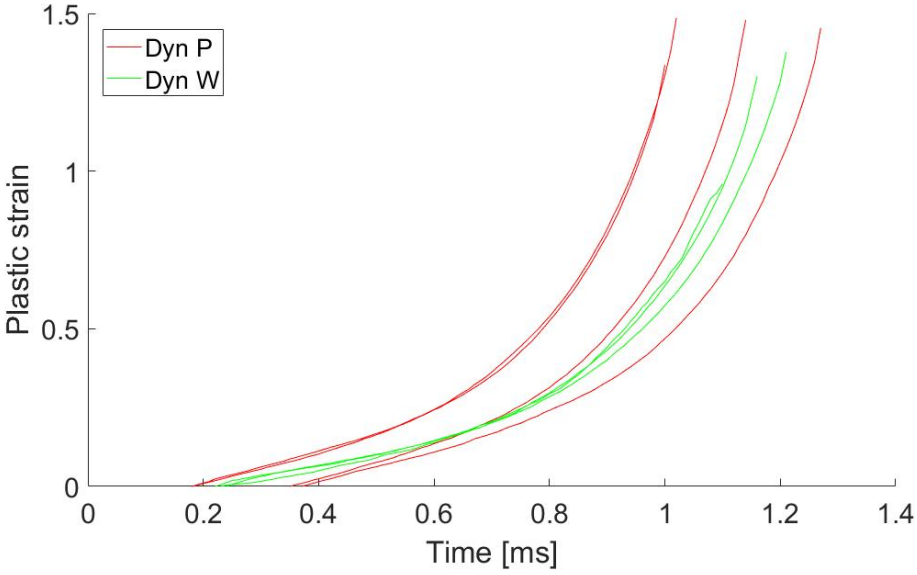

(a) Plastic strains in time

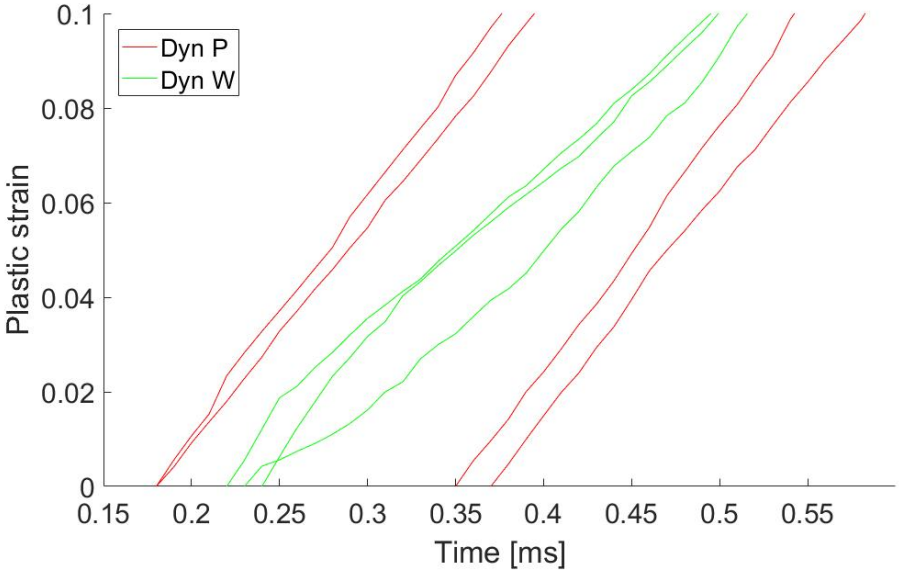

(b) "Linear" part at small strains

Figure 6.14: Plastic strains in time, dynamic material tests

From the results of each material test, the calculated true stress σ was obtained at three representative plastic strain values, at $p_1 = 0.00$, at $p_2 = 0.05$ and at $p_3 = 0.10$. Further, having calibrated the Voce parameters for all the materials, the *Voce* term in Equation 6.5 was calculated for the same three representative strains for each material. Having obtained σ, *Voce* and $\dot{p}$ for each material test, the plots in Figure 6.15 and in Figure 6.16 were obtained. Since the block material only had been tested with the slow going quasi-static material tests, it would not be possible to get a C-value for the block by itself. The block and the plate was therefore assumed to have the same C-value, knowing that both parts were made of steel S355.

Linear curves were created to represent the scattered data points in a best possible way, as illustrated i Figure 6.15b and in Figure 6.16b. To give equal importance and weight to all the three test velocities used, the linear polynomials were based on only three average points from each of the representative plastic strains, one average point for each of the three test strain rates. There were for example more results from dynamic material tests than from the fast going quasi-static tests. If all the points were weighted equally, the results from the dynamic test would have been more important than the results from the fast going quasi-static tests in the calculations of C. One could also argue that the dynamic tests should be given more importance since more tests were performed and therefore those results are more reliable. However, as Table 6.5 illustrates, the difference of the two approaches did not change the C-values much. For this thesis the C-values based on the mean points are used.

Table 6.5: C values for the different materials

	Steel S355 (plate and block material)	Weld material
C, mean points	0.0247	0.0233
C, all points	0.0237	0.0232

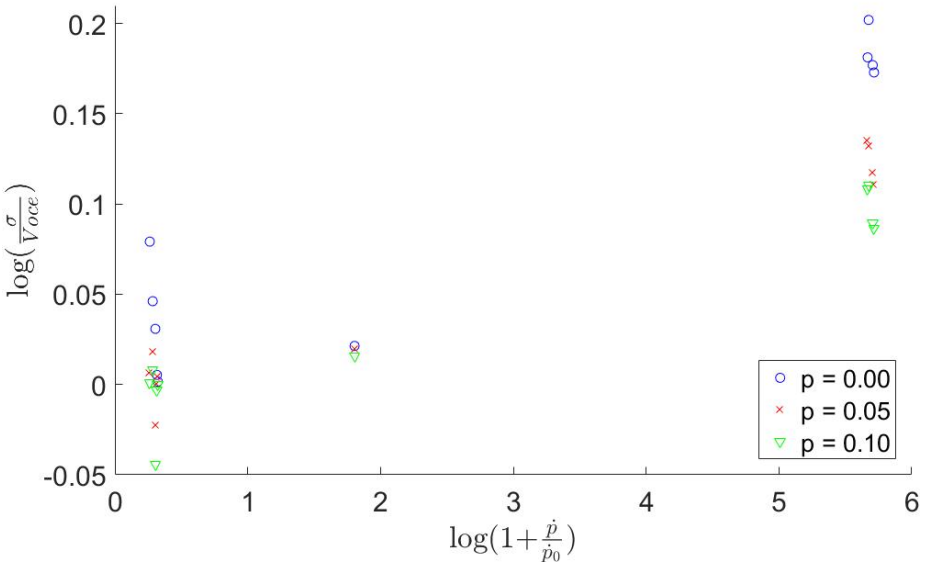

(a) Points to calibrate C, steel S355

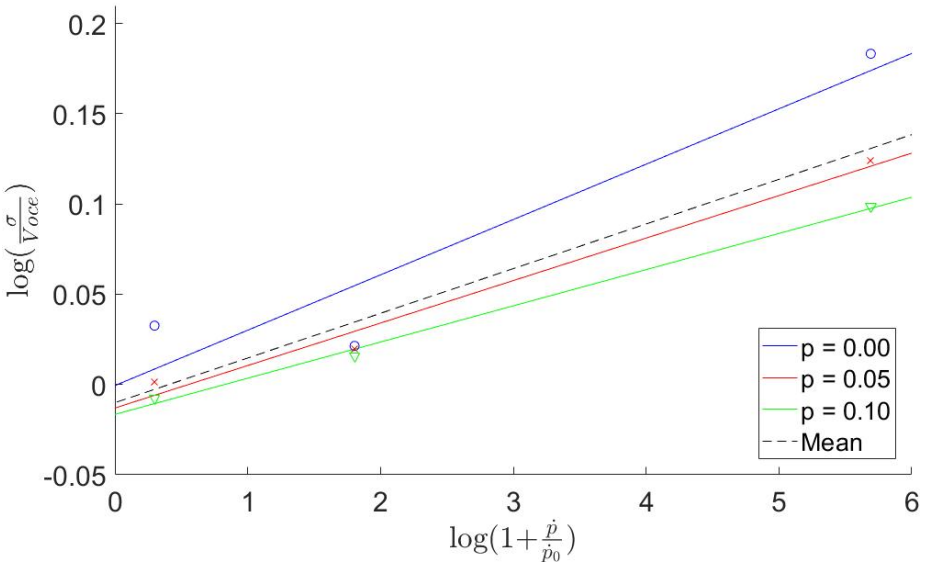

(b) Linear polynomial curve fitted to the mean points, steel S355

Figure 6.15: Calibrating C for the steel S355 material

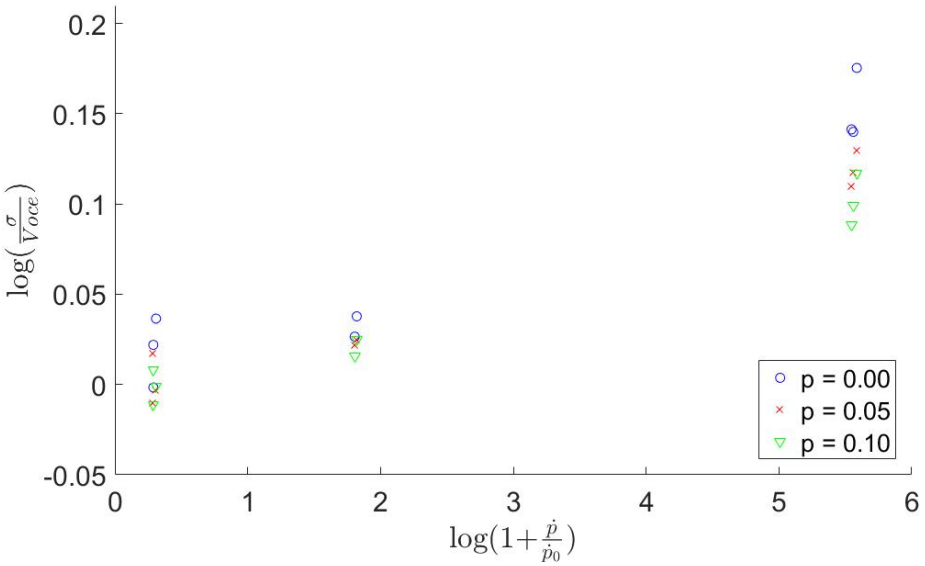

(a) Points to calibrate C, weld material

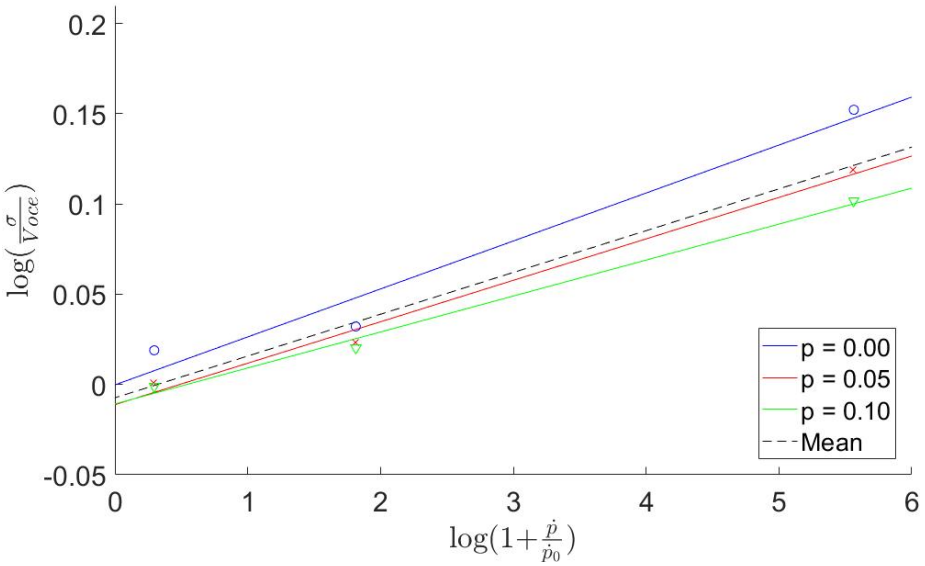

(b) Linear polynomial curve fitted to the mean points, weld material

Figure 6.16: Calibrating C for the welds

6.4.2 Fracture criterion

The Cockroft-Latham fracture criterion [10] was used in the numerical simulations of the dynamic component tests. Assuming tension, the criterion can be written as

$$W = \int_0^p \sigma_I dp \leq W_c \tag{6.7}$$

where W is the plastic work per unit volume σ_I is the principal stress, p is the equivalent plastic strain and W_c is the critical plastic work per unit volume. To use the fracture criterion it was necessary to obtain the critical plastic work W_c for each material. To do this, the equivalent plastic strain p and the principal stress σ_I was tracked from the core element of the numerical simulations of the material tests. The selected element is illustrated in Figure 6.17. The fine mesh where the smallest elements were 0.125 mm was used here.

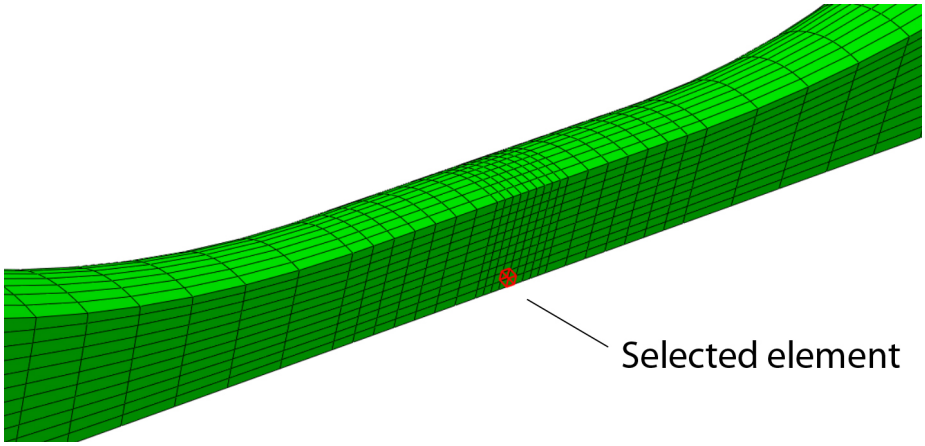

Figure 6.17: Selected element in the core of the material test

Without an integrated fracture criterion in the numerical simulation, the curves with plastic strain and principal stress went beyond the real fracture point. To stop the curves at the correct place, the reduction in diameter at fracture for the material tests, illustrated in Figure 6.8, in Figure 6.9 and in Figure 6.10 was used. The tracked strain and stress was synchronized with the reduction in diameter in the simulations, and in that way the critical diameter gave the time of fracture. In this way the curves in Figure 6.18 were obtained. The area under each curve was calculated to obtain the critical plastic work per unit volume W_c for each material. The results are given in Table 6.6.

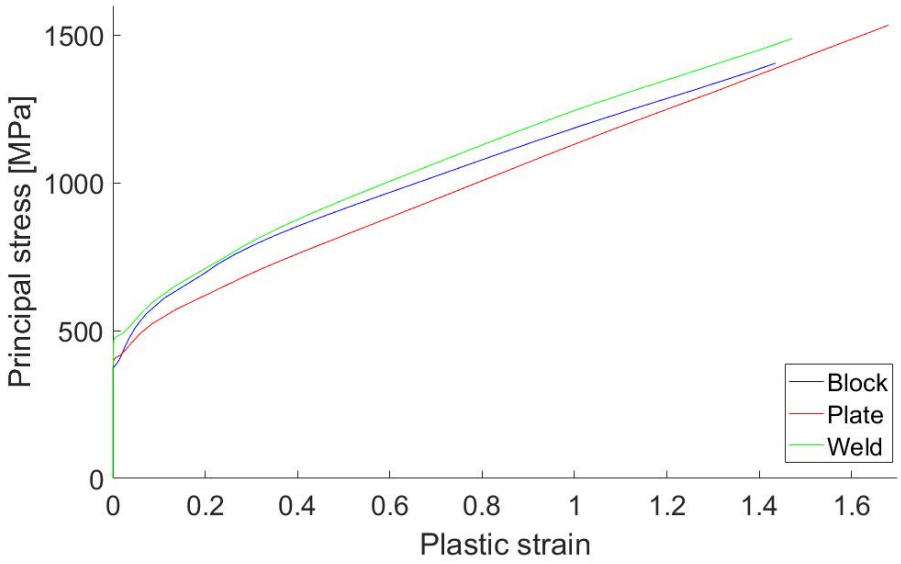

Figure 6.18: Curves used to integrate W_c

Table 6.6: Critical plastic work for the different materials

	Block	Plate	Weld
W_c [MPa]	1448	1716	1564

6.5 Scaling the strength of the weld

As mentioned in Section 5, it was necessary to create a larger weld to be able to machine the material test specimens for the weld material. Ideally the new weld should have had the same material properties as the welds from the component test specimens, however that is difficult to fully achieve. The bigger weld was welded with several passes. For each new layer with welds, the existing welds were reheated, giving a thermal history that probably produced different material properties than for the fillet welds of the component specimens, which were welded with one pass.

To decide whether the material properties of the welds in the component test specimens were different from those in the material test specimens, Vickers hardness tests [8] were performed by SINTEF Materials and Chemistry. The Vickers hardness tests indicates the capacity of the test material to resists plastic deformations during a standardized applied load. A small diamond with a pyramid form, was pushed into the material with a given force leaving an indent in the material. The hardness in the test material is given as

$$HV = \frac{F}{A} \tag{6.8}$$

where F is the force applied and A is the area of the created indent in the test material. A part of an unused component test specimen was tested with the Vickers hardness test in various points, as illustrated in Figure 6.19. The mean hardness in the weld in the component test, illustrated with the blue dots, was 221.2 HV.

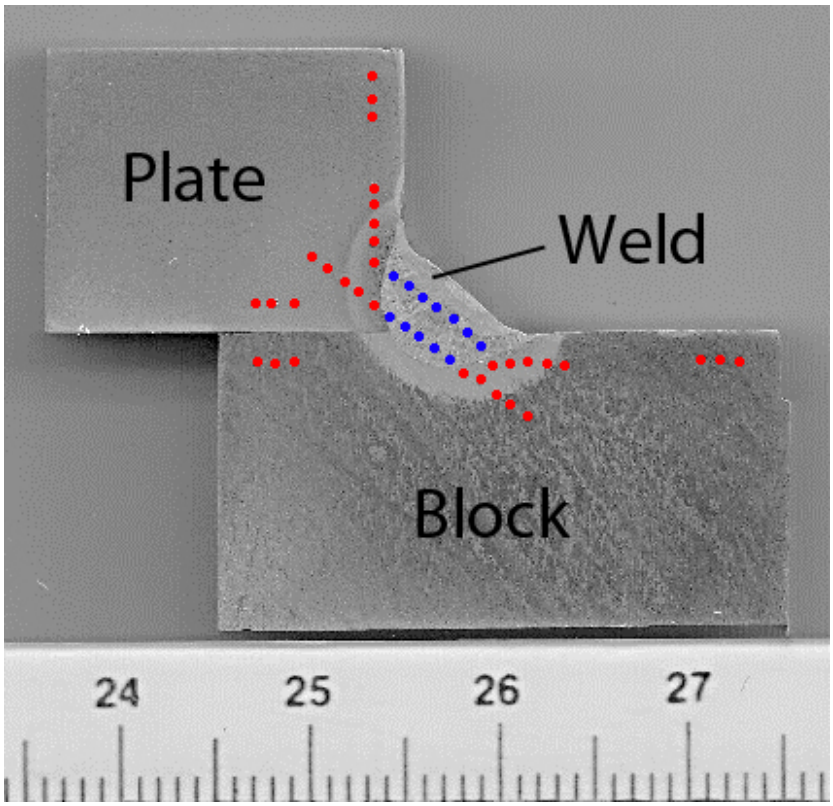

Figure 6.19: Part of a component test with positions of the indents from the Vickers hardness tests. Blue dots are in the weld material.

Similar tests were performed on the weld material used in the material tests. The two cylinders used for the material tests were carved out centrally from the weld, as illustrated in Figure 5.2b. The hardness of the material tests for the welds was therefore assumed to be best represented by the two central points marked in blue in Figure 6.20. The mean hardness in the central part of the big weld was 182.5 HV.

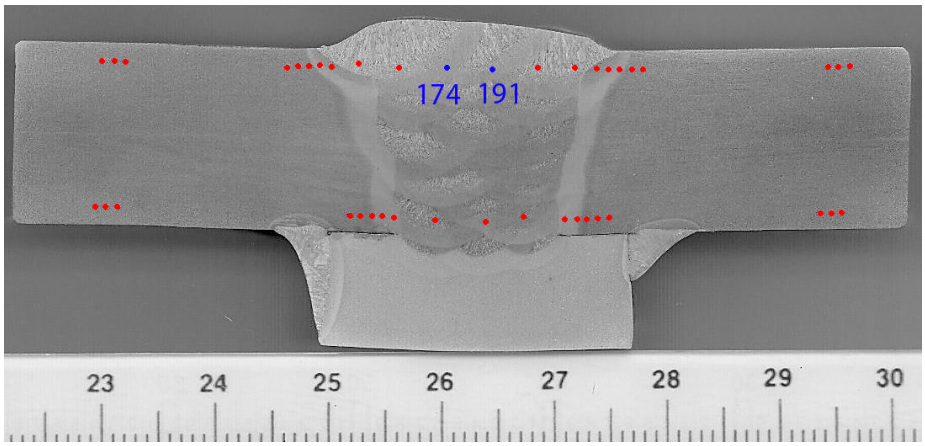

Figure 6.20: Positions for the Vickers hardness tests on the weld material for the material tests

The mean hardness in the weld material from the component test is about 21.2% higher than the mean hardness in the selected points of the bigger weld used in the material tests. To account for this difference, the yield stress in the welds was scaled up accordingly. From the material calibrations, the yield stress for the weld material resulted 450 MPa. Scaling it up by 21.2%, the yield stress for the welds resulted 545.4 MPa. The other Voce parameters for the welds remains unchanged, see Table 6.7.

Table 6.7: Scaled up Voce terms for the weld material

	σ_y	Q_1	Θ_1	Q_2	Θ_2	Q_3	Θ_3
Weld	545.4	200	2200	300	200	50	100

6.6 Effects of the material parameters in the numerical models

In the numerical models different material parameters were used. The elastic, the plastic, the viscous, the thermal and the fracture properties were all used to define the behaviour of the different materials. To get a better understanding of the influence from the different material properties, a simple one-element dynamic tension model was created as cube with 1 mm edges.

To create the one-element model, one corner of the cube was placed in the origin of a Cartesian coordinate system, and the edges of the cube were parallel to the X, Y and Z directions of that coordinate system. The four nodes contained in the plane defined by X=0 was constrained from displacement in the X-direction. The nodes on the opposite side of the cube was pulled in the

positive X-direction using a smooth step velocity going from 0 to 10^4 mm/s during the step time that was set to 1 ms. The two planes Y=0 and Z=0 were defined as planes of symmetry to avoid rotation and to get pure tension in the element.

The idea was to carry out several simulations using the different material properties and comparing the results, and in that way to better understand the influence from each parameter. The plastic strain and principle stress was tracked in the element during the simulations and as an example, the results for the block material are presented in Figure 6.21. The results from the other materials were very similar.

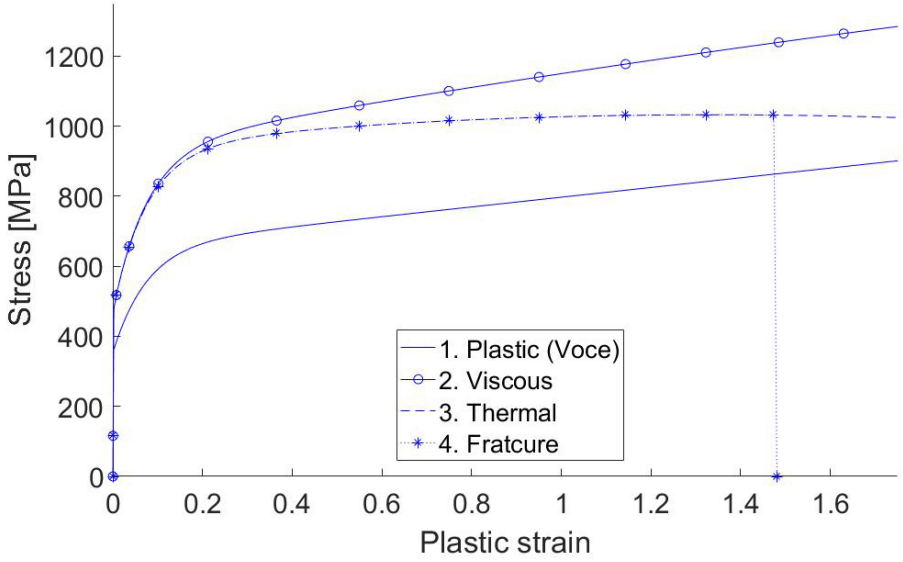

Figure 6.21: Element tests with material properties from the block

The first simulation was carried out using only elastic and plastic material properties. As expected, this simulation gave a perfect match to the created Voce curve. In the second simulation, by adding the viscous material properties, the strain rate hardening gave an evident increase in strength. The velocities in these simulations were purposely given very high values to clearly see the the effects from the strain rate dependent material properties. Further, in the third simulation, by adding the thermal properties the element had clear softening with the increasing strain. Finally the fracture criteria was inserted, and notice that the this curve is the same as the third one until fracture.

7 Modelling and simulating component tests

Four different numerical models were created, one for each component test type. All the simulations were preformed using Abaqus 6.14 and the SIMLab material model library. The two quasi-static numerical simulations, one with transverse fillet welds and the other with longitudinal fillet welds, were executed with implicit analysis. The two corresponding dynamic simulations were executed with explicit analysis.

Neglecting possible irregularities in the test specimens or the experiments, both the types of test specimens could be assumed symmetric about the two planes illustrated in Figure 7.1. Using the symmetric proprieties, it was sufficient to run simulations using only one quarter of the test specimen.

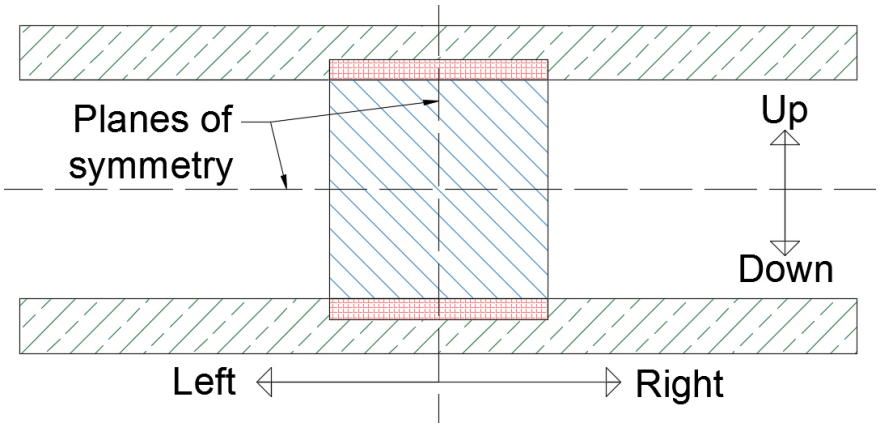

(a) Symmetry planes for the test specimen with transverse welds

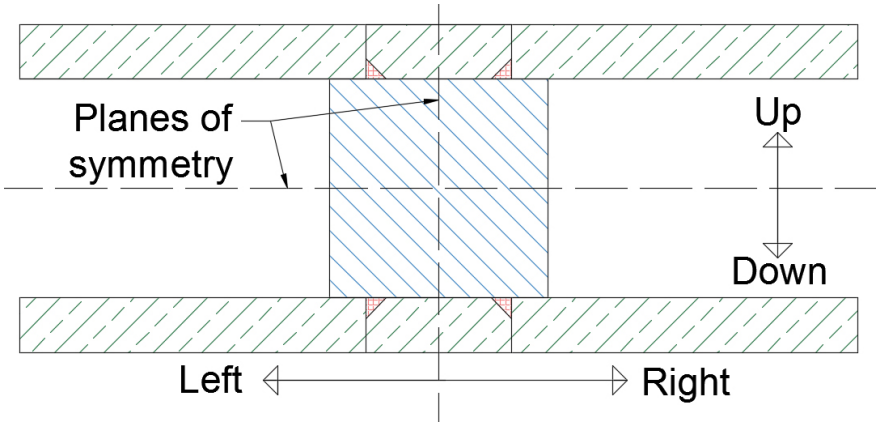

(b) Symmetry planes for the test specimen with longitudinal welds

Figure 7.1: Planes of symmetry

7.1 Building the numerical models

7.1.1 Parts

The test specimen was created as one part with 3D solids, as illustrated in Figure 7.2 and in Figure 7.3. The part included the block, the weld and the plate. The weld was created with a perfect triangular form with a throat size of 4 mm. It was necessary to create a gap between the plate and the block to define the two as two different bodies and to avoid that they were attached under the plate. This gap was created by giving the plate a very small inclination of 0.01°from the root of the weld as the figures illustrates. Notice that the inclinations of the plates in the drawings are dramatically exaggerated.

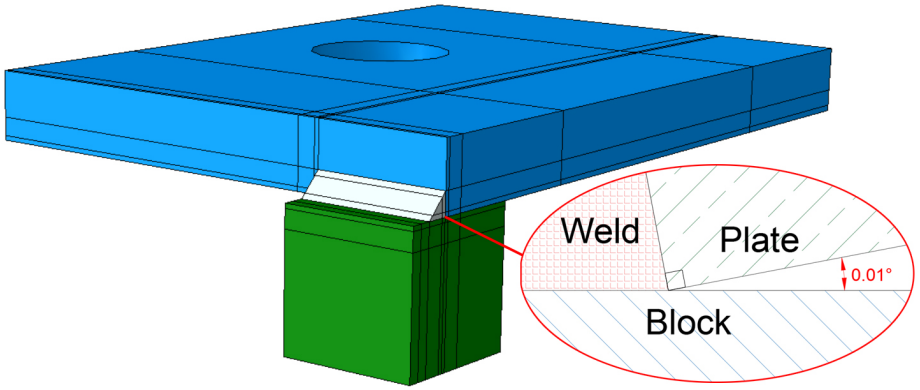

Figure 7.2: The test specimen part with transverse fillet welds

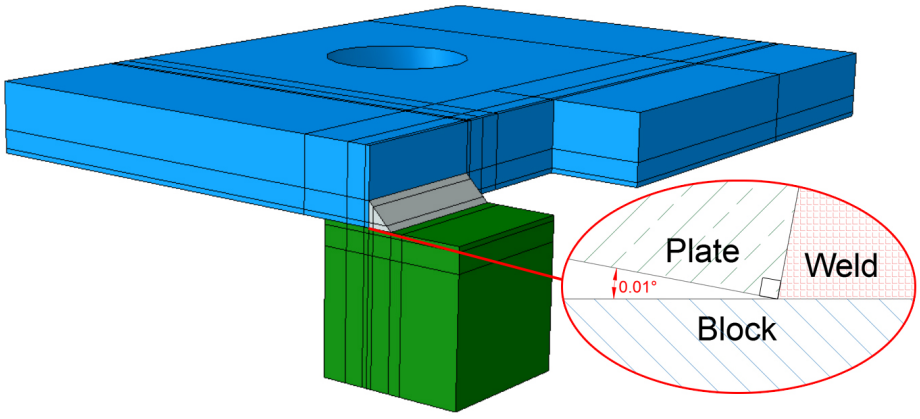

Figure 7.3: The test specimen part with longitudinal fillet welds

Further the parts for the nose and the bolt were created as 3D solids. One quarter of the nose was created without the end plate, only with the cylindrical front part. Half of a bolt was created with the washer, but without the bolt head and without bolt threads. Figure 7.4 illustrates the assembly of all the parts for the component test specimen with transverse fillet welds. The assembly was similar for the numerical simulation of the test specimen with longitudinal fillet welds.

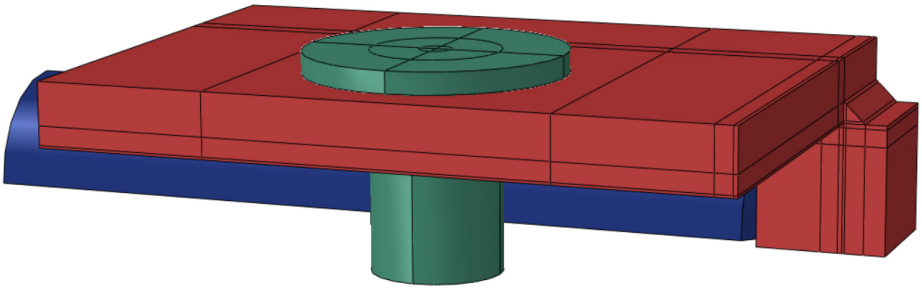

Figure 7.4: Assembly with all the parts for the test specimen with transverse fillet welds

7.1.2 Material parameters

The material parameters for the different materials were calibrated in Section 6. The component test specimen part was divided into sections for the block, the plate and the weld. The different sections were given their respective material properties according to Table 7.1 for the elastic properties and Table 7.2 for the plastic properties.

Table 7.1: Elastic material parameters

Young's modulus [MPa]	Poisson's ration
210 000	0.3

Table 7.2: Plastic material parameters, Voce terms for the materials

	σ_y	Q_1	Θ_1	Q_2	Θ_2	Q_3	Θ_3
Block	360	298	4000	20000	140	-	-
Plate	384	140	2300	600	300	50	100
Weld	545.4	200	2200	300	200	50	100

For the dynamic simulations, the different materials in the component test specimen part were also given their dynamic material parameters according to Table 7.3 and Table 7.4. The nose and the bolt were given purely elastic properties in both the quasi-static and the dynamic simulations, assuming that these parts would not obtain any plastic deformations anyway.

Table 7.3: Thermal softening properties for steel alloys [9]

T_r (K)	T_m (K)	ρ (kg/m^3)	C_p (J/kg K)	χ	m
293	1800	7821	452	0.9	1.0

Table 7.4: Viscosity and fracture properties for the materials

	Block	Plate	Weld
C	0.0247	0.0247	0.0233
W_c [MPa]	1448	1716	1564

7.1.3 Boundary conditions, interactions and loads

First of all, the nodes in the symmetry planes were constrained from displacements perpendicular to the current planes. Further, all the nodes in the bolt part were fixed in all directions so the bolt could hold back the plate during deformations. The bolt was not perfectly fixed in the experimental set-up, but its small displacement was assumed to be of little importance to the test results.

The fixture from the experimental set-up was not created as a part for the numerical simulations. Without it the plate was free to bend downwards into the space where the fixture should have been. To avoid this, the part of the underside of the plate that would have been in contact with the fixture was restrained from vertical displacement. This last boundary condition did not give a significant difference in the results.

A general contact interaction with frictionless tangential behaviour and a hard normal behaviour was created. This Contact interaction was applied between the fixed bolt and the plate, between the nose and the block and between the block and the plate. The last one was to avoid that the block was pushed up into the plate during deformations.

For the quasi-static numerical tests, the load was created, similar to the experiment, as a displacement of the rear side of the nose towards the block. The front of the nose, being initially surface to surface with the back of the block, would in this way push the block forward.

For the dynamic tests, the load was applied as a mass with initial velocity. An analytical rigid plate was created parallel to the rear end of the nose. A

reference point on the rigid plate, representing a quarter of the trolley, was created and given a mass of 358.5 kg. This rigid plate was tied to the rear end of the nose, just as the trolley was in the experiment. The dynamic assembly for the numerical simulation of the component test with longitudinal fillet welds is illustrated in Figure 7.5. The assembly for the numerical simulation of the component test with transverse fillet welds was similar. Further, the rigid plate was restrained from any rotations or any displacement other than the displacement towards the block. Finally the the rigid plate, including the reference point, and the nose were given an initial velocity towards the block to create the impact.

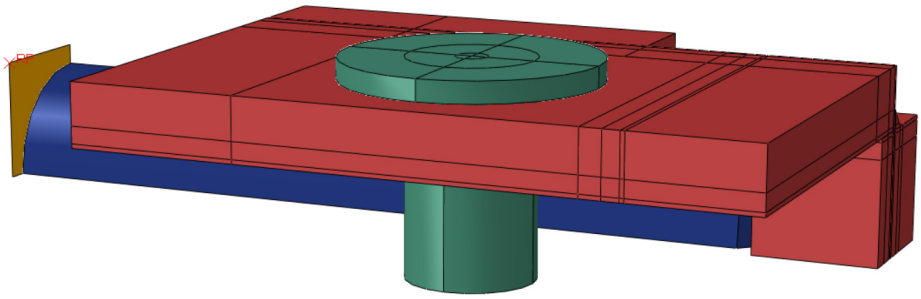

Figure 7.5: Assembly with all the parts for the dynamic test specimen with longitudinal fillet welds

The load from the numerical simulations was tracked, similar to the experiment, with a fictitious strain gauge on the nose. The fictitious strain gauge was an element on the surface of the nose about 135 mm from the front of the nose. The element was in that way in the same place as the strain gauges in the experiment. The strain in the longitudinal direction of the nose was tracked in this element during the simulations. Because the deformation of the nose was purely elastic, the load applied was calculated using Hook's law, given as

$$F = EA\varepsilon \tag{7.1}$$

where E is the Young's modulus, A is the area of the full cross section of the nose and ε is the tracked strain. The velocities used in the experiment were set to the mean velocities from the experiments, according to Table 7.5.

Table 7.5: Mean initial speed of trolley

	Dyn T	Dyn L
v_0 [mm/s]	2453	2353

7.1.4 Meshing the parts

The bolt and the nose were meshed with a relatively coarse mesh as illustrated in Figure 7.6. Six-node linear triangular prism elements were used in the core of both the parts, while the rest was meshed with eight-node brick elements.

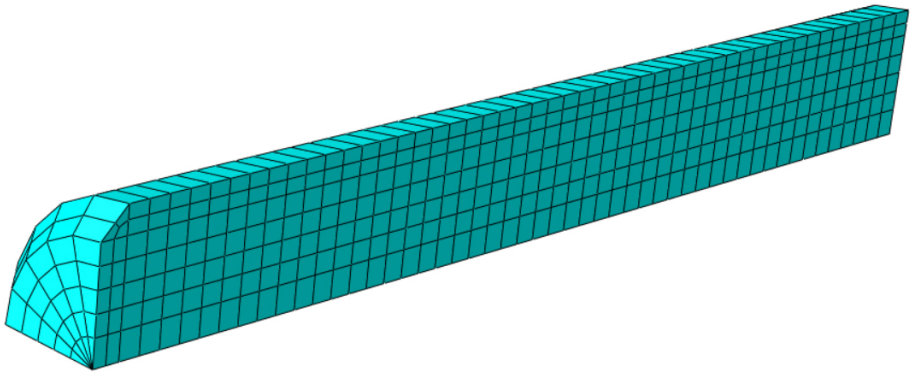

(a) Meshing the nose

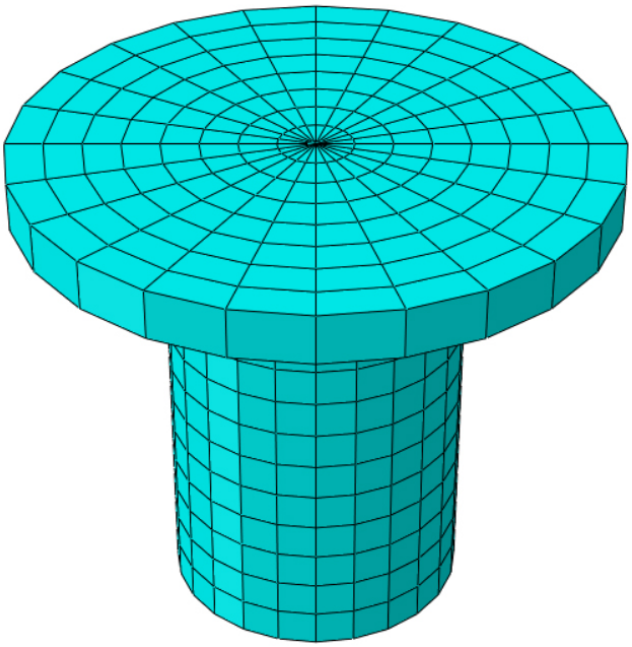

(b) Meshing the bolt

Figure 7.6: Mesh for nose and bolt

The component test specimen part was the critical part in these simulations and the plastic deformations were assumed to be concentrated in and around the weld, particularly around the weld root. To save computational cost, the mesh of the test specimen was generally coarse, but it was gradually refined closer to the weld. Simulations were executed with different meshes to get a better understanding of the mesh sensitivity. The finest mesh used had cubic elements around the root weld with element size of 0.125 mm. The finest meshes for the two different types of component test specimens are illustrated in Figure 7.7. In general the elements in all the parts in the quasi-static simulations were fully integrated, while the elements in the dynamic simulations used reduced integration to save computational expense.

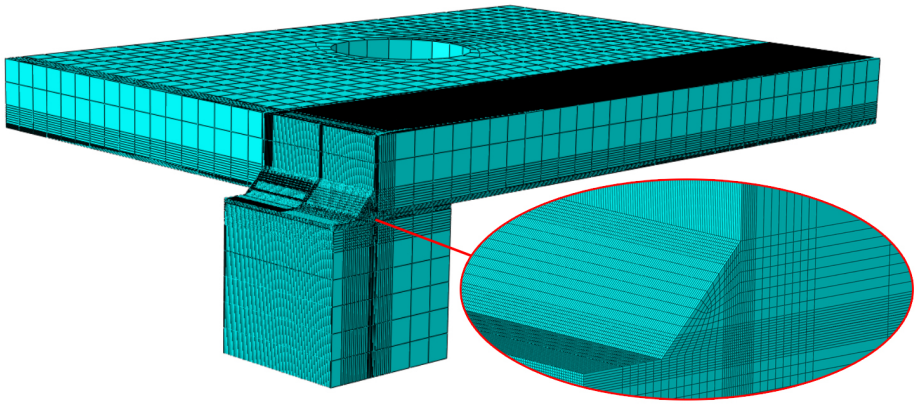

(a) Finest mesh for the component test specimen with transverse fillet welds

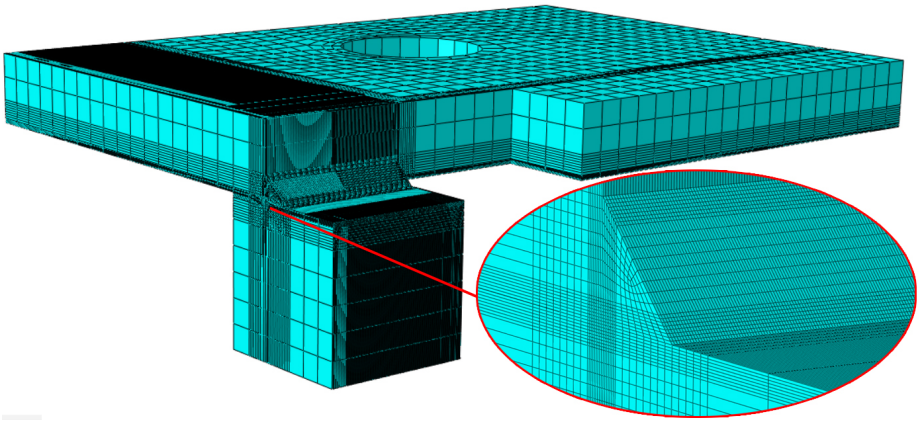

(b) Finest mesh for the component test specimen with longitudinal fillet welds

Figure 7.7: Mesh for nose and bolt

7.2 Results from numerical simulations

Relative displacement of the block was tracked in the same way in the numerical model as had been done with DIC in the experiments. The displacements of pairs of nodes, with one node on the block and another on the plate, were tracked during the simulations. The positions of the nodes were similar to the positions of the points in the experiment, see Figure 7.8. The displacements of the selected nodes on the plate was subtracted from the displacements of the pair nodes on the block, resulting in the relative displacement between the two nodes in the pair. The average value of the relative displacements of the node pairs was defined as the total mean relative displacement of the block.

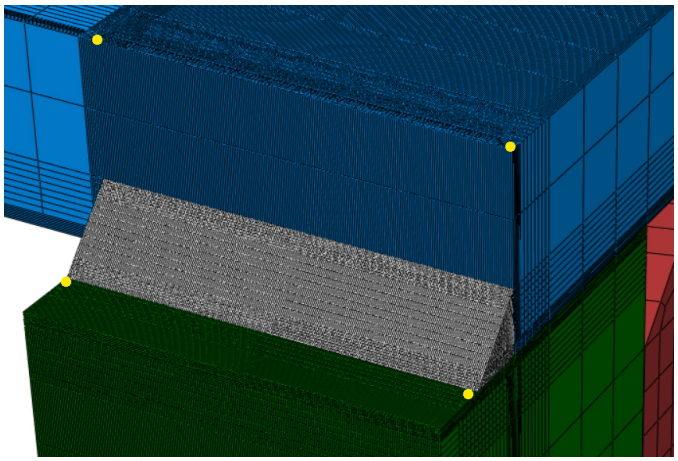

(a) Component test specimen with transverse fillet weld

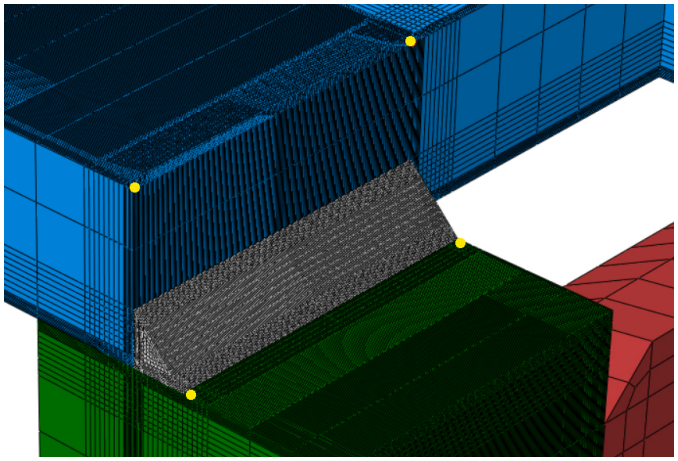

(b) Component test specimen with longitudinal fillet weld

Figure 7.8: Nodes used to track relative displacement of the block

7.2.1 Numerical simulations of the QS T component tests

The quasi-static component test specimen with transverse fillet welds was simulated with three different meshes, as illustrated in Figure 7.10. The deformation and the stresses in the figure were extracted at a frame when the relative displacement of the block was around 0.8 mm. That is roughly where the fracture occurred in the experiment for this type of component tests, see Section 4.1.1. Notice in the figure that the local stresses in and around the root of the weld seem to increase when refining the mesh. The load and the relative displacement of the block was obtained, and the results for the different meshes are presented in Figure 7.9. The applied load was clearly reduced by refining the mesh.

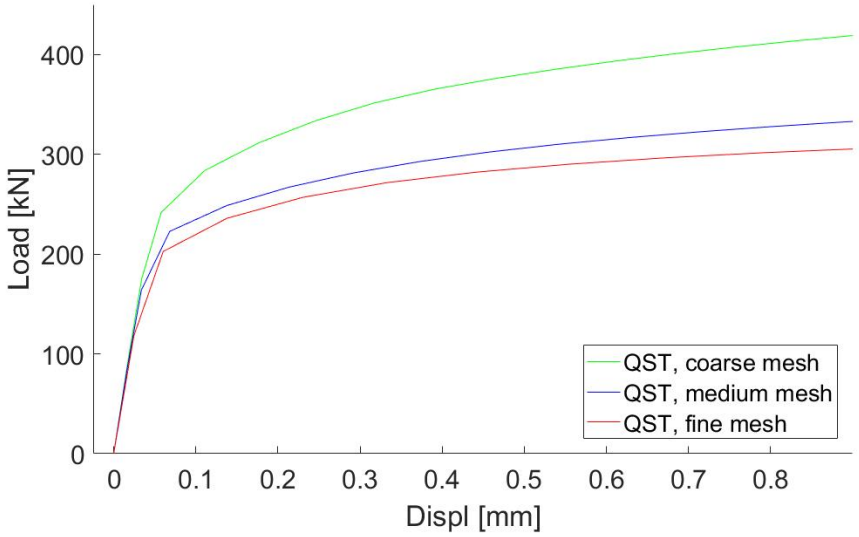

Figure 7.9: Numerical simulations of the QS T component tests

7.2.2 Numerical simulations of the QS L component tests

Similar simulations were carried out for the quasi-static component test specimen with longitudinal fillet welds. The QS L component tests fractured approximately when the relative displacement of the block was at 3.0 mm, see Section 4.1.2. Hence the deformation and the stresses from the three meshes in Figure 7.11 were extracted at a frame where the relative displacement of the block was around 3.0 mm. Notice that the the stress scale is different than for the QS T component tests. The local maximum stresses had a much higher value in the simulations of the QS L component tests than for the QS T component tests. The results from the simulations, presented in Figure 7.12, indicate that the mesh sensitivity of the QS L component tests corresponds to that for the QS T component tests, and that the applied load was reduced by refining the mesh.

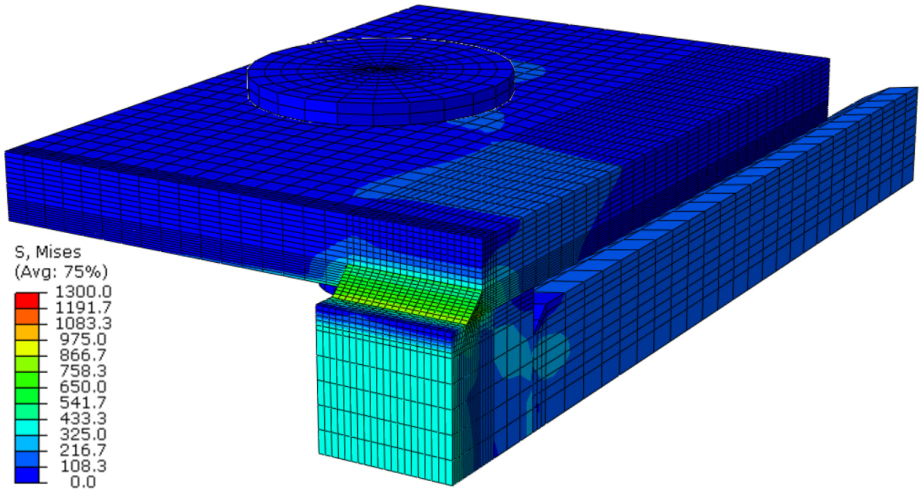

(a) Component test with medium mesh, smallest element size: 0.5 mm

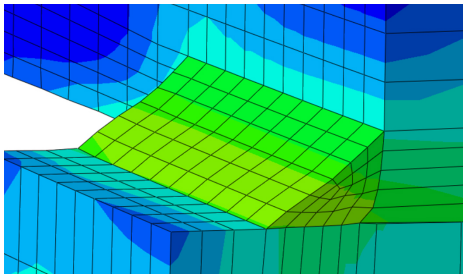

(b) Coarse mesh, smallest element size: 2 mm

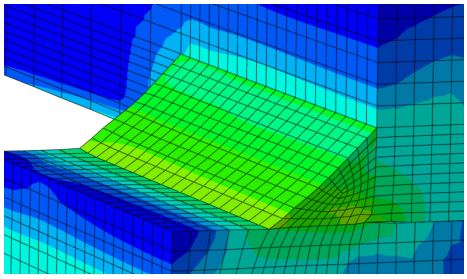

(c) Medium mesh, smallest element size: 0.5 mm

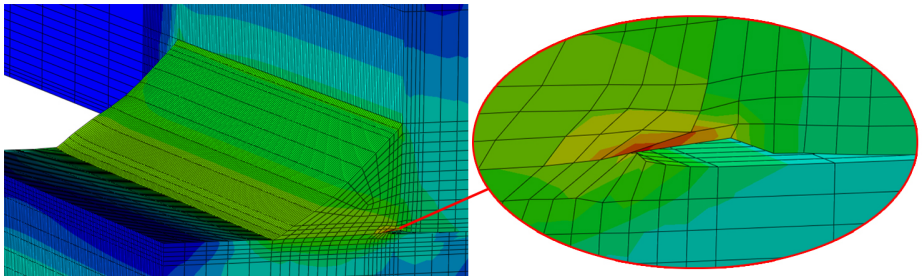

(d) Fine mesh, smallest element size: 0.125 mm

Figure 7.10: Deformations and stress distributions in the QS T simulations, extracted when the relative displacement of the block was around 0.8 mm

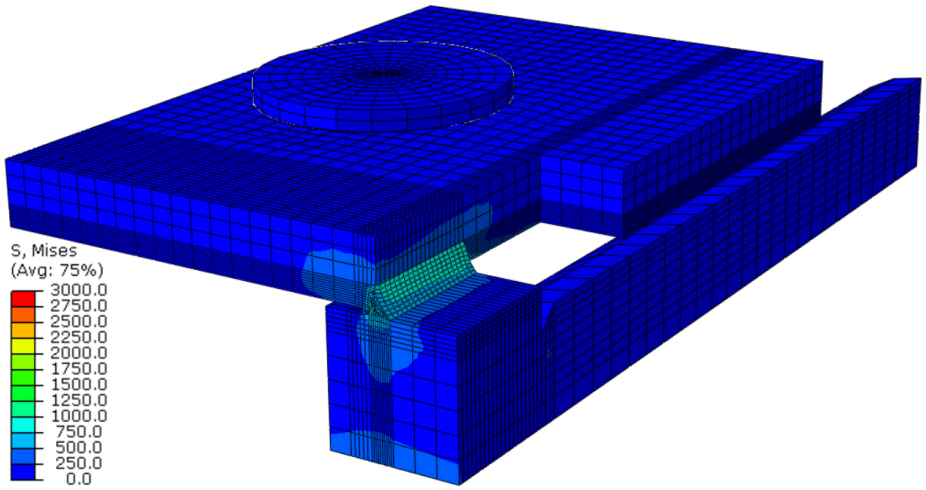

(a) Component test with medium mesh, smallest element size: 0.5 mm

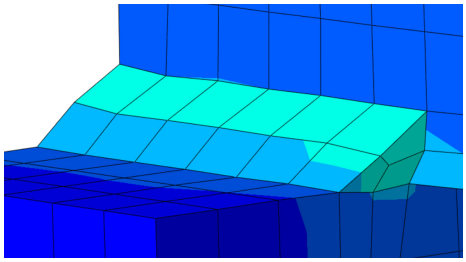

(b) Coarse mesh, smallest element size: 2 mm

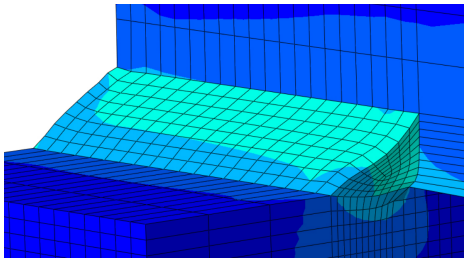

(c) Medium mesh, smallest element size: 0.5 mm

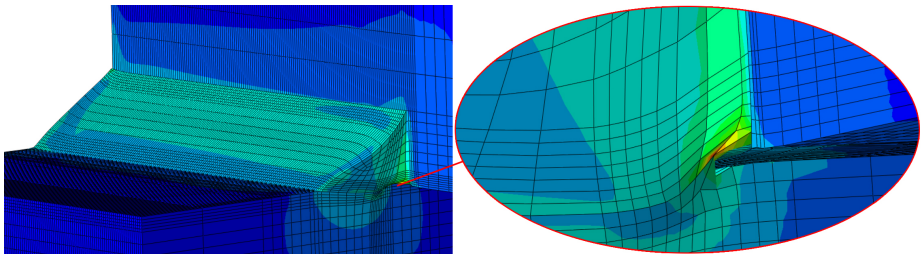

(d) Fine mesh, smallest element size: 0.125 mm

Figure 7.11: Deformations and stress distributions in the QS L simulations, extracted when the relative displacement of the block was around 3.0 mm

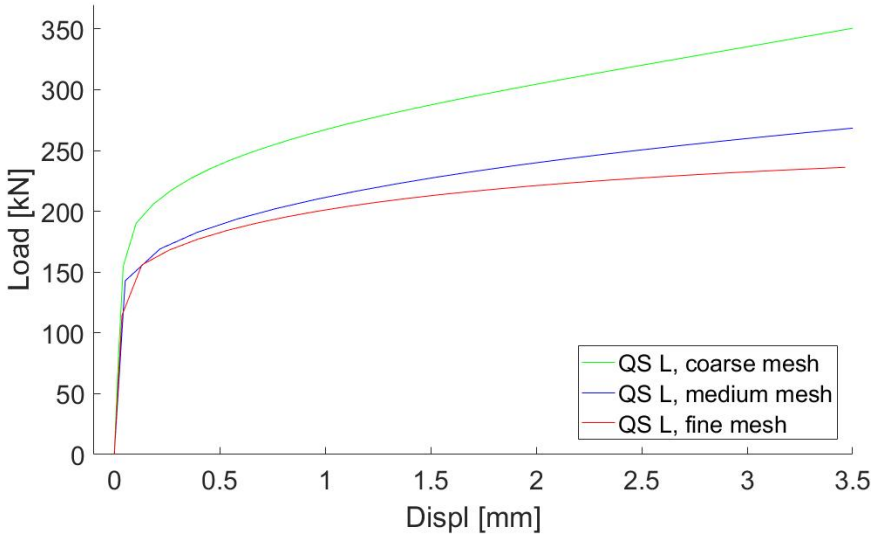

Figure 7.12: Numerical simulations of the QS L component tests

7.2.3 Numerical simulations of the Dyn T component tests

The numerical simulations of the dynamic component tests with transverse fillet welds were carried out with two different meshes. The meshes were the same as the coarse mesh and the fine mesh used in the QS T simulations. As mentioned, a fraction criterion was inserted into the dynamic simulations. When the criterion was reached in an element, the element was deleted from the model, simulating local fracture. The deformations and stresses in Figure 7.13 were extracted from the frame prior to the first element deletion in the model. The first element deletion in the Dyn T simulation with the fine mesh occurred when the relative displacement of the block had reached 0.79 mm. There was no element deletion for the Dyn T simulation with the coarse mesh. The results of the Dyn T simulations are presented in Figure 7.14.

7.2.4 Numerical simulations of the Dyn L component tests

Two different meshes were also used to carry out the numerical simulations of the dynamic component test with longitudinal fillet welds. The two meshes used were equal to the coarse mesh and the fine mesh in the QS L simulations. The first element deletion in the Dyn L simulation with the fine mesh occurred when the relative displacement of the block had reached 0.92 mm. There was no fracture in the Dyn L simulation with the coarse mesh. Figure 7.15 illustrates the stresses and deformations prior to fracture in the Dyn L component test with fine mesh. The results from the Dyn L simulation are presented in Figure 7.16.

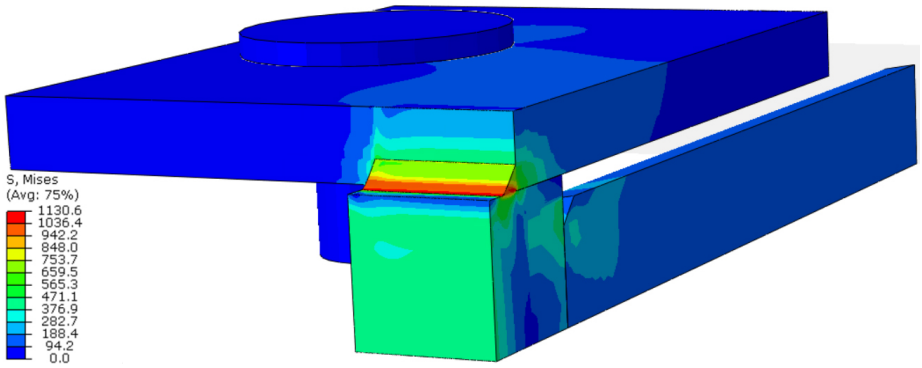

(a) Dyn T simulations, deformations and stress distribution with the fine mesh

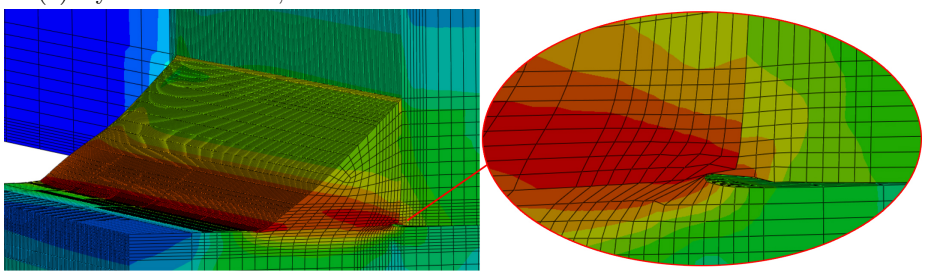

(b) Dyn T simulations with the fine mesh, smallest element size: 0.125 mm

Figure 7.13: Dyn T simulations with the fine mesh

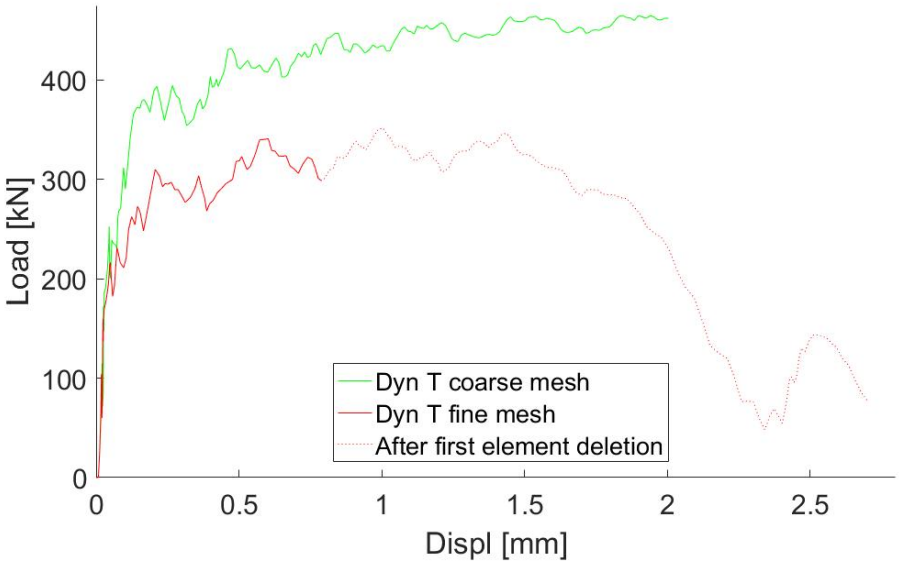

Figure 7.14: Numerical simulations of the Dyn T component tests

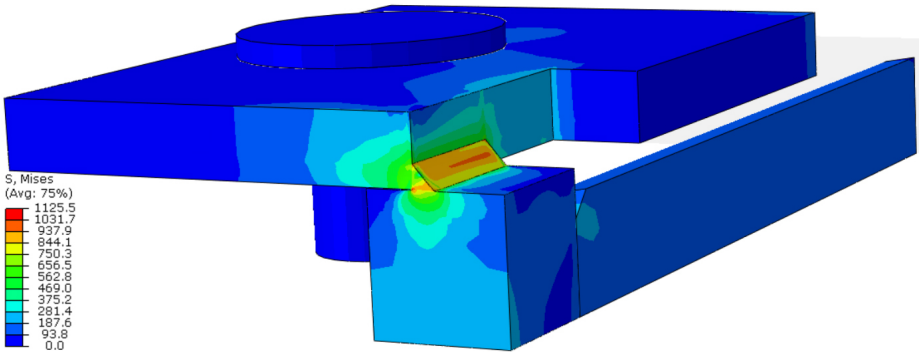

(a) Dyn L simulations, deformations and stress distribution with the fine mesh

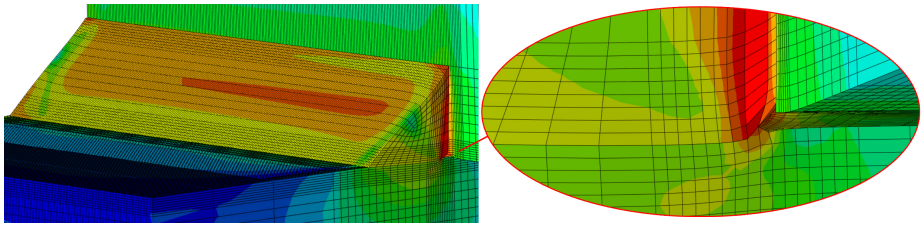

(b) Dyn L simulations with the fine mesh, smallest element size: 0.125 mm

Figure 7.15: Dyn L simulations with the fine mesh

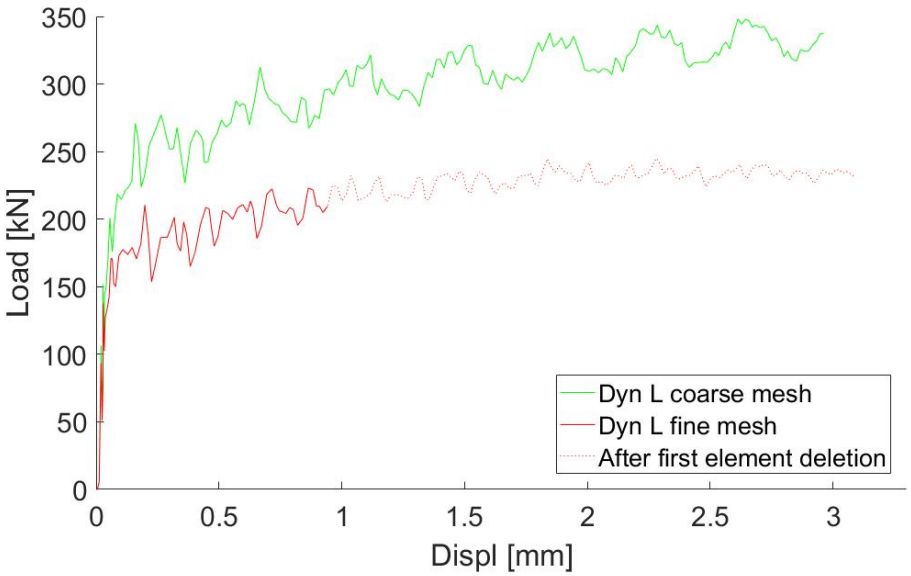

Figure 7.16: Numerical simulations of the Dyn L component tests

8 Discussion

8.1 Response to different load rates

The material tests, described in Section 5, were carried out with three different deformation rates. The block material was only tested with the slow going quasi-static rate, but the plate and weld materials were both tested with all three deformation rates, as illustrated in Figure 8.1. The reasons why the material response was different for the different deformation rates is discussed in the following paragraphs.

8.1.1 Strain rate hardening

When exposing a material to higher strain rates, the material can respond with strain rate hardening causing it to increase its strength [11, 12]. This is caused by the viscous properties in the material. A viscous material, such as honey, is characterised by its strain rate dependency. Stirring slowly in the honey is easy, but with increased stirring speed the honey becomes much stronger and the stirring becomes difficult. Also solids such as steel has viscous properties, and can become stronger at higher strain rates. It was therefore no surprise that the dynamic material tests gave higher stresses than the quasi-static material tests for both materials.

8.1.2 Thermal softening

With high strain rates, thermal softening can also play an important role in the material behaviour. Generally when a material is plastically deformed, heat energy is created where the deformation is occurring. When the strain rates are low, the created heat energy can be conducted throughout the material and diffused into its surroundings. The local temperature in the deformation zone is therefore not significantly increased at low deformation rates.

When the strain rates are high on the other hand, the heat energy has far less time to be conducted away from the deformation zone. This effect can cause an accumulation of heat energy causing local heating of the material in the center of the deformation zone. The stress strain properties of materials changes with temperature [13, 14]. The strength of steel for example, is gradually reduced when the steel is heated above around 150°. Hence, when a deformation zone is heated, that zone also looses some strength. With a consistent load, the reduced strength will cause a cycle of further deformations and further local heating, particularly in the center of the deformation zone. This effect is called thermal softening and can cause a weak point in the material and therefore reduce the stress-strain curve.

It was expected to be seen some effects of thermal softening in the results of dynamic material tests. And, quite so, the curves from the dynamic material tests seem to have reduced inclinations after yielding with respect to the curves

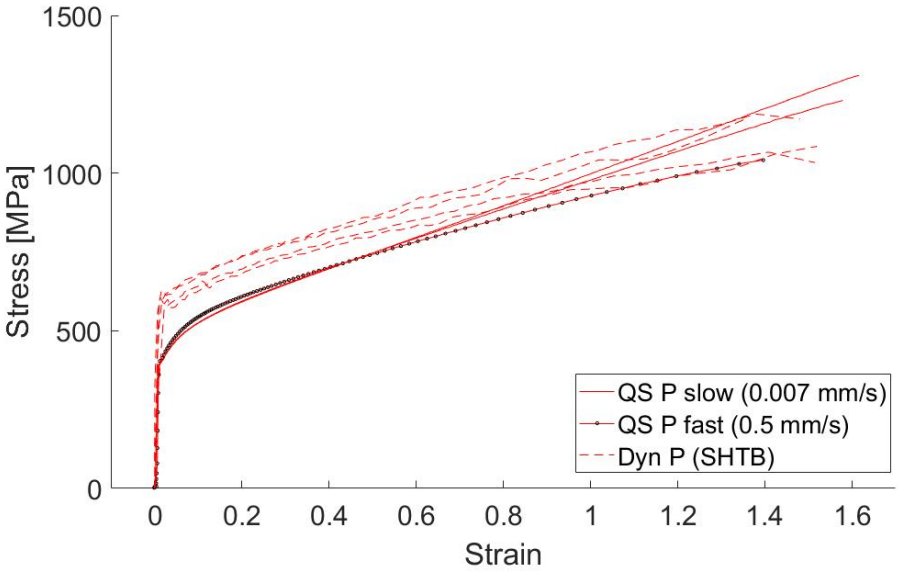

(a) Comparing material tests, plate material

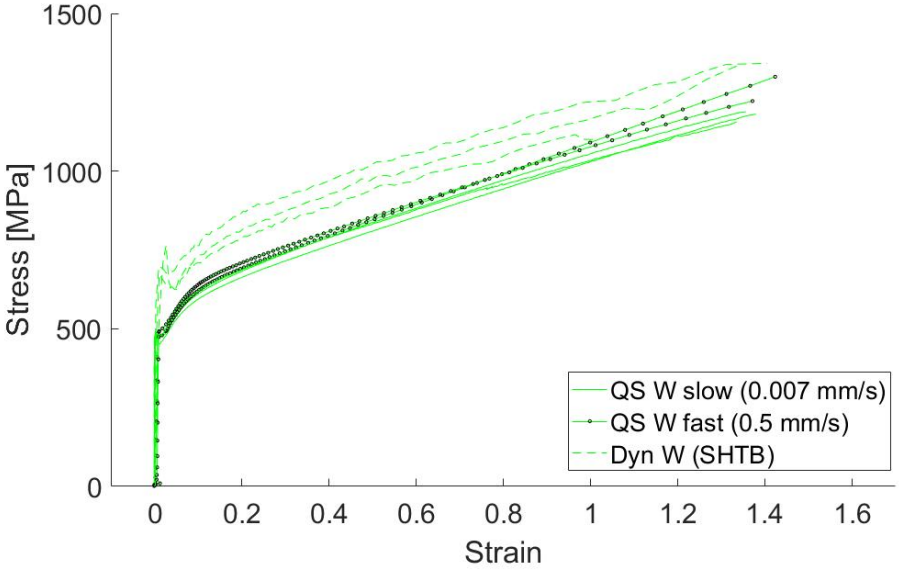

(b) Comparing material tests, weld material

Figure 8.1: Comparing the response to different strain rates for each material

from the slow going quasi-static material tests. However, the effects of thermal softening were not expected to be seen in any of the quasi-static tests. The fast going quasi-static tests for the welds, illustrated in Figure 8.1b, has an increased stress curve as a result of strain rate hardening. Just as expected, the curves do not give any indication of softening.

The results from the fast going quasi-static test of the plate material on the other hand have almost the same inclination as the respective dynamic tests after yielding, see Figure 8.1a. This behaviour looks very similar to the effects of thermal softening, but the test specimen was not expected to be significantly heated up during this test. The softening could be caused by other factors such as irregularities in the material test specimen. With only one successful fast going quasi-static test for the plate, it is hard to conclude anything for sure.

8.2 Comparing results

8.2.1 Experimental results

As presented in Figure 8.2, the component tests with transverse fillet welds had a stronger bahaviour with less deformation capacity than the component tests with longitudinal fillet welds. This difference was as expected [5].

Further it was expected to see an increase in the strength for the dynamic component tests with respect to the quasi-static component test because of the strain rate hardening. However, the increase in strength for the dynamic tests was not evident in the results, given in Figure 8.3 and in Table 8.1. The mean maximum load from the dynamic tests was slightly higher than for the quasi-static tests. However, the differences are small and besides the trend in the tests actually shows quite similar results in the stress-strain curves.

Table 8.1: Mean values of max load, relative displacement at fracture, and throat measure for the different types of component tests

	Transverse		Longitudinal	
	QS T	Dyn T	QS L	Dyn L
Mean max load [kN]	346	370	213	219
Mean rel displ. [mm]	0.73	0.88	2.71	1.51
Mean a [mm]	4.4	4.2	4.0	4.0

The reason why there was not a bigger difference between the results of the dynamic and the quasi-static component tests is not obvious. One explanation could be that the effect of the thermal softening more or less equalized the effect from the strain rate hardening. The deformation zones around the welds were quite small which would increase the concentration of thermal softening and perhaps give the thermal softening a larger significance in the overall response.

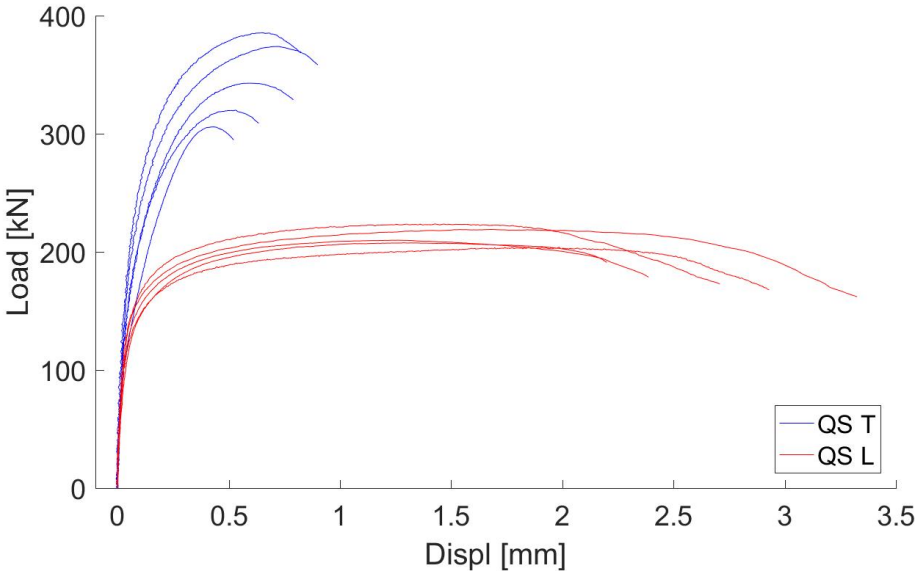

(a) Comparing all quasi-static component tests

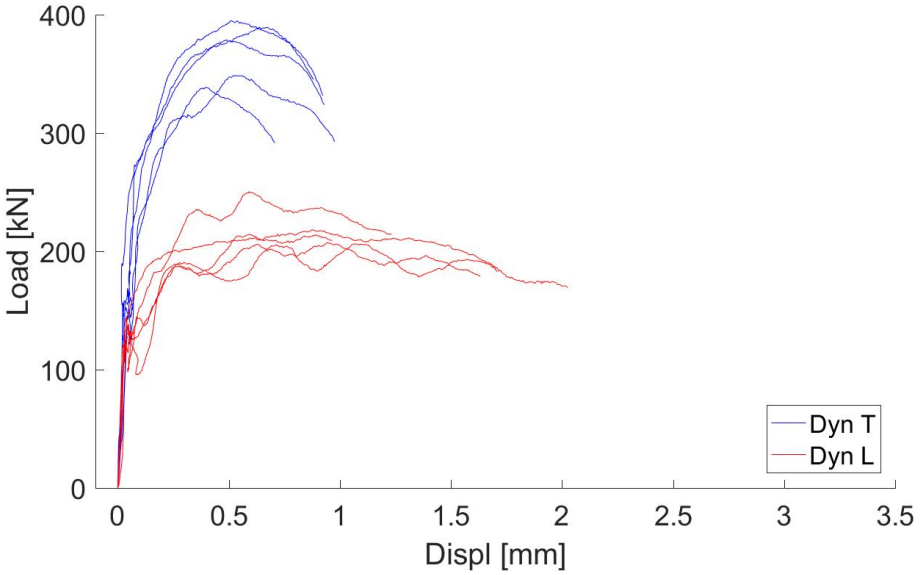

(b) Comparing all dynamic component tests

Figure 8.2: Comparing the results from the component test with transverse and longitudinal fillet welds

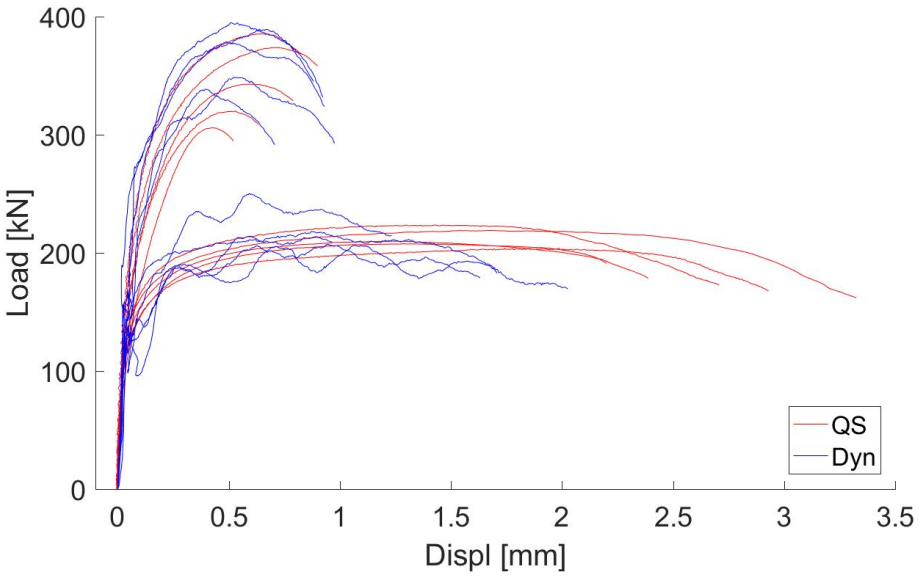

Figure 8.3: Comparing the results from all component tests

One clear difference between the results from the quasi-static component tests and the dynamic component test is the smoothness of the curves. The results from the quasi-static tests gave very smooth curves while the curves from the dynamic tests seem to oscillate. The reason for this is simply because of the stress wave propagation during the the impact of the dynamic tests. At impact, the colliding parts will vibrate and the contact force will therefore oscillate.

Another observation is that the deformation capacities were different for the dynamic and the quasi-static component tests with longitudinal fillet welds. The relative displacement of the block at fracture for the Dyn L component tests was roughly reduced with around 40% with respect to that for the QS L component tests. This effect was not present for the component tests with transverse fillet welds where the deformation capacities were quite similar for the dynamic and the quasi-static component tests.

The decreased deformation capacity in the Dyn L tests could be explained as a result of thermal softening. The deformations in the Dyn L tests were quite big, in fact they were almost twice as big as for the Dyn T test. Big deformations in a short amount of time cause local temperature heating which would increase the local ductility. However, if all the plastic deformations in the component were happening in a small deformation zone, the overall deformation capacity could have been reduced even if the local ductility was increased.

8.2.2 Numerical results

Comparing the results from the dynamic and the quasi-static component simulations from Section 7.2, using the results from the simulations with the fine meshes, the curves in Figure 8.4 were obtained. As expected, and similar to the experimental results, the model with the transverse fillet welds proved stronger than the model with longitudinal fillet welds. Further, the response of the dynamic simulations indicated a slightly stronger behaviour than for the quasi-static tests. Expecting some strain rate hardening in the dynamic tests, this was more or less as anticipated

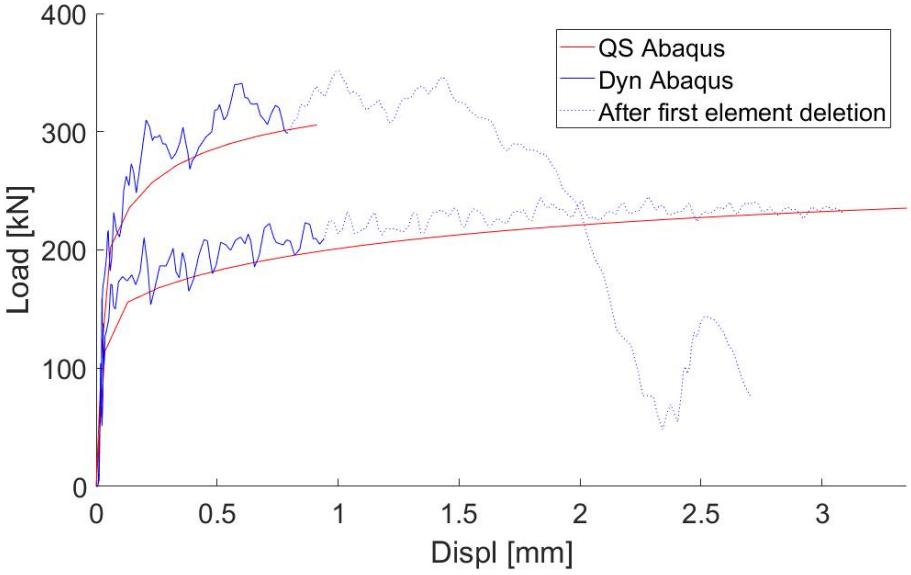

Figure 8.4

One curious and unexpected observation is that the two dynamic simulations started their fracture with a similar relative displacement of the block. It was expected that the fracture of the Dyn L component tests would come at a bigger relative displacemnt of the block. However, simulating the actual crack propagation during fracture is a difficult task and has not been prioritised for this thesis. Hence, it is difficult to say how representative the results of the dynamic simulations are after their first element deletion. It is also hard to define a specific time for when global fracture had occurred. The first element deletion ideally gives an indication of when crack propagation starts, but there can be big global deformations also during the crack growth before fracture.

8.2.3 Comparing simulations and experimental results

Figure 8.5 compares the numerical results, using the simulations with the fine meshes, with the experimental results. Notice that the quasi-static simulations were carried out with three different weld sizes. This was to get a better understanding of the significance of the throat size in the response of the component tests. Changing the throat size with 0.5 mm, which was a change of 12.5% of the original 4.0 mm throat size, gave roughly a 10% change in the strength of the component tests. The dynamic tests were only tested with 4.0 mm throats.

There is a clear resemblance between the results from the experiment and from the simulations. However, there is one obvious difference. When the load in the experimental quasi-static tests reached a certain level, the load curve flattened out and after a while started decreasing. This effect is not present in the results from the numerical simulations. The reason for this is that the materials defined in the quasi-static numerical simulations were perfectly elastic-plastic.

Another observation is the differences in strength from the numerical simulations and the experiments. The general trend, perhaps with the exception of the Dyn L component tests, was that the numerical models with the 4.0 mm welds had lower strength than the component test specimens in the experiments, particularly for the specimens with transverse fillet welds. There could be several reasons for this discrepancy. One obvious reason is that the average throat size for the transverse welds were larger than the 4.0 mm used in the simulations according to Table 8.1.

Another possible, and perhaps the most probable, source of discrepancy could be the simplification of the weld geometry used in the simulation. While the simulation was created with perfectly triangular welds, that is seldom the case in the real world. Figure 8.6, which is the same image used in Figure 6.19 from the Vickers hardness test, illustrates an example of the real weld geometry from a piece of a component test specimen. Notice that the perfectly triangular weld, marked in black, is a somewhat poor reproduction of the real weld geometry, marked in red.

Producing the component test specimen, the weld was burned into the base materials, increasing the effective area of the weld with respect to the weld with the perfectly triangular shape. This certainly also increased the overall strength of the component test specimens. Besides, the material around the weld material, indicated in blue, has clearly been effected by the heat in the welding process. The Vickers hardness tests show that the base material in this zone had increased strength with respect to the unaffected zones of the base materials. Non of these effects were inserted into the numerical model. The weld in the numerical model was simply created perfectly triangular and there was no heat effected zone around the welds either. By improving this, a more accurate result would be expected.

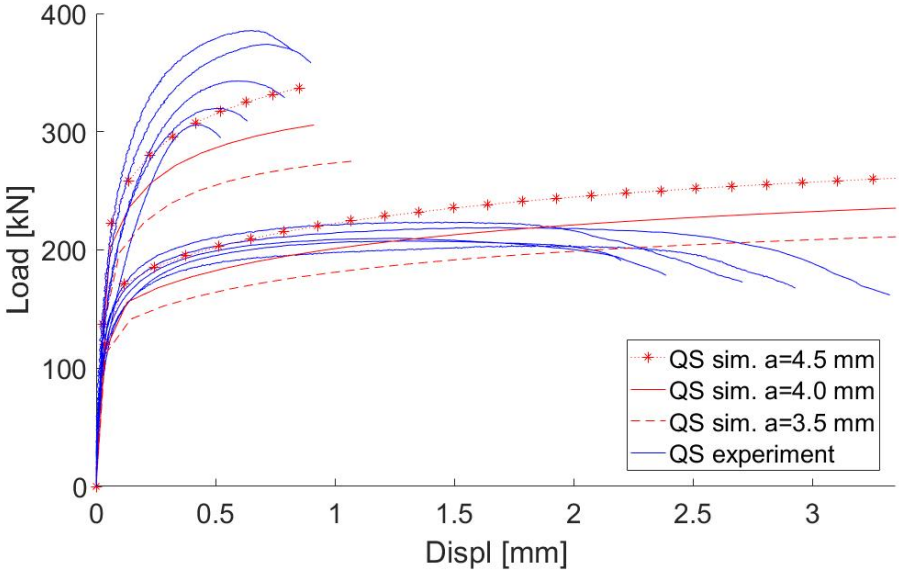

(a) Comparing quasi-static results

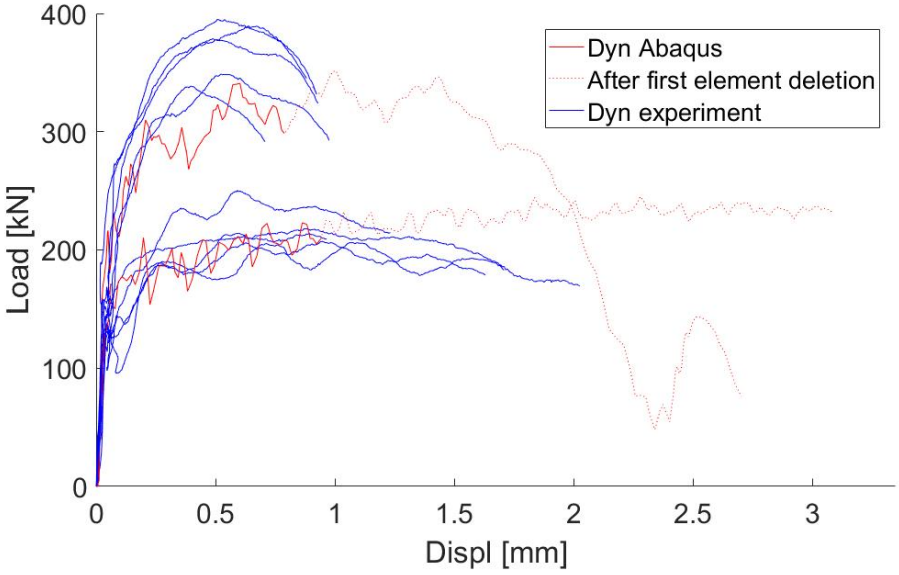

(b) Comparing dynamic results

Figure 8.5: Comparing numerical and experimental results

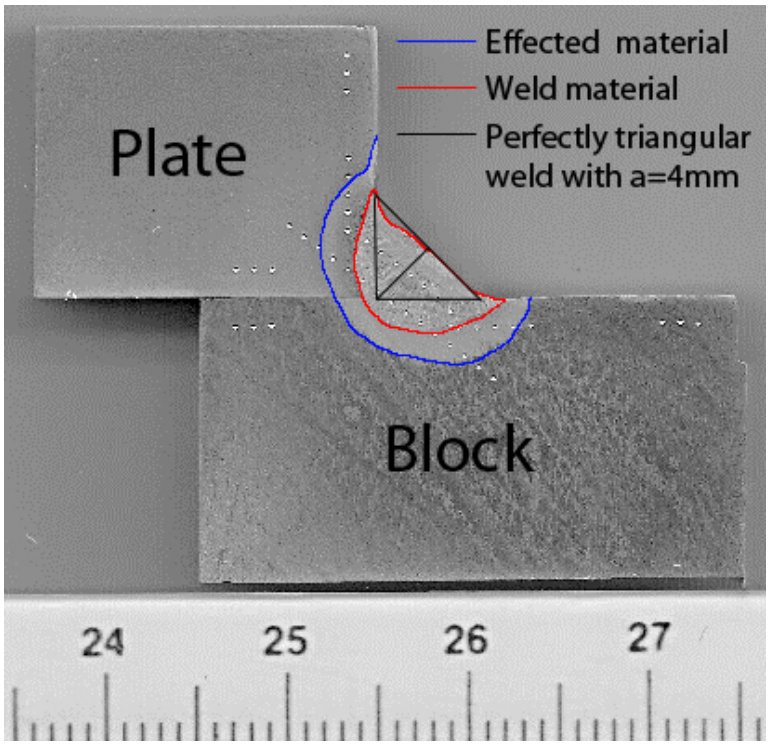

Figure 8.6: Real weld geometry

8.3 Comparing results to Eurocode calculations

The maximum resistance force for transverse fillet welds, according to the Eurocode, is calculated using Equation 2.5. Having two equally big welds, maximal resistance of the component test with transverse fillet weld is

$$F_{max,T} = \frac{f_u \cdot A_{w,tot}}{\sqrt{2} \cdot \gamma_{M2} \cdot \beta_w} = \frac{f_u \cdot 2 \cdot a \cdot l_{eff}}{\sqrt{2} \cdot \gamma_{M2} \cdot \beta_w} \tag{8.1}$$

Moreover, the maximum resistance force for longitudinal fillet welds, accordin to Eurocode, is calculated using Equation 2.8. Having four equally big welds, the maximum resistance force for the component test with longitudinal fillet welds is

$$F_{max,L} = \frac{f_u \cdot A_{w,tot}}{\sqrt{3} \cdot \gamma_{M2} \cdot \beta_w} = \frac{f_u \cdot 4 \cdot a \cdot l_{eff}}{\sqrt{3} \cdot \gamma_{M2} \cdot \beta_w} \tag{8.2}$$

Assuming $l_{eff} = 60.0$ mm for the transversal welds and $l_{eff} = 30.0$ mm for the longitudinal welds, and using the mean measured throat sizes from the component test specimens, the maximum resistance forces were calculated and presented in Table 8.2.

Table 8.2: Comparing results to Eurocode calculations

	Transverse		Longitudinal	
	QS T	Dyn T	QS L	Dyn L
Mean a [mm]	4.4	4.2	4.0	4.0
Mean max load, P [kN]	346	370	213	219
F_{max}, Eurocode [kN]	169	162	126	126
F_{max}/P [%]	48.8	43.7	59.2	57.5

Comparing the results it seems that the resistance forces calculated with the Eurocode roughly were between 40-60% of the measured applied loads. The main reason for these differences is because the calculations used in Eurocode are presented with various safety factors to cover for possible discrepancies in materials used, in loads applied, discrepancies due to poor craftsmanship, etc. Further, the formulas in the Erocode are based on static loading. The mean maximum loads measured in the dynamic tests were not significantly different from the mean maximum loads measured in the quasi-static loads. Hence there is no motive, found in this study, to alter the formulas in the Eurocode for the use of impact loading.

8.4 Possible sources of discrepancies

The material parameters used in the numerical simulations were extracted from the material tests. However, some of the materials had few successful material tests which could lead to questioning the credibility of these results.

Simplifications in the numerical models have already been mentioned as possible sources of discrepancies for the geometry of the welds. However other simplifications were carried out as well. For example, the component tests were assumed to be symmetric about two planes. There will always be some small differences in the material or the geometry in a test specimen causing some small asymmetries, but these variations can safely be neglected. However as mentioned in Section 3.3.3, the bolts used in most of the component tests had bolt threads in the lower hole of the plates and not in the upper holes. This was a possible source of asymmetry in the component test specimens that might have created some rotations of the block.

If the plates had any plastic deformations because of the contact with the screws thread in the bolt, it would signify that some of the energy, that was supposed to deform the lower welds, was going to the plate hole instead. If this really was the case, the upper welds would get bigger deformations than the lower ones, and that would cause a rotation of the block. To measure the rotation of the block, the displacement of the selected points on the block and the plate was used. Subtracting the mean relative displacement of the underside of the block from the mean relative displacement of the upper side of the block,

the rotations in Figure 8.7 were obtained. The two quasi-static tests that were tested with the longer bolt are marked in red. All the other quasi-static tests were also tracked for comparison and marked in blue.

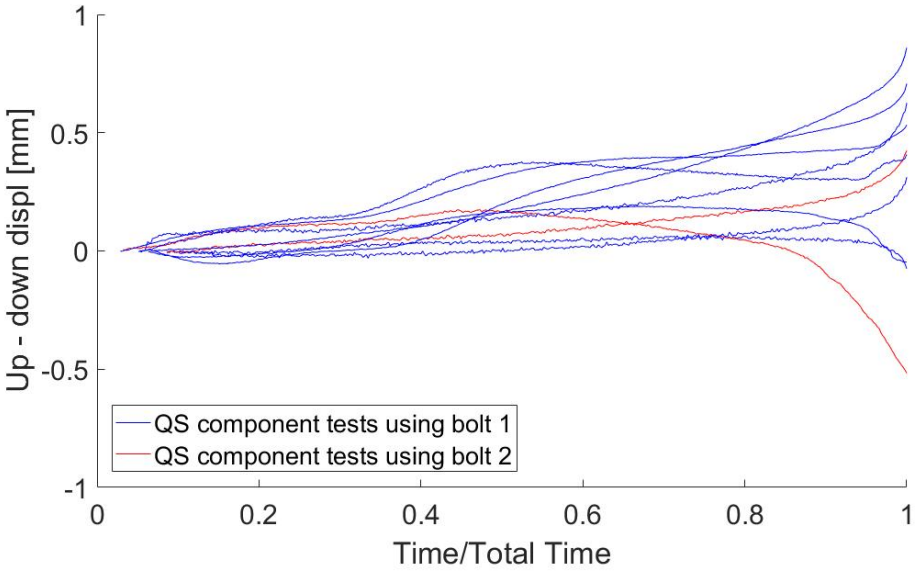

Figure 8.7: Difference in relative displacement of the upside and the underside of the block in all the quasi-static component tests

There seems to have been a general trend for the component tests to have bigger relative displacement on the upper side of the block than on the underside. The only component test with a clear opposite rotation was one of the two component tests where the longer bolts were used. This could indicate that the bolts played a part in these rotations. However, it could also be completely random, and the general trend to rotate in that direction could be caused by other factors. Having only carried out two tests with the longer bolt, it is very hard to conclude. Further, it is hard to know how important these rotations were to the overall response of the component tests.

When creating the numerical models for the different component tests, all the contact between the different parts were assumed frictionless. This was of course a simplification, and could have caused some small discrepancies in the results. However, friction is not believed to have played a major role for the component tests in this study.

The biggest source of discrepancies for the results of the numerical simulations is however still assumed to be the geometry of the weld, as mentioned in Section 8.2.3.

9 Concluding remarks

Twenty component tests were successfully carried out. As expected, the component tests with transverse fillet welds showed higher strength and less deformation capacity than the component tests with longitudinal fillet welds. The mean maximum loads measured in the component tests with longitudinal fillet welds were roughly about 60% of the mean maximum loads measured for the component tests with transverse fillet welds. Unexpectedly, the strengths of the component tests were not, at least not significantly, increased at impact with respect to at quasi-static loading. It is believed that the effects of thermal softening could have equalised the effects of strain rate hardening in the impact tests.

The deformation capacity for the component tests with longitudinal fillet welds was significantly decreased at impact with respect to for the quasi-static loading. The deformation capacity at impact was about 56% of the deformation capacity at quasi-static loading. The reason for this was again believed to be because of thermal softening, which could have caused a decreased deformation zone.

Numerical FE-simulations were created, using Abaqus 6.14, and material tests were carried out. The material properties extracted from the material tests were inserted into the numerical models to give best possible simulations. The results from the numerical simulations were similar to the results from the experimental test, indicating that the simulations were rather accurate. However, the match in the results were not perfect. The most important source of discrepancies is believed to be the simplification of the weld geometry in the numerical simulations.

Finally the results from the tests were compared to calculations from the Eurocode. The regulations from the Eurocode are presented with various safety factors, and it was therefore expected that the results from the component tests would give higher strengths than the calculations based on the design codes. In fact, the resistance forces calculated with the Eurocode were roughly between 40-60% of the measured applied loads in the experiments. There was not found any motive to change the formulas in the code for impact loading

9.1 Suggestions for further work

In this study, all the welds in the component tests were created with a throat size of approximately 4 mm. All the tests were carried out in room temperature and only two different loading rates were used. Moreover, only two weld orientations were tested and all the welds were fillet welds. Besides, the materials used, both in the welds and in the base materials, were the same for all the tests. To get a best possible comprehension of how welded materials respond to different loadings, it could be interesting to further investigate these variables.

References

[1] Grimsmo EL, Clausen AH, Aalberg A, Langseth M. (2016) A numerical study of beam-to-column joints subjected to impact. *Engineering Structures*. **120**, 103–115

[2] Grimsmo EL, Aalberg A, Langseth M, Clausen AH. (2016) Failure modes of bolt and nut assemblies under tensile loading. *Journal of Constructional Steel Research*. **126**, 15–25

[3] Grimsmo EL, Clausen AH, Aalberg A, Langseth M. (2015) An experimental study of static and dynamic behaviour of bolted end-plate joints of steel. *International Journal of Impact Engineering*. **85**, 132–145

[4] Larsen PK. (2010) Dimensjonering av stålkonstruksjoner. **2.utg**

[5] Butler LJ, Kulak GL. (1971) Strength of fillet welds as a function of direction of load. *Welding Journal, Welding Research Supplement*. **36(5)**, 231-234

[6] Chen Y, Clausen AH, Hopperstad OS, Langseth M. (2011) Application of a split-Hopkinson tension bar in a mutual assessment of experimental tests and numerical predictions. *International Journal of Impact Engineering*. **38**, 824-836

[7] Vilamosa V, Clausen AH, Fagerholt E, Hopperstad OS, Børvik T. (2014) Local Measurement of Stress–Strain Behaviour of Ductile Materials at Elevated Temperatures in a Split-Hopkinson Tension Bar System. *Strain: An International Journal for Experimental Mechanics*. **50(3)**, 223-235

[8] Smith RL, Sandland GE. (1922) An Accurate Method of Determining the Hardness of Metals, with Particular Reference to Those of a High Degree of Hardness. *Proceedings of the Institution of Mechanical Engineers*. **1**, 623–641

[9] B ørvik T, Dey S, Clausen AH. (2008) Perforation resistance of five different high-strength steel plates subjected to small-arms projectiles. *International Journal of Impact Engineering*. **36(7)**, 948-964

[10] Cockroft MG, Latham DJ. (1968) Ductility and the workability of metals. *Journal of the Institute of Metals*. **96**, 33-39

[11] Cao Y, Ahlström J, Karlsson B. (2014) The influence of temperatures and strain rates on the mechanical behavior of dual phase steel in different conditions. *Journal of Materials Research and Technology*. **4(1)**, 68-74

[12] Hopperstad OS, Børvik T. (2015) Materials Mechanics Part I

[13] Cooke GME. (1988) An introduction to the mechanical properties of structural steel at elevated temperatures. *Fire Safety Journal*. **13**, 45–54

[14] Poh KW. (2001) Stress-strain-temperature relationship for structural steel. *Journal of Materials in Civil Engineering*. **13(5)**, 371-379

[15] NS-EN 1993-1-8:2005/NA:2009, Eurocode 3: Design of steel structures, Part 1-8: Design of joints

[16] NS-EN 1993-1-8:2005/NA:2009, 4.5.3.2

[17] NS-EN 1993-1-8:2005/NA:2009, NA.2.2(2)

[18] NS-EN 1993-1-8:2005/NA:2009, Table 4.1

[19] http://folk.ntnu.no/egilf/ecorr/doc/